INSTITUTO SUPERIOR TÉCNICO
Universidade Técnica de Lisboa

Structural assessment based on photogrammetry measurements and finite element method

Aleix Cubells i Barceló

Thesis in partial fulfillment of the requirements for Master Degree in

Naval Architecture and Marine Engineering

Jury

Chairman: Doutor Carlos António Pancada Guedes Soares

Supervisor: Doutor Yordan Ivanov Garbatov

Member: Doutor Manuel Filipe Simões Franco Ventura

May 2012

ACKNOWLEDGMENTS

First and foremost, I would like to express my deep gratitude to Prof. Doutor Yourdan Garbatov for giving me the opportunity to develop the present thesis. Working with him has been a very challenging experience, from the starting point with an interesting issue, up to the final steps, where relevant achievements have been reached. His profound knowledge, as well as his supportive attitude, has been very influential to my daily work.

A deep hearted thanks to my colleagues, who have been following my master's studies from Barcelona all this time and who have been next to me every day. I also want to kindly thank my girlfriend Laia for having cared for me and my mind.

Last but not least, a very special gratitude to my parents Albert and Rosalia for being so close to me all the time, for encouraging me to fight for my dreams and for trusting on my capacities.

RESUMO

O objectivo da presente tese é desenvolver uma nova abordagem para modelar as imperfeições geométricas iniciais de placas de navios utilizando fotogrametria analítica. Esta técnica é capaz de fazer medições das distorções de placas e tomar a forma da superfície dominante, incluindo os desvios dos bordos e as assimetrias. Tendo estes dados, é possível gerar modelos fiéis de placas baseadas em funções polinomiais. Finalmente, a resistência última das placas pode ser estudada realizando um cálculo baseado nos elementos finitos através dum código comercial.

Sete chapas, três não-reforçadas e quatro reforçadas, foram modeladas e estudadas neste trabalho. Para cada placa, dois modelos de imperfeição inicial foram gerados: um, com base em medições fotogramétricas e o outro, com base nas funções trigonométricas de Fourier. Ambos os modelos são submetidos às mesmas condições de carga de compressão e de contorno, a fim de estudar o comportamento através das curvas de força de tensão de resposta.

O presente trabalho também estuda a utilização da fotogrametria para medir o nível de corrosão de placas de aço. Baseando-se nas fotografias estereográficas, uma nuvem de pontos é gerada para modelagem da rugosidade da superfície das placas. A dispersão dos pontos é usada para calcular a profundidade de corrosão. A conclusão é que a abordagem proposta nesta tese é capaz de gerar superfícies dasplacas duma maneira fiável e versátil e pode ser usada para avaliar diferentes modos de falha.

Palavras-chave:imperfeiçoes iniciais, placa, resistência última, modo de colapso, corrosão, fotogrametria, ajuste a superfícies

ABSTRACT

The objective of the present thesis is to develop a new approach to model the initial geometrical imperfections of ship plates by using the analytical Photogrammetry. This technique is able to take measurements of the distortions of the plates and to catch the dominant surface shape, including the out-of-plane of the edges and the asymmetries. Having this data, it is possible to generate faithful models of plates based on polynomial functions. Finally, the maximum load-carrying capacity of the plates can be analysed by performing a nonlinear finite element analysis using a commercial finite element code.

Seven plates, three un-stiffened and four stiffened, have been modelled and analysed in this study. For each plate, two initial imperfection models have been generated: one, based on photogrammetric measurements and the other, based on the trigonometric Fourier functions. Both models are subjected to the same uniaxial compressive load and boundary conditions in order to study the behaviour through the strength-strain response curves.

The present work also studies the use of the Photogrammetry to measure the level of corrosion degradation depth of steel plates. Relying on the stereographic photographs, a dense cloud of points modelling the roughness of the surface of the plates is generated and the points' dispersion is used to compute the corrosion depth. The conclusion drawn is that the approach proposed in this thesis is able to generate ship plate surface faithfully in a versatile and reliable way and it can be used to evaluate different failure modes.

Keywords: initial imperfections, plate, ultimate strength, buckling, photogrammetry, corrosion, surface fitting

TABLE OF CONTENTS

LIST OF FIGURES

LIST OF SYMBOLS

a	plate length
ASR	average stress ratio
a_i	coefficient of a polynomial function
b	plate breadth
β	slenderness
COV	coefficient of variation
D	plate's flexural rigidity
δr	radial distortion
E	Young modulus
GOF	goodness of fitness
i, j	indexes
k	buckling coefficient, index
K1, K2, K3	radial distortion parameters
λ	scale factor
m, n	number of half sine waves on a bucked mode
MSE	mean squared error
N	in-plane uniaxial load
N_x, N_y	plate's membrane forces per unit length in x and y direction
π	Pi number
$\mathcal{P}$	class of a polynomial function
$p(x, y)$	bivariant polynomial function
R_d	reduction factor due to the initial deflection
R_r	reduction factor due to residual stress
$R - square$	coefficient of determination
$R_{w\varphi k}$	rotation matrix
Adj. R-squ.	adjusted coefficient of determination
RMSE	root mean squared error
σ_0	Yield stress
SSR	sum of the squares of the regression
SST	total sum of the squares of the residuals
ε	strain

ε_{YP}	Yield strain
$\sigma_{u,o}$	ultimate stress of intact plate
σ_{YP}	material Yield stress
σ_u	ultimate stress
t	plate thickness
ϕ_u	non-dimensional ultimate strength
u, v	plate displacement in x and y direction respectively
v	Poisson ratio
w_o	initial deflection
w	out-of-plane deflection
w, φ, k	rotation parameters
$X\ Y\ Z$	primary coordinate system
$X_A Y_A Z_A$	coordinates of an arbitrary point a in primary coordinate system
$x\ y\ z$	secondary coordinate system
$X_0 Y_0 Z_0$	coordinates of the perspective centre of the secondary system
x_a, y_a	coordinates of an arbitrary point a in the secondary coordinate system

1.INTRODUCTION

1.1. STATEMENT OF THE PROBLEM

Ship structures are predominantly made of steel plates and stiffeners forming panels. They have widely been used as primary structural components due to the simplicity of fabrication and their high strength-weight ratio. During the service lifetime, these panels are subjected to axial loads and bending moment stresses making the structure susceptible to failure. One of the major stability losses is due to buckling of plates, which are part of stiffened panels. Nowadays there is still insufficient knowledge about their behaviour.

Structures fail when performing the function for which they have been designed and to evaluate their capacity, Limit State functions are used. There are four types of limit states: Serviceability Limit State, Ultimate Limit State, Fatigue Limit State and Accidental Limit State. From the point of view of design, these types of limit states might be considered to assess the present status of structural safety [1].

For structural design of ships, the most important criteria is strength, and to evaluate it the Ultimate Limit State (ULS), or simply Ultimate Strength approach is used. The so called permissible stress approach, which is based on linear elastic stress assessment does not allow to determine the true margin of structural safety since the ultimate limit state remains unknown [2].

The plates and stiffened panels of the deck and the bottom are subjected to compressive stresses due to sagging and hogging bending moments, making them susceptible to failure by instability. The stiffened plates can buckle in four different forms: plate induced overall buckling (PI), stiffened overall buckling (SI), stiffener tripping (ST) and plate buckling (PB).

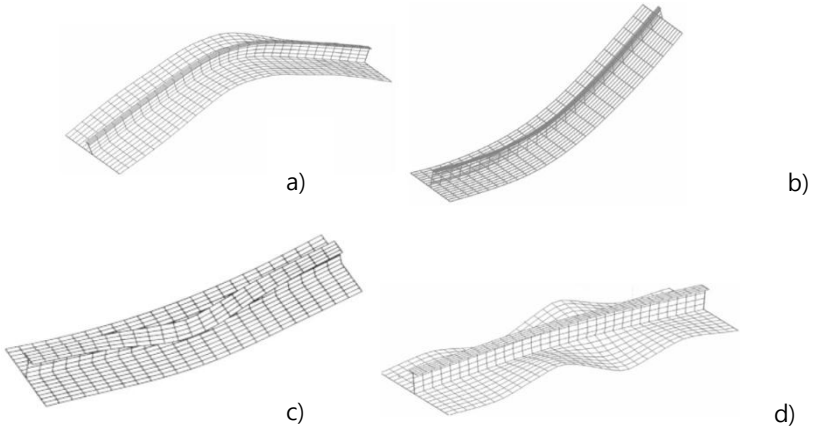

Figure 1.1 Modes of Buckling a) Plate induced Overall Buckling (PI) b) Stiffened Induced Overall Buckling (SI) c) Stiffener Tripping (ST) d) Plate Buckling (PB)

The overall buckling can be induced by the failure of the plate of the stiffened panel. When plate-induced buckling (PI) occurs, it is observed that the panel deflects away from the plate. The stiffened-induced failure

(SI) is associated with the yielding in compression in the stiffener. Both plate-induced and stiffened-induced failure modes have a very stable post-buckling response.

On the other side, Stiffened tripping (ST) consists of twisting of the stiffener about its line of attachment with the plate. It is also known as lateral torsional buckling of the stiffener and it occurs when the stiffeners of a panel has the high flexural rigidity and low torsional rigidity. Stiffener tripping is characterized by a rapid drop in load capacity that occurs because of the loss of stiffener rigidity, what makes this failure to be more critical than other failure modes.

Finally, plate-buckling failure (PB) is characterized by buckling between stiffeners, what transfers the load from the plates onto the stiffeners. As a result, the stiffeners may fail by flexural buckling. This failure mode may happen under in plane loading, under distributed lateral loads, or a combination of both. The resulting loss of effectiveness due to plate buckling is addressed in design phases by the so-called effective plate width theory [3].

The analysis of the ultimate strength of ship structures, taking into account all possible failure modes, is not trivial because of the interaction of various factors such as geometry/material properties, loading, boundary conditions, residual stresses and post-weld out-of-plane initial imperfections. The material, with which ship plates are commonly made, is mild or high tensile steel and they can be square or rectangular. As indicated previously, the loads might be considered either in plane loading, distributed lateral load due to water pressure or the combination of both. The boundary conditions are related to the design of the structure and depend on the position of the plate inside of the structure. The latter factor, the out-of-plane initial imperfections, is the principal factor to be evaluated in this thesis.

The initial imperfections are generated by production processes such as welding, manoeuvring, cutting and so forth and their influence is of high relevance. During the years many authors such as Carlsen [4], Guedes Soares [5], Frankland [6]andSmith [7], have been studied how the ultimate strength of a plate is affected by the presence of initial imperfections, proposing design methods and equations to predict the ultimate strength. All the authors considered that the deformations of a plate might be expressed in Fourier expansion series as follows:

$$W_{0,exp} = \sum_{i=1} W_{0,i1} sin\left(\frac{i\pi x}{a}\right) sin\left(\frac{\pi y}{b}\right) \tag{1.1}$$

where$W_{0,i1}$ is the amplitude of the initial deflection. The number of terms that best represents the initial imperfections, as well as the amplitude of each of them, has been the milestone of the investigations along the years. Initially, it has been approached the initial geometrical imperfections is affecting only to the amplitude of deformation. Later, the efforts were focused also to the shape of the deformations, and the buckling mode of the plates since it was observed that they were of high importance.

Guedes Soares and Gordo [8] outlined that the initial geometry of the plate is very influential when the plate behaves inside of the pre-buckling regime, owed to the fact that the deformations are of less magnitude. In this sense, a high reduction in plate strength was found to be from 48% to 71%. They proved how determinant the initial deformation mode and the maximum amplitude are, and show the importance of evaluating them.

1.2. AIM AND SCOPE

Up to now, the initial imperfections of plates have been represented using trigonometric functions in which both the number of terms and the amplitudes were deduced from statistical examinations of plate samples. The present thesis aims to develop a methodology that is based on photogrammetric techniques and it is able to measure the initial deformations directly from the plates. Having these measurements, it is possible to create a model of the plate and to perform a structural analysis based on Finite Element Method (FEM).

Photogrammetric measurements permit to catch the shape of plates directly, instead of performing a study relying on statistical regressions. The models generated by trigonometric functions present two implicit characteristics, the first one is that the edges of the plate will always be equal to 0, and hence, it is assumed that there are no deformations on the edges, and the second, is that in those cases when the Fourier function is used, the response model will be symmetric. These characteristics are rarely found in the real plates. Photogrammetric measurements easily overcome these difficulties, being possible to generate models of complex shapes and taking into account the out-of-plate edges.

Photogrammetry has been developed for many years now and it is currently used in an impressive range of fields such as geology, medicine, architecture and several areas of engineering. This technique has been proven to be accurate as well as versatile and the challenge is to find the way to adapt it to procedures such as strength assessment, whether to post-production stages or during the operational ones.

To demonstrate the feasibility of using Photogrammetry techniques in structural assessments, it has been carried out an analysis of a sample of 7 panels, 4 stiffened and 3 un-stiffened. To do so, a functional methodology has been designed in a way that the data involved in the procedure are fairly managed and the reliability of the results is ensured. This methodology developed in this thesis is composed of three parts: Photogrammetry, Fitting Surface and Finite Element Analysis.

1.3. ORGANIZATION OF THE THESIS

The thesis is divided into nine other chapters that are organized as follows: Chapter 2 presents a state of art of both Photogrammetry and initial imperfections of plates; Chapter 3 is addressed to briefly present the theoretical background of the strength assessment of steel plates; Chapter 4 is dedicated to treat the theoretical background of Photogrammetry; Chapter 5 is focused on surface fitting procedures; Chapter 6 is done a sensitive analysis of the photogrammetric techniques; in the Chapter 7 it is presented a study case where seven specimens are studied. A methodology integrating all the techniques that are necessary to carry out the analysis is presented, applied and the results are discussed; finally, the chapter 8 discusses the conclusions of the present work and traces the future work.

2.STATE OF ART

2.1. PHOTOGRAMMETRY

Photogrammetry techniques have been used since 1800 when the idea of representing objects from images started to be attractive. One hundred years later, this technology has been applied in several areas, being predominant geological and terrestrial representations. More recently, the development of the technology permitted its application for close-range measurements when the size of the object to be measured and the camera-to-object distance are both less than 100m. Nowadays it is being used for measurements of medical, archaeological, architectural and industrial elements, as well as accident reconstruction.

In the following it is outlined some recent works in which the close-range technology is used successfully, showing out its potential in measuring processes.Koelman [9]presented an industrial application of CAD that concerned the measurements and re-engineering of the shape of a complete ship hull and ship parts. In his study, he considered separately the 3D model measurements and the topological proprieties. Besides this, it was focused on modelling a large model scale and it was considered those cases where close-range study were needed such as ship repair phase, where measurements of flat constructions is a goal. Furthermore, in his work he presents a comparison between laser and photogrammetric techniques concluding that the latter is more appropriate for ship hull inverse engineering measurements.

Zaplatic [10]also presented a procedure of dimensional and shape control of a sub-assembled section in shipbuilding based on photogrammetry. Such procedure allowed them to carry out a survey of the fabrication quality, being able to check out the flatness and the curvatures and compare the measured values with the CAD drawings. The importance of this quality control strives in the fact that inaccurate sub-assembled blocks in shipbuilding carry to an inefficient production. Despite the accuracy of the measurement not been presented in this study, it concludes that the procedure was able to control the deviation of sub-assembled sections making an important production improvement.

Julia Armestoa, Lubowieckab [11]performed a strength assessment of the timber roof structure of an historical house using photogrammetric techniques. He not only took the measurements of the structure but also performed a FEM analysis. He proved the feasibility of representing a 3D model of a structure with most of the irregularities catch, such as out-of-plane distortions or damage to the girders' cross sections. Despite the fact he faced difficulties when modelling the target, it was demonstrated the ability of Photogrammetry for FEM analysis due to the nature of the data.

Ljubenkov[12] used photogrammetry methods as a solution for the propulsion alignment of a ship when launched. In that work, it is presented a procedure in which measurements of the structure deflection in the machinery space and displacements of the main engine are taken before and after the launching. For that experiment there were taken 600 photos to capture 202 measuring points. After the launching, they succeed obtaining structure deflections up to 3 mm at the narrowest parts of the hull with an accuracy of 0.2 mm.

Remondino and Menna [13] presented new developments in terrestrial 3D surface reconstruction and object

modelling using digital images, reporting some tests conducted using low cost digital cameras and commercial or in-house software and concluded that a successful image matcher and surface measurement approach should (1) use accurately calibrated cameras and images with strong geometric configuration, (2) use local and global image information, to extract all the possible matching candidates and get global consistency among the matching candidates, (3) use constraints to restrict the search space, (4) consider an estimated shape of the object as a priori information and (5) employ strategies to monitor the matching results.

The results of a digital photogrammetric survey, performed on the 81-foot Italian Navy motor yacht "Argo", were presented by Menna, Ackermann [14]. 540 circular coded targets were uniformly positioned on the hull surface, and approximately 75 circular code targets were positioned on both the screw propellers. A 12 Mega pixels DSLR camera was used for the image acquisition. About 400 pictures of the boat surface and 60 images per screw propeller were taken with both parallel and convergent camera axes. A photogrammetric approach for measuring weld-induced initial distortions in plated structures was presented by Chen, Garbatov [15], [16, 17]. Compared with initial imperfection classifications, a new equation to predict the initial imperfections of very-thin-walled structures has been developed.

An optical system using structured light and close-range Photogrammetry was presented by Grytten, Fagerholt [18]for taking full-field continuous measurements of out-of-plane deformation of a loaded plate. In that experiment a model was generated by taking measurements of the plate using one camera, recorded images of the pattern while it was being deformed due to a punching force applied in the centre of the plate. In addition, two cameras were used to check the results obtained. From the model generated, it was carried out a structural analysis using FEM, and the results were compared with the real plate deformations. After the tests, it was concluded that there was a great similarity between force-displacement curves, and in particular between the measured and simulated out-of-plane displacement profiles.

In the field of civil engineering, Jiang, Jáuregui [19]presented a literature review of close-range Photogrammetry applications in bridge deflection measurements. A list of experiences carried out from 1985 to 2003 was presented stating that most of them reached an order of accuracy of about 1mm. One of the experiences listed was presented by Whiteman [20]in which two video-camera system were used to measure vertical deflections in a concrete beams during destructive test. Despite of the camera resolution not being as high as a photographic CCD, a precision of 0.25mm was reached, demonstrating the feasibility of obtaining measurements even with low-resolution video camera.

Dias-da-Costa [21] presented a procedure based on Photogrammetry and image post-processing to measure surface displacements in laboratory test. The aim of that study was to overcome the drawbacks of the traditional methods of measurements. Among those drawbacks were the limitations in hardware positioning, the costs of the equipment and human resources; and time-consuming data processing, as it happens with Displacement-Transducers (LVDT). Therein, it was compared the results obtained by Photogrammetry methods with the measurements coming from LVDT elements. The results showed a high correlation between the values obtained from both systems. The coefficient of determination equals to 0.9994.Similarly, Bambach [22]used a photogrammetric procedure to accurately capture the full surface transverse buckling deformations of the flanges and webs. In his work, he investigated edge-stiffened flanges structures numerically modelled and validated against the experimental results captured by photogrammetric procedures.

Photogrammetry is also used for medical applications, for example for monitoring the so-called back desire Scoliosis. Sechidis, Tsioukas [23] used 3 video cameras connected to a computer for the automatic extraction of the 3D surface model of a human back. For this procedure least squares epipolar image matching techniques were used to find conjugate points and reconstruct the back surface. For medical purposes there is much other experience as has been shown by Petros [24].

Luhmann [25] presented a study summarizing recent developments and applications of digital Photogrammetry in industrial measurements. Therein it refers to new concepts for close-range Photogrammetry applications owing to the availability of video and digital cameras in combination with direct access to the digital image data generated. On one hand, off-line system can be regarded as fully accepted 3D measurement tools that applied in a large variety of industrial application areas, yielding a typical measurement precision on the object in a range of 1:100000 to 1:200000 that is 0.1 mm for an object of 10 mm size. On the other hand, on-line Photogrammetry systems have the capability of providing measurements in a real time, however, they are less accurate, approximately from 1:4000 to 1:10000.

To summarize, it can be concluded that after more than one hundred and fifty years of development, close-range Photogrammetry has been progressed sufficiently in terms of accuracy and practicability. Many experiences have been proven the potentialities of this technique in several fields and the current and quick progress of the cameras and computer processors, make this technology even more eligible modelling structures ensuring high accuracy results.

2.2. INITIAL IMPERFECTIONS OF PLATES

The ultimate compressive strength (UTS) of plates is very important from the design and safety point of view for marine structures. It is well known that the capacity of plates is decreased because of the fabrication procedures imperfection, so the UTS significantly depend on the initial welding distortions and residual stresses. In this sense, many equations have been proposed along the years with the intention of characterizing the initial imperfections. Karman and Sechler [26] proposed an equation relating the ultimate strength and the plate slenderness,

$$\beta = \frac{b}{t}\sqrt{\frac{\sigma_0}{E}} \tag{2.1}$$

Frankland [6], introduced quadratic terms to the former equation and Gerard modified the equation in 1957 to characterize plates with plastic behaviour. Finally, Faulkner [27], proposed a formula for simply supported plates with elasto-plastic behaviour that became one of the most widely used equations on marine structures. Faulkner also found that the presence of the residual stresses reduces the compressive strength by as much as 20% and that the relationship between the non-dimensional amplitude of the initial distortions and the slenderness ratio may be defined as,

$$\phi_u^{Fa} = \begin{cases} 1, & if\ \beta \leq 1 \\ \frac{2}{\beta} - \frac{1}{\beta^2} & if\ \beta \leq 1 \end{cases} \tag{2.2}$$

$$\left(\frac{W_{max}}{t}\right)_{Fa} = 0.10\,\beta^2 \tag{2.3}$$

Most of the research concerning the effect of welding distortions concentrates only on the maximum initial distortion amplitude, however, the evidence indicates that the welding distortion shape also significantly affects the ultimate compressive strength [28].

A new formulation was proposed in order to divide the ultimate strength in various terms in an equation that considers two reduction parameters to the maximum ultimate strength,($\phi_{u=}\phi_u R_d R_r$).The first of these parameters regards the initial deflection and the second one, with the residual stresses due to welding. Across several years, the authors proposed formulas to evaluate the values for $R_d R_r$ such as Carlsen [29], Guedes Soares [30], and Cui [31].

Among other authors, Dowling and Frieze [32] alerted the fact that the first buckling mode was not necessary the worst scenario, being necessary to focus to the problem beyond the maximum initial deflection. Antoniou [33] presented a study with 2000 measurements of plates were taken based on the principal mode of deflection. As a result, he proposed a new expression relating the initial deflections as a function of the plate slenderness,

$$\left(\frac{W_{max}}{t}\right)_{A} = 0.12\,\beta^2 \tag{2.4}$$

Carlsen [4]analysed a typical "hungry horse" shape of initial imperfections in full-scale stiffened panels. This typical shape was found to have the same load-deflection curve with an initial imperfection pattern of three half-sine waves along the length of the plate and one half-sine wave cross across the width of the panel [3].

[34] carried out an analysis of initial plate distortions of merchant ships concluding that the dominant distortion, mainly induced by the welding processes followed a sine wave forms. He proposed three levels of initial imperfections and residual stresses in average, slight and severe. These three levels correspond to the mean, 3 and 97 percentile values of maximum post-welding distortion he found from the regression analysis of their data. Smith also found the "hungry horse" to be a predominant shape in his observations.

$$\left(\frac{W_{max}}{t}\right)_{Sm} = \begin{cases} 0.025\beta^2 & Slight \\ 0.1\beta^2 & Average \\ 0.3\beta^2 & Severe \end{cases} \tag{2.5}$$

Kmiencik [35] carried out a statistical and regression analysis of a database of initial imperfections obtained from Polish shipyards. This database was composed of 1998 measurements of plates of different ships. All plate measurements were collected during the construction process by using mechanical tools. From his analysis, Kmiencik concluded that the plate's initial imperfections can be described using a Fourier series with three terms in the longitudinal direction and one term in transversal direction for plates with an aspect ratio a/b=3.

$$W_{0,exp} = \sum_{i=1}^{3} W_{0,i1}\, sin\left(\frac{i\,\pi x}{a}\right) sin\left(\frac{\pi y}{b}\right) \tag{2.6}$$

The characteristics of initial imperfections in the panels and stiffeners were discussed byYao [36], as well as bucking and ultimate strength of ship structures subjected to combined bi-axial thrust and lateral pressure. From these studies, it was observed that welding residual stresses reduce both buckling strength and ultimate strength, and the mode of initial deflection has minor effect on the ultimate strength. In this sense, [34]outlined that when the magnitude of lateral pressure actions is relatively large, the effect of the plate initial deflection shape on the plate ultimate strength is small. This is because the plate initial deflection shape becomes almost identical after the application of lateral pressure actions regardless of different magnitudes and shapes of plate initial deflections before the application of in-plane compressive actions

Some codes such as ECCS and Eurocode 3 introduces the concept of equivalent out-of-straightness to derive design equations for buckling, which is able to capture the combined effect of initial distortions and residual stresses [28]. On the other hand, Fujikubo [37]found that the classification society rules can also give somewhat unsafe results with high transverse compression and high initial deflections, what indicates that further investigation might be necessary.

The analysis of various uncertainties related to the prediction of the ultimate strength of a stiffened panel has been presented in [38]. The effect of different structural parameters on the uncertainty was evaluated based on Monte Carlo simulation and an ANOVA methodology was used to determine the most relevant parameters. The ultimate strength was predicted by the finite element method and the influence of plate thickness, Young modulus, yield and ultimate tensile strain of material, the shape of the initial geometry imperfection and slenderness ratios have been accounted for.

More studies have been concentrated in accounting for all parameters that are involved in buckling of stiffened steel plates. Sheikh, Grondin [39] presented a parametric study identifying the factors that may dominate the strength and modes of failure of stiffened steel plates. 11 parameters, grouped in four groups (geometric properties, elastic properties, loading and deformation), were investigated and evaluated and a new formulation was presented. The sixth of those parameters refer to the initial imperfections [40].

[34] carried out experimental studies to verify the existence of interaction of plate buckling and overall buckling in a stiffened steel panel under uniaxial compression. They based their work on the parameters proposed by Sheikh, Grondin [39] and concluded that the method was successful in predicting the interaction buckling failure mode.

Kamiski and Amadhl [28]affirmed that the existing simplified methods might be not sufficiently good to achieve a more advanced buckling and ultimate strength design of ship plating, meaning that more sophisticated solution methods are needed. He outlined the increasing interest in the evolution of weld induced residual stresses and distortions. The prediction of UTS in design stages allows calculating more precisely the amount of strength degradation. Having this information, it is possible to identify favourable procedures that maximize the load carrying capacity of structures. In this sense, the present thesis is aimed to develop a procedure to predict accurately the initial distortions of steel plates and thus, the maximum capacity.

3.STRENGTH ASSESSMENT OF STEEL PLATES

3.1. PLATE THEORY DEVELOPMENT

The first study about general plate behaviour was presented by Lagrange in 1813. He introduced some corrections to the formulation of the French mathematician Germain, who developed a plate differential equation, though lacking the warping effects in her formulation:

$$\nabla^4 w = \frac{\partial^4 w}{\partial x^4} + 2\frac{\partial^2 w}{\partial x^2 + \partial y^2} + \frac{\partial^4 w}{\partial y^4} \tag{3.1}$$

[34] and Poisson [41]were the first to formulate the problem of plate on the basis of general equations of the theory of elasticity through expanding the characteristic quantities into series in power of distance from a middle surface. In 1829, Poisson expanded the Garmin-Lagrange plate equation to the solution of a plate under static loading. Nevertheless, he assumed that the rigidity is constant.

It is considered that the first satisfactory theory of bending of plates was introduced by Navier [42], who related the plate thickness with the rigidity. He proposed a faithful method to transform the differential equation into algebraic expressions by the use of the Fourier trigonometric series. He also was the first to derive the governing equation for thin rectangular plates subjected to direct compressive forces. In 1850, Kirchoff [43]presented an important study in which some hypothesis were introduced that are widely known as Kirchoff hypothesis and became fundamental for an analytical analysis of plates based on linear, elastic and small deflection theory:

- The material of the plate is elastic, homogeneous, and isotropic.
- The plate is initially flat.
- The deflection, h (the normal component of the displacement vector) of the mid-plane is small compared with the thickness, w of the plate (w>0.3h). The slope of the deflected surface is therefore very small and the square of the slope is a negligible quantity in comparison with unity.
- The straight lines, initially normal to the middle plane before bending, remain straight and normal to the middle surface during the deformation, and the length of such elements is not altered.
- The stress normal to the middle of the plane is small compared with the other stress components and may be neglected in the stress–strain relations.
- Since the displacements of a plate are small, it is assumed that the middle surface remains unstrained after bending.

At the end of the 19th century, shipbuilders changed the materials of ship construction, from wood to structural steel. This change was very fruitful in the development of various plate theories. Timoshenko, Woinowsky-Krieger [44]studied the buckling behaviour of rectangular plates subjected to non-uniform direct compressive load and also developed solutions for circular plates considering large deflections and the formulation of elastic stability problems. Among other authors, Timoshenko also presented a comprehensive

analysis of linear and nonlinear buckling problems for thin plates of various shapes. In his studies, he derived the differential equation that governs the plate's deflection taking into account the membrane stresses:

$$\nabla^4 w = \left(\frac{12(1-\nu^2)}{Et^3}\right)\left(p(x,y) + N_x\frac{\partial^2 w}{\partial x^2} + 2N_{xy}\frac{\partial^2 w}{\partial x \partial y} + N_y\frac{\partial^2 w}{\partial y^2}\right) \quad (3.2)$$

where $p(x,y)$ is the load to plate's plane and $N_x N_y N_z$ are the external membrane forces per unit length acting on the plate. For ship structures,this equation might be reduced accounting only the longitudinal loads as can be seen in Figure 3.1.

$$\nabla^4 w = \left(\frac{12(1-\nu^2)}{Et^3}\right)\left(-N_y\frac{\partial^2 w}{\partial y^2}\right) \quad (3.3)$$

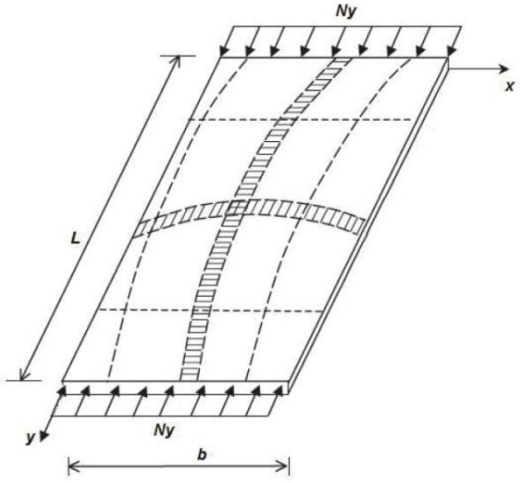

Figure 3.1 Plate under uniaxial in-plate forces

Bryan [45]was the first to use the energy method to solve the buckling problem for a simply supported plate subjected to direct, constant compressive forces acting in one and two directions and Cox [46] presented a study where solutions of various buckling problems for thin rectangular plates in compression was presented.

However, these formulations, as well as Kirchhoff hypothesis, fail in design of ship plating because there are initial imperfections to the welding processes and residual stresses and due to the lateral pressure acting over the hull plates to be accounted. Because of that, analytical solutions for real problems in the field of ship platting have limited applications and numerical procedures are needed.

3.2. BUCKLING AND POST-BUCKLING OF THE PLATES

Thinner plates are present in naval structures and they are often subjected to compressive and shearing loads acting in the middle plane of the plate, what is called in-plane loads. Under certain conditions, plate

buckling may occur. Buckling, or elastic instability of plates is very important for their failure may be attributed to such instability instead of a lack of their strength.

The stability analysis of thin plates starts considering an ideal thin, elastic plate, which is assumed initially to be perfectly flat and subjected to external in-plane loads. In this hypothetical situation, there would be no any deflections and thus, no bending and twisting neither moments nor transverse shear forces either. Such plane stress condition is known as flat configuration of equilibrium.

The initial configuration of plate equilibrium under applied in-plane loads may be stable or unstable. It is considered the initial configuration to be stable if the plate tends to come back to initial equilibrium state after a 'perpendicular' infinitesimal disturbance is applied and later removed. Contrarily, the initial configuration of equilibrium is said to be instable if the plate finds an equilibrium state other than the initial one. Summarizing, the transition of the plate from stable state of equilibrium to unstable is referred to as buckling or structural instability, being the smallest load producing such known as buckling load. The importance of buckling is on the appearance of deflection patterns, which may conduce rapidly to very large lateral deflection and thus, large bending stresses and eventually to complete failure of the plate [47].

Linear buckling analysis of plates makes possible to determine accurately the critical buckling loads, which are of practical importance in the stability analysis of thin plates. To do so it is necessary to consider four important assumptions: a) the plate is initially perfectly flat; b) any changes in the plate dimensions are neglected prior buckling; c) all the applied loads do not change neither in magnitude nor in direction and finally d) the plate bending is described by Kirchhoff's plate bending theory.

On the other side, it is possible to formulate the problem taking into account small initial imperfections, the sum of the initial curvature plus the deflection due to loads applied: $w = w_0 + w_1$, where w_1 is the solution of Equation (3.1), corresponding to a flat plate subjected to in-plane load, and $w_0$is the curvature due to lateral force or due to production processes such as welding. This is valid only if w_0 is small compared with the plate thickness and it cannot be applied for large-deflections. The resultant w is introduced to Eqn (3.2)and following form:

$$\nabla^4 w = \left(\frac{12(1-\nu^2)}{Et^3}\right)\left(p + N_x \frac{\partial^2(w_0 + w_1)}{\partial x^2} + 2N_{xy} \frac{\partial^2(w_0 + w_1)}{\partial x \partial y} + N_y \frac{\partial^2(w_0 + w_1)}{\partial y^2}\right) \tag{3.4}$$

In practical case, the initial deflection can be expressed into the following Fourier series,

$$W_0 = \sum_{m=1,3\ldots}^{\infty} \sum_{n=1,3\ldots}^{\infty} \alpha_{m,n} \sin\left(\frac{m\,\pi\,x}{a}\right) \sin\left(\frac{n\,\pi\,x}{b}\right) \tag{3.5}$$

and,

$$W_1 = \sum_{m=1,3\ldots}^{\infty} \sum_{n=1,3\ldots}^{\infty} b_{m,n} \sin\left(\frac{m\,\pi\,x}{a}\right) \sin\left(\frac{n\,\pi\,x}{b}\right) \tag{3.6}$$

where a and b are the longitudinal and transversal sides of the plate, respectively, m and n indicates the number of half sine waves on the buckled mode. $\alpha_{m,n}$is the initial amplitude of the m and n half sine wave and $b_{m,n}$ is the amplitude of the half sine waves due to both initial deformation and in-plane loads,

$$b_{m,n} = \frac{\alpha_{m,n}\, N}{\frac{\pi^2 D}{a^2}\, m + \left(\frac{n^2 a^2}{m^2 b^2}\right)^2 - N} \tag{3.7}$$

where N is the applied in-plane uniaxial load.

According to the equilibrium method, it is possible to find the critical buckling load for a simply supported plate subjected to a uniformly distributed compressive edge load acting on a plate as shown in Figure 3.1 by seeking the solution that satisfies the following equation,

$$\sum_{m=1}^{\infty}\sum_{n=1}^{\infty}\left[\pi^2 D\left(\frac{m^2}{a^2}+\frac{n^2}{b^2}\right)^2 - \left(N_y\right)_\sigma \pi^2 \frac{m^2}{a^2}\right] w_{m,n} sin\left(\frac{m\pi x}{a}\right) sin\left(\frac{n\pi x}{b}\right) = 0 \tag{3.8}$$

One of the solutions is to assume$w_{m,n} = 0$, nevertheless, it corresponds to equilibrium in the unbuckled, flat state of the plate. Another solution is obtained by setting to zero a part of the equation,

$$\pi^2 D\left(\frac{m^2}{a^2}+\frac{n^2}{b^2}\right)^2 - \left(N_y\right)\pi^2 \frac{m^2}{a^2} = 0 \tag{3.9}$$

from which

$$\left(N_y\right) = \frac{\pi^2}{b} D\left(m\frac{b}{a}+\frac{n^2}{m}\frac{a}{b}\right)^2 \tag{3.10}$$

This expression returns various values for N_y depending on the number of half sine waves considered$m$=1,2,3,... and n = 1,2,3, ... The lowest value attained among the several values obtained is the critical one $\left(\mathrm{N_y}\right)_\sigma$ and the corresponding m and n values that conduce to it is the mode of deformation. Evidently, the smallest value for $\left(N_y\right)$ is obtained for $(n = 1)$,

$$\left(N_y\right)_\sigma = \left(\frac{mb}{a}+\frac{a}{mb}\right)\frac{\pi^2 D}{b^2} = K\frac{\pi^2 D}{b^2} \tag{3.11}$$

where$K$is the so-called buckling load parameter, is a non-dimensional quantity coefficient and depends on plate dimensions and boundary conditions. For a given value of$m$, the variation of buckling load parameter depends only on the aspect ratio of plate (a/b), so the critical buckling load is obtained by selecting the value for m that makes Eqn (3.11) minimum. By solving the equation that satisfies $(dK/dm) = 0$ it is found that the minimum values of the critical load are given for buckling load parameters $K = 4$, that is, when the width of the plate dimensions, b fits in its length, a, by whole numbers. In this case, a bent plate is subdivided into square cells of side dimensions$b$.

The variation of the buckling load parameter K as a function of aspect ratio a/b for m=1,2,3,4 is shown in Figure 3.2. This figure permits to find the mode of deformation a plate will buckle for a given aspect ratio.

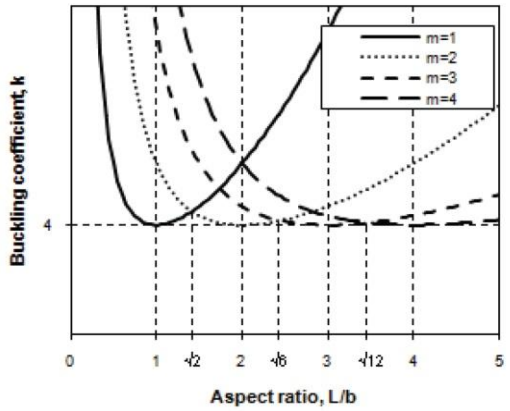

Figure 3.2 Buckling load parameter load variation

However, the linear buckling analysis presents two drawbacks. Firstly, the assumptions to be initially considered reducing the analysis to a limited range of cases, which despite being of relevant importance, do not allow to be applicable to real plate problems. The critical values of applied in-plane forces are found from the solution of the governing differential Eqn (3.2),which is impossible to find its analytical solution in the general case, and only exact solutions may be found in a some cases, yet important in terms of theoretical demonstration. The other important drawback is that this analysis is not able to describe the plate behaviour after buckling that, differently to the beam cases, it is of high importance in plate capacity assessment. While a small increase in the critical load for beams produce a complete collapse, the load-carrying capacity of plate is not exhausted and can carry stresses higher than the critical one, being possible the bring the load-carrying capacity up to twice the critical load. The reason of such behaviour might be explained by the effect of large deflections that consists in the presence of stretching in the middle of the plate and by the fact, the edges of the plate are usually constrained to remain straight. This constraint is usually achieved by the use of stringers that usually supports the edges of the plates.

The post-buckling state may increase the strength of structures so its consideration is of great importance in the design of ship structures among others. By considering that it is possible to achieve a considerable weight saving, the analysis of post-buckling behaviour of plates is governed by the nonlinear, large-deflection of thin plates bending theory[26]:

$$\nabla^4 w = \frac{\partial^4 w}{\partial x^4} + 2\frac{\partial^2 w}{\partial x^2 + \partial y^2} + \frac{\partial^4 w}{\partial y^4} = \frac{1}{D}\left(p + \frac{\partial^2 \phi}{\partial y^2}\frac{\partial^2 w}{\partial x^2} + \frac{\partial^2 \phi}{\partial x^2}\frac{\partial^2 w}{\partial y^2} - 2\frac{\partial^2 \phi}{\partial y \partial y}\frac{\partial^2 w}{\partial y \partial y}\right) \quad (3.12)$$

Because of the nonlinearity of the governing differential equations of this analysis, the mathematical difficulties to solve it are considerable and exact solutions are seldom to be obtained. So that, the most generally used techniques for the treatment of post-bucking of plates are based on numerical methods [47] and some analyses for plates subjected to transverse and to biaxial loading have been presented in [8, 48].

3.3. CORROSION

The environment in which marine structures operates is complex and strongly affects their capacity. Different types of corrosion may be seen wasting the material such as general corrosion, pitting corrosion, stress corrosion cracking, corrosion fatigue, fretting corrosion, weld corrosion and bacterial corrosion among others. General corrosion is the most common form found in marine structures and is spread over the surface and it is reflected in a generalized decrease of the plate thickness.

Another important corrosion type is pitting corrosion, which results in pits in the material surface. Pitting may behave in a different ways penetrating down to a certain depth, or even pitting corrosion might penetrate horizontally. Whatever form it has, it is considered to be dangerous because it may cause structural strength decrease or leakage and eventually pollution incidents [49].

The corrosion deterioration may be modelled based on three fundamental approaches. The first one considers the deterioration to be linear what induces an overestimation, because the corrosion reduces the plate capacity not only because of the thickness reduction but also because of its random behaviour[50, 51]. The second approach takes into account the nonlinear corrosion degradation[52, 53]. The difficulty of this method is to determine its descriptors that will be used to generate the degradation in accordance to the real one..A corrosion wastage based on a non-linear time-dependent corrosion model accounting for various immersion environmental factors, including the effects of salinity, temperature, dissolved oxygen, pH and flow velocity including the effect of ship's service life in different routes has been developed in [54-56].

This thesis will take into account corrosion with the model developed in [57, 58]. The model is based on the second approach [53]considering the statistical characteristics of marine immersed corrosion. On the other hand, this thesis is developing a new corrosion model based on photogrammetric measurements.

4. PHOTOGRAMMETRY

Photogrammetry is an approach that can determine the size and the shape of objects through analysing images previously recorded by a photographic or video camera. The Photogrammetry approach must be used with a precaution since good results can only be produced from suitable images, so that, some skills are necessary to be taken[59]. Thompson [60] stated that "photogrammetric methods of measurement are useful in the following conditions: first, when the object to be measured is inaccessible or difficult to access; second, when the object is not rigid and its instantaneous dimensions are required; third, when it is not certain that the measures will be required at all; fourth, when it is not certain, at the time of measurement, what measures are required; fifth, when contours of the surface of the object is required and sixth, when the object is very small".

Photogrammetry is divided in two differentiate techniques, analytical and digital. While the principal objective of the present work is to develop a model for the initial imperfection of plates, which is based on analytical Photogrammetry, there is some interesting advantages when using digital Photogrammetry, for example, in corrosion assessment. Because of that, the analytical part of Photogrammetry is studied in more detailed than the digital one.

4.1. INTRODUCTION

The developments in photogrammetry, from around 1850, have followed four development cycles as: Plane table photogrammetry (1850 to 1900), Analog photogrammetry (1900-1960), Analytical Photogrammetry (1960-recent), Digital photogrammetry, which started few years ago being present in the photogrammetric industry more and more, as it can be seen, each cycle corresponds to a single technique. In 1849, Aimé Laussedat, a French military office engaged in mapping, was the first of using terrestrial photographs for topographic map compilation and he is referred to as the "Father of Photogrammetry", despite he called his works as "Iconometry". Albreacht Meydenbauer in Germany was occupied with the survey of architectural monuments, when he suggested the use of cameras for photographic reconstruction of architectural plans, what he called in 1865, "Photogrammetry" [61].

Plane table Photogrammetry, which marked the first cycle, is an extension of the conventional plane table surveying. Each exposure station was determined by resection and plotted on the plane table. The exposed photos were oriented on the plane table and the directions of the different objects were transferred onto the map sheets. With the advent of photography and the ability to make exposures from the air, it was soon found that there were military applications to this technology. As to the mathematics, Sebaastian Finsterwalderwasthe first to make measurements from photographs, when measuring the rapidly advancing and retreating of a Glacier in the Alps in 1889. He described the principles of modern double-image Photogrammetry and the methodology of relative and absolute orientation. In addition, he introduced the necessity of redundant rays to recreate the proper geometry and used least squares theory to describe the relationship of the vectors between corresponding rays [62].

The second cycle corresponds to the analog Photogrammetry incorporates two important developments. The first one is the stereoscopy, which became widely used, and the second one is the development of the airplanes by the Wright brothers in the early 1900. At that time, US Geological Survey began to use Photogrammetry for topographic mapping. Carl Pulfrich developed by Carl Zeiss in Jena the first stereo-comparator, even though Henry Fourcade is also known as the inventor of a stereoscopic method of surveying. Eduard von Orel developed the Zeiss Orel stereoutograph, which permitted drawing of contours from terrestrial photographic stereo images. Many authors, such as Heinrich Wild, Santoni, Poivilliers and Brock developed new techniques for aerial Photogrammetry that makes evolve the new technology. Also new cameras were invented in this period, making them most suitable for aerial images.

The invention of the computer in 1941 and 1943 made significant advances to photogrammetric developments after 1950. This event influenced the third cycle proposed by Konecny. In 1953HellmutSchmid developed the principles of modern multi-station analytical Photogrammetry using matrix notation. This approach included a "rigorously correct least squares solution, the simultaneous solution of any number of photographs and a complete study of error propagation" [62]. Duane Brown included self-calibration, which improved the accuracy and reliability of the photogrammetric adjustment, as well as he developed a number of high-accuracy, large format and close-range photogrammetric cameras. His work also included adjusting for decentring distortion and principal point calibration. Finally, he was the first to use retro-reflecting targets, which offered significant improvements. Because of all his developments, Duane Brown was the first to achieve accuracy better than 1:1,000,000 on a project.

The last cycle is influenced by the introduction of the Digital Photogrammetry. One of the pioneers was Gilbert Luis Hobrough. His contributions involved the development of an electronic dodging printer and after some other contributions, he developed the Gestalt Photo Mapper, an automated ortho-photographic system utilizing correlation of stereo imaging.

4.2. ANALYTICAL PHOTOGRAMMETRY

In those projects where the object size and the camera-to-object distance are both less than 100 m, the terrestrial Photogrammetry is defined as close-range Photogrammetry[19]. Contrary to the terrestrial Photogrammetry, where all the aerial photos are taken perpendicular to the land, in close range images are obtained from camera positions all around the object. Camera axes are only parallel in special cases, usually they are converging, pointing towards the middle of the object [63].

4.2.1. Coordinate Transformations

The position of an object in space can be defined by a three-dimensional Cartesian co-ordinate system: the origin, the scale and the orientation of which can be arbitrarily defined. When having more than one photo, it is necessary to convert between coordinates in systems, what it is known as co-ordinate transformation. It can be divided into three parts: scale change, translation and rotation. The scale change along the three axis depends on the factor λ and may be represented by the vector equation $x = \lambda X$, where $X = [X\ Y\ Z]^t$ is the position vector of a point in the primary coordinate system and $x = [x\ y\ z]^t$ is the position vector of the point in the scaled coordinate system. As for the translation of axes, they may be represented by the following vector equation: $x = X - X_0$, where X is the position vector of a point, in the primary coordinate

system, $X_0 = [X_0 Y_0 Z_0]^t$ is the position vector of the origin of the secondary coordinate system, relative to the primary coordinate system and$x = [x\ y\ z]^t$ is the position vector of the point in the secondary coordinate system.

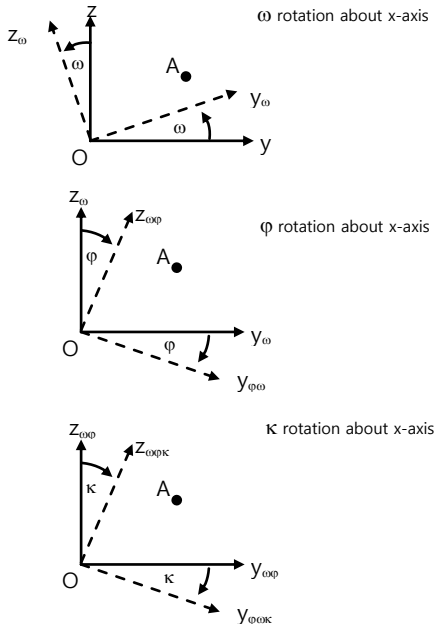

Figure 4.1Sequential rotation of axis

The rotational process is not as trivial as the other transformations. It may be expressed as a result of the three independent sequential transformations, correspondent to each axis. For a given point, called A, in a coordinate system (x, y, z), if a rotation ω is made clockwise about the x-axis, the position vector of A in the rotated system $(x_w y_w z_w)$ is given by the vector equation $[x_w y_w z_w]^t = R_w\ [x\ y\ z]^t$, where

$$R_w = \begin{bmatrix} 1 & 0 & 0 \\ 0 & cos\, w & sin\, w \\ 0 & -sin\, w & cos\, w \end{bmatrix} \tag{4.1}$$

The same process is followed by the axis y_w for a given rotation φ. This rotation is added to the given before and the coordinates of A in the $(x_{w\varphi}\, y_{w\varphi}\, z_{w\varphi})$ will be $[x_{w\varphi}\, y_{w\varphi}\, z_{w\varphi}]^t = R_w R_\varphi\ [x\ y\ z]^t$, where

$$R_\varphi = \begin{bmatrix} cos\, \varphi & 0 & -sin\, \varphi \\ 0 & 1 & 0 \\ sin\, \varphi & 0 & cos\, \varphi \end{bmatrix} \tag{4.2}$$

Finally, when a rotation $k$is clockwise about the $z_{w\varphi}$ axis, the coordinates of A in the $(x_{w\varphi k}\, y_{w\varphi k}\, z_{w\varphi k})$ system will be $[x_{w\varphi k}\, y_{w\varphi k}\, z_{w\varphi k}]^t = R_w R_\varphi R_k\ [xyz]^t$, where

$$R_k = \begin{bmatrix} \cos k & \sin k & 0 \\ -\sin k & \cos k & 0 \\ 0 & 0 & 1 \end{bmatrix} \tag{4.3}$$

At this point, it can be done the matrix product $R_w R_\varphi R_k$ denoted as $R_{w\varphi k}$

$$R_{w\varphi k} = R_w R_\varphi R_k = \tag{4.4}$$

$$= \begin{bmatrix} \cos\varphi \cos k & \sin w \sin\varphi \cos k + \cos w \sin k & -\cos w \sin\varphi \cos k + \sin w \sin k \\ -\cos\varphi \sin k & -\sin w \sin\varphi \sin k + \cos w \cos k & \cos w \sin\varphi \sin k + \sin w \cos k \\ \sin\varphi & -\sin w \cos\varphi & \cos w \cos\varphi \end{bmatrix}$$

or

$$R = \begin{bmatrix} \gamma_{11} & \gamma_{12} & \gamma_{13} \\ \gamma_{21} & \gamma_{22} & \gamma_{23} \\ \gamma_{31} & \gamma_{32} & \gamma_{33} \end{bmatrix} \tag{4.5}$$

It is possible to express the relationship between two coordinate systems, if the second one is translated by $(X_0 Y_0 Z_0)$, and the scale along each axis is multiplied by λ and the axis rotates by $w, \varphi \; and \; k$.

$$X = X_0 + \lambda^{-1} R^t x \tag{4.6}$$

or

$$\begin{bmatrix} X \\ Y \\ Z \end{bmatrix} = \begin{bmatrix} X_0 \\ Y_0 \\ Z_0 \end{bmatrix} + \lambda^{-1} \begin{bmatrix} \gamma_{11} & \gamma_{12} & \gamma_{13} \\ \gamma_{21} & \gamma_{22} & \gamma_{23} \\ \gamma_{31} & \gamma_{32} & \gamma_{33} \end{bmatrix} \begin{bmatrix} x \\ y \\ z \end{bmatrix} \tag{4.7}$$

The transformation is then defined by seven parameters, $X_0, Y_0, Z_0, w, \varphi, k$ and λ. This transformation is described as conformal one because the shape of the object defined by coordinates in one system is unchanged by the transformation [63].

4.2.2. Single Camera geometry

The basic concept for building a functional model in a close range Photogrammetry is the central perspective projection. Being a point called a, three-dimensional positioned point in the space, and its projection onto the *projection plane*, it is defined as a straight line passing through AO, where O is the perspective centre. At the same time, it defines the straight line POP as an orthogonal one to the projection plane and the distance OP as the *principal distance* denoted as C.

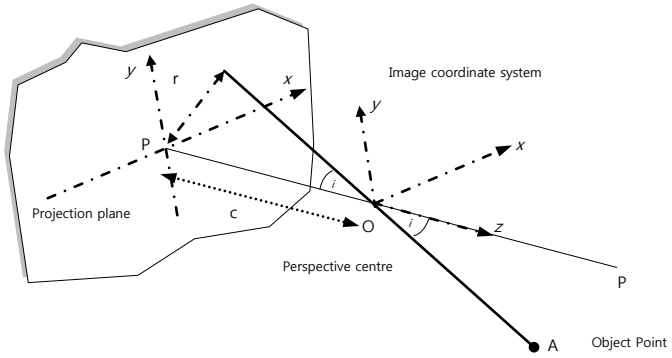

Figure 4.2Central Perspective Projection

In order to derive the functional relationships between the position of the object A and its projection on the *projection plane*, two co-ordinate systems may be introduced. The primary system ($X\,Y\,Z$) is arbitrarily located in the object space. In this system, the coordinates of the perspective centre of the secondary system are ($X_0Y_0Z_0$), and the coordinates of the point A are ($X_AY_AZ_A$). The secondary system ($x\,y\,z$) has its origin in O, where the perspective centre is. The z-axis coincides to the orthogonal lines POP, and the x-axis and y-axis are parallel to the ones from the *projection plane.* Once both coordinates system are defined, it is possible to write the vectors relative to the primary coordinate system: $X_A = X_0 + S$ where S is the position vector of A relative to O. It is collinear with x_a but in opposite sign:

$$X_A = X_0 - \mu R^t x_a \tag{4.8}$$

in matrix notation:

$$\begin{bmatrix} X_A \\ Y_A \\ Z_A \end{bmatrix} = \begin{bmatrix} X_0 \\ Y_0 \\ Z_0 \end{bmatrix} - \mu \begin{bmatrix} \gamma_{11} & \gamma_{12} & \gamma_{13} \\ \gamma_{21} & \gamma_{22} & \gamma_{23} \\ \gamma_{31} & \gamma_{32} & \gamma_{33} \end{bmatrix} \begin{bmatrix} x_a \\ y_a \\ -c \end{bmatrix} \tag{4.9}$$

where μ is a scalar quantity, greater that zero and γ_{ij} are elements of the rotation matrix R.

If now it is considered the same relationship, but this time expressing the primary coordinate system to the secondary one, it is obtained the reverse transformation:

$$x_a = \mu^{-1} R(X_0 - X_A) \tag{4.10}$$

in matrix notation

$$\begin{bmatrix} x_a \\ y_a \\ -c \end{bmatrix} = \mu^{-1} \begin{bmatrix} \gamma_{11} & \gamma_{12} & \gamma_{13} \\ \gamma_{21} & \gamma_{22} & \gamma_{23} \\ \gamma_{31} & \gamma_{32} & \gamma_{33} \end{bmatrix} \begin{bmatrix} X_0 - X_A \\ Y_0 - Y_A \\ Z_0 - Z_A \end{bmatrix} \tag{4.11}$$

where the third equation can be explicitly written byμ^{-1} resulting in the following equations:

$$x_a = \frac{-c\,[\gamma_{11}(X_0 - X_A) + \gamma_{12}(Y_0 - Y_A) + \gamma_{13}(Z_0 - Z_A)]}{[\gamma_{31}(X_0 - X_A) + \gamma_{32}(Y_0 - Y_A) + \gamma_{33}(Z_0 - Z_A)]} \tag{4.12}$$

$$y_a = \frac{-c\,[\gamma_{21}(X_0 - X_A) + \gamma_{22}(Y_0 - Y_A) + \gamma_{23}(Z_0 - Z_A)]}{[\gamma_{31}(X_0 - X_A) + \gamma_{32}(Y_0 - Y_A) + \gamma_{33}(Z_0 - Z_A)]} \tag{4.13}$$

These equations are referred to the photogrammestrists as *collinearity equations.*

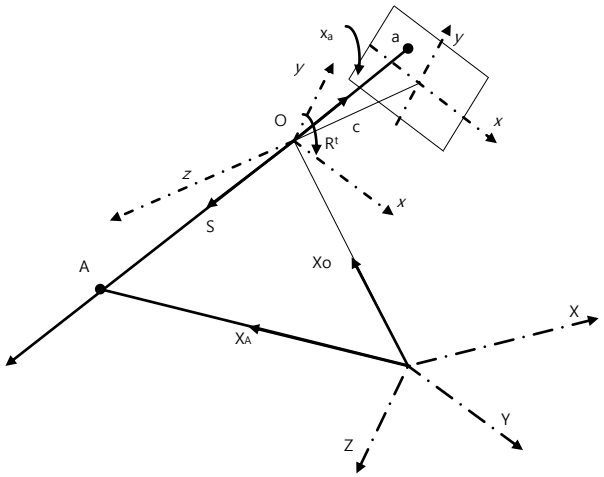

Figure 4.3 Collinear condition

4.2.3. Calibration

The objective of the calibration is to identify how much the geometry of image information in a real camera differs from the geometry of a central perspective projection. The lenses are typically identified as the main element distorting the images and the variation in angular magnification with angle of incidence are usually interpreted as a radial lens distortion. To calculate the distortion, it is necessary to define two concepts: the *fiducial*, as a physical point in the image and the *principal point*, which is defined by a line through the lens nodal points and perpendicular to the image plane intersecting the image plane. The distortion might be expressed as a polynomial function of the radial distance from the fiducial to the principal point:

$$\delta r = K_1 r^3 + K_2 r^5 + K_3 r^7 \tag{4.14}$$

where δr is the radial displacement of an image point, $r^2 = (x - x_0)^2 + (y - y_0)^2$, (x, y) are the fiducial co-ordinates if the image point,defined by the coordinates (x_0, y_0) are the fiducial co-ordinates of the point of the principal point, and K_1, K_2 and K_3 are the coefficients, which depend upon the camera focal setting. The

distortion is usually resolved into two components:

$$\delta r_x = \delta r(x - x_0)/r \tag{4.15}$$

$$\delta r_y = \delta r(y - y_0)/r \tag{4.16}$$

Typical radial lens distortion curves for some commercial CCD camera lenses are illustrated in Figure 4.4.

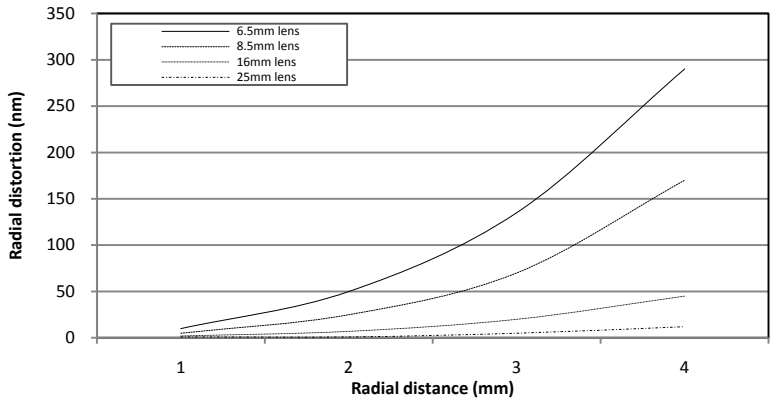

Figure 4.4Lens distortion curves for 25, 16, 8.5 and 6.5 mm

On the other hand, there is another element, introducing deviations in the representation of the central perspective projection that is called *tangential lens distortion* and is caused by misalignment of the components of the lenses. This displacement might be represented by two polynomials, one for the displacement in the direction of the x-fiducial axis and another for the displacement in the y-fiducials:

$$\delta x = P_1[r^2 + 2(x - x_0)^2] + 2P_2(x - x_0)(y - y_0) \tag{4.17}$$

$$\delta y = P_2[r^2 + 2(y - y_0)^2] + 2P_1(x - x_0)(y - y_0) \tag{4.18}$$

where P_1 and P_2 are coefficients that depend on the camera focal setting.

Measurements of the photo coordinatesx_a and y_a of the image of the target *A* give rise to two collinearity equations 4.13) and (4.14)-.If the three elements of interior orientations,x_a, y_a and $c$are known from camera calibration and the space coordinates (X_A, Y_A, Z_A)in the object space coordinate system are also known, the two collinear equations will have six unknowns $(X_0, Y_0, Z_0, w, \varphi, k)$, these unknowns correspond to the *exterior orientation* and their evaluation is called *resection.*

4.2.4. Geometry using two cameras

Considering Figure 4.5, if the elements if the exterior orientation of the two cameras with perspective centres at O_1 and O_2 are known, the object space coordinates (X_A, Y_A, Z_A) of the target A can be evaluated from the

measurements of the photo-coordinates (x_1, y_1) and (x_2, y_2) of their homologues a_1 and a_2. Collinearity equations are the basis of the present method. Since there are three unknowns X_A, Y_A and Z_A and four equations, a least squares estimation is necessary. This process is known as *intersection.*

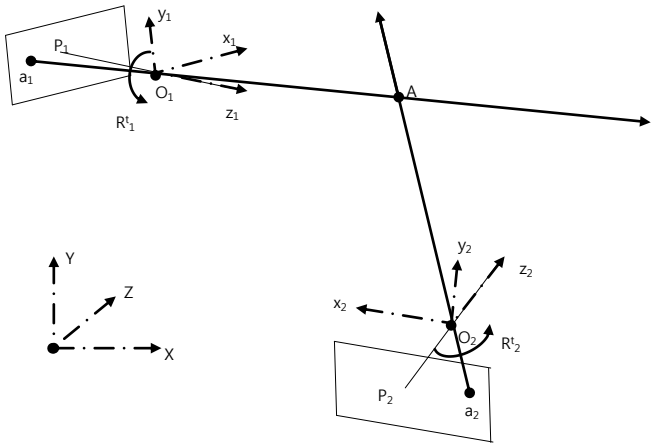

Figure 4.5 Intersection

A linear least squares estimation of the coordinates of the target A can be derived by regarding all terms in the collinear equations. Independent resections of the cameras followed by the intersections of the object space targets using pairs of cameras and homologous points are common procedures in a close range Photogrammetry[63]. Nevertheless, these procedures do not take profit in terms of precision and reliability as it can be possible. A multi-station convergent bundle adjustment can raise the accuracy of the results, however being necessarily higher computational requirements.

4.2.5. Multi-station convergent geometry

In the previous section, it has been treated the relationships between the coordinates of a certain point in the space and their coordinates in the projection plane. In this section, it is studied the relationships between one point and its projections in more than one projection plane, in other words, cameras.

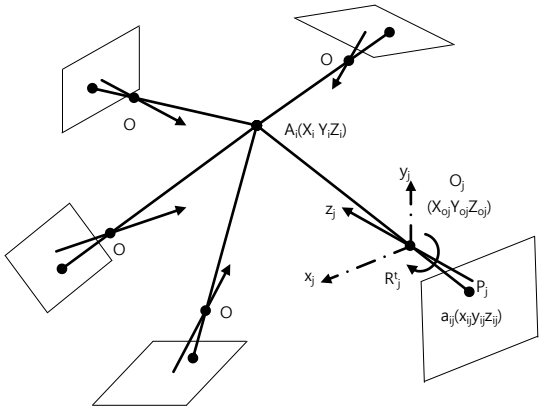

Figure 4.6 Multi-station convergent configuration

In Figure 4.6, five cameras are shown, disposed around a point, which gives rise to an image point a_{ij} in the camera j. The collinearity equations are:

$$x_{ij} = \frac{-c\,[\gamma_{j,11}(X_0 - X_A) + \gamma_{j,12}(Y_0 - Y_A) + \gamma_{j,13}(Z_0 - Z_A)]}{[\gamma_{j,31}(X_0 - X_A) + \gamma_{j,32}(Y_0 - Y_A) + \gamma_{j,33}(Z_0 - Z_A)]} \tag{4.19}$$

$$y_{ij} = \frac{-c\,[\gamma_{j,21}(X_0 - X_A) + \gamma_{j,22}(Y_0 - Y_A) + \gamma_{j,23}(Z_0 - Z_A)]}{[\gamma_{j,31}(X_0 - X_A) + \gamma_{j,32}(Y_0 - Y_A) + \gamma_{j,33}(Z_0 - Z_A)]} \tag{4.20}$$

If the previous calibration of the camera has been processed, the distortion parameter. (coefficientsK_1, K_2 and K_3 representing geometrical radial lens distortion and coefficients $P_1 P_2$, representing the geometrical effects of lens decentring) should be included in the equations. Then, the left-hand of the collinearity equations are defined as follows,

$$\begin{aligned} x_{ij} - x_{oj} + (x_{ij} - x_{ij}) r_{ij}^{-1}\left(K_{1j} r_{ij}^3 + K_{2j} r_{ij}^5 + K_{3j} r_{ij}^7\right) + P_{1j}\left[r_{ij}^2 + 2\left(x_{ij} - x_{oj}\right)^2\right] \\ + 2P_{2j}\left(x_{ij} - x_{oj}\right)\left(y_{ij} - y_{oj}\right) \end{aligned} \tag{4.21}$$

$$\begin{aligned} y_{ij} - y_{oj} + (y_{ij} - y_{ij}) r_{ij}^{-1}\left(K_{1j} r_{ij}^3 + K_{2j} r_{ij}^5 + K_{3j} r_{ij}^7\right) + P_{1j}\left[r_{ij}^2 + 2\left(y_{ij} - y_{oj}\right)^2\right] \\ + 2P_{2j}\left(x_{ij} - x_{oj}\right)\left(y_{ij} - y_{oj}\right) \end{aligned} \tag{4.22}$$

To facilitate the calculations, these equations can be written in vector form,$F(x, b, a) = 0$,where "x" is a vector representing the *u* elements whose values are required; "b" is a vector representing the *m* measured elements, including all the photo coordinates x_{ij} and y_{oj} ; and "a" is a vector representing the known constants. This formula is known as a *functional model* of the Photogrammetry based on collinearity equations and it is used to evaluate "x" for a given values of "b" and "a". Generally, no unique solution for "x" exists, but the least squares estimation provides a means for obtaining one.

4.2.6. Application of Analytical Photogrammetry

Analytical Photogrammetry is capable to measure deformed plates. To do so it is necessary to define certain points to be measured as regard of the multi-station condition. If many of the points belonging to the surface of a plate are measured, it is possible to generate a point of clouds representing the deformation trend of the surface. The way to proceed with these techniques are explained in more detailed in Section 0.

4.3. DIGITAL PHOTOGRAMMETRY

The photogrammetric technique studied in known as analytical Photogrammetry. There is another technique that is based on digital procedures and with which refine surface meshes are generated. Digital Photogrammetry (DP) is intended to generate a dense pattern of points from photographs, named the Dense Surface Model (DSM). Such dense pattern of points is in accordance to the surfaces' objects and surface models might be taken.

This technique is extendedly used in many fields, being the most relevant architecture and preservation of buildings, archaeological digs, for museum and curatorial activities, geotechnical projects, medicine and of course, civil and mechanical engineering.

In digital Photogrammetry the photos have to be taken in a paired stereo configuration and the object's surfaces appearing in them should be of certain characteristics, being the most important its texture and reflective surfaces induce inexact results. Due to its aim, DP can be thought of as camera-based 3D 'Laser-Scanner'. In fact, both systems generate DSM and each one shows some lights and drawbacks depending on the projects to be studied. A deeper comparisons of both systems may be found in [10, 64].

Dense Surface Modelling is based on an algorithm that searches for image patches that 'look' alike from an existing oriented project composed of stereographic photographs. When a good match is found between two photographs, the orientation and camera data allows the program to compute the correct 3D location of the surface point corresponding to the image patch [65].

Owing to the distortions produced by the lens, the object in the photo appears to be of different size and shape compared to the real dimensions and since the digital Photogrammetry is based on the whole image, it is necessary to deform it to undo the deformations and this procedure is known as Idealization.

The way of taking the photographs for a Dense Surface Modelling project is completely different from the one of the analytical case. While in the analytical Photogrammetry, the photos should be taken in 'multi-station' form, in digital case they have to be stereographic. Photographs in pairs with an overlap on the surface of interest, where the camera is to be kept in a similar orientation for both images with a shift sideways is shown in Figure 4.7.

From the whole procedure, a surface model is obtained, where the shapes of the objects are represented and from which a cloud of points may be generated. Such cloud of points can be of whatever density, which is decided as a function of the necessities of the project. Mote dense points on the surface permits a more detailed analysis to be performed.

Digital Photogrammetry is used in two ways. The first one is to take measurements of the deformed surfaces in order to generate models of them as it is done with the analytical Photogrammetry. The other one is to focus on the catch of the surface roughness in order to assess the corrosion shape and depth for an example. Both of these analyses are presented in Chapter 7.

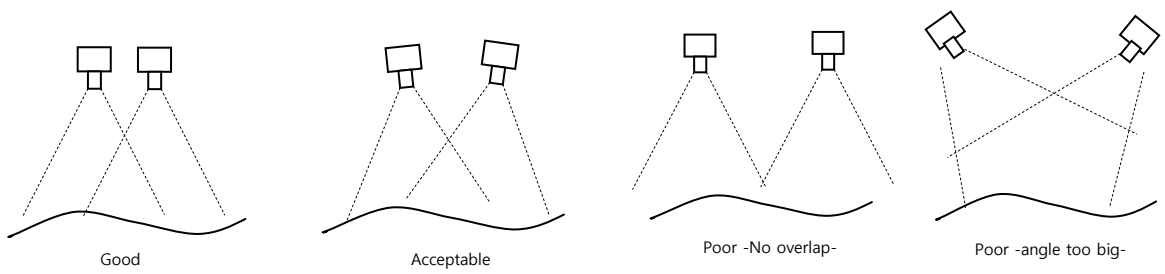

Figure 4.7 Setups for a pair of camera stations

4.4. COMPARISON

Analytical Photogrammetry requires some previous setups for a project to be processed such as special points to be attached onto the object as will see in Section 7.2.1. On the other hand, the digital Photogrammetry can proceed without any preparation of the project. The digital procedures may be more convenient, however, it presents some disadvantages.

The first problem is related to the characteristics of the surface, where erroneous information is obtained if it is reflective. The steel plate specimens analysed in this work are corroded and therefore, not reflective at all, but it should be taken into account if painted plates of a ship hull are to be studied. Digital Photogrammetry presents other aspects to be considered, especially related to the light. The digital Photogrammetry relies on the pixel characteristics as colour and light, so that the object has to be equal in both photographs and that means that the light and shadows should be the same. Because of that, it is not possible to use flash in digital procedures as it is for analytical projects, and that means more light environmental dependency is involved. In addition, the digital Photogrammetry requires extremely sharp images, avoiding any blurry area leading to either high illuminated object or very expensive lens.

5.SURFACE FITING

In the following chapter a mathematical method to generate surfaces, fitted to a cloud of points generated with photogrammetric techniques is presented. The goal is to generate mathematical functions that represent the initial imperfections that might be further introduced to ANSYS and to carry out FEM analysis. The whole method is developed in the Chapter 7.

The reason of using mathematical functions instead of directly using the mesh obtained from photogrammetric techniques relies on the fact that the important information to be considered into the structural analysis is rather the trend of the shape than the plate particularities. It means that the data is filtered and smoothed. Moreover, the exchange of mesh data between software often causes erroneous results due to incompatibilities between software.

The method used to generate such mathematical functions is based on third polynomial functions. This method is presented as well as other mathematical methods such as interpolant, Lowess, or trigonometric Fourier Series Functions. In this chapter, and in Section 7.3.1, comparisons have been carried out in order to justify the convenience of using polynomial functions and what are the best features to be set-up to obtain the best results. Those comparisons rely on statistical parameters that are known Goodness of Fit (GOF).

Polynomial fitting is commonly used by geographers to decompose observations on a spatially distributed variable into a component associated with any regional trends present in the data, such procedure receives the name of *the trend surface analysis*. This technique is suitable for those problems in which the data points that are sparse inside is of well-defined limits and the output variable changes smoothly as for example: temperatures, humidity, etc.

The whole process of space fitting is developed here by using Matlab software, which incorporates a tool called *Sftool* that carries out surface fittings using several methods.

5.1. TYPES OF SURFACE FITTING

The Interpolant Fit category fits a surface that passes through all the points, which are composing the set of data. The resultant surface is considered 'perfect' if the residuals obtained are zero, nevertheless, it does not mean that this fit represents faithfully the real plate. This may be explained by the fact that the resultant surface is composed of the squares between the points, that is, unreal sharp corners are generated. By definition, the function of an interpolant fitting is a piecewise linear surface that cannot be used to generate the node properties in the finite element model. Because of that, it is only useful to analyze graphically the shape of the deformation plate surfaces.

Another fitting technique is called Lowess. The name "Lowess" is derived from the term "locally weighted scatter plot smooth". The smoothing process is locally considered because each smoothed value is determined by neighbouring data points defined within the span percentage of the total number of data points in the data set-. The process is weighted because the regression weight function is defined for the

data points contained within the span. This fitting type is also not useful for the goal of this thesis since it is intended to be used for other purposes.

As for the Polynomial fitting, this method is based on the bi-variant polynomial functions where the third coordinate is a function of the other two axes. They can be of several degrees to better fit to the data points and their adjustment is reached by means of modifying the polynomial coefficients. The determination of the coefficients that fits best is done by the least squares. This technique boasts an impressive versatility and accuracy in performing fittings, and because of that, it is proposed to be used to build models for FEM analysis.

In addition, Matlab allows introducing custom functions to be adjusted to set of points. By the Least squares method, Matlab is able to compute the coefficients belonging to the mathematical function so the residuals are minimized. This tool is used in the section 7.3.1to carry out fittings based on trigonometric Fourier functions, which is the most suitable method for the initial imperfection estimation and the results will be compared with the polynomial ones.

5.2. GOODNESS OF FITTING

As previously exposed, the aim of this chapter is to find a fitting method, which is able to perform a surface model that faithfully represents the data points and to carry out the comparisons, it is necessary to define the parameters to rely on. These statistical parameters are grouped and known as Goodness of Fitting (GOF). As it is common in the statistical literature, the GOF might be used in various senses. Generally, a good fit refers to a model, which explains a high proportion of the variability in the data, and is able to predict new observations with a high certainty. In addition, a good fit is such in which the model coefficients can be estimated with a little uncertainty. The parameters composing this group are:

- Sum of the Squares due to error (SSE),
- R-Square,
- Adjusted R-Square,
- Root mean Squared error (RMSE)

The sum of the Squares due to Error (SSE) is a parameter that measures the global deviation of the values from the predicted response values to the data point values, that is, the residuals. A value closer to 0 indicates that the model has small random error component and that the fit is more faithful to the data points. It is also known as SSE,

$$SSE = \sum_{i=1}^{n} w_i (y_i - \hat{y}_i)^2 \tag{5.1}$$

y_i is the data point value and $\hat{y}_i$ is the predicted response value.

R-Square is a statistic measure showing how successful the fit is in explaining the variation of the data. In other words, R-square is the square of the correlation between the data point values and the predicted response values. It is also called the square of the multiple correlation coefficient or the coefficient of

determination and might be found as R^2. It is defined as the ratio of the sum of squares of the regression (SSR) and the total sum of the squares (SST).

$$SSR = \sum_{i=1}^{n} w_i(\widehat{y_i} - \overline{y_i})^2 \tag{5.2}$$

$$SST = \sum_{i=1}^{n} w_i(y_i - \overline{y_i})^2 \tag{5.3}$$

the R-Square might be defined now as

$$R - square = \frac{SSR}{SST} = 1 - \frac{SSE}{SST} \tag{5.4}$$

By definition, R-square can take only a value between 0 and 1. The closer to 1, the greater proportion of variance is accounted for by the model. An R^2 of 0.82 means that the fit explains 82% of the total variation in the data about the average. There is an important issue to be considered in evaluating the quality of a fit by relying on the R-square. If the number of fitted coefficients in the model is increased, the R-square will also increase although the fit may not improve in a practical sense. To prevent this situation it is necessary to use the degrees of freedom adjusted R-square.

Adjusted R-Square: A degree of freedom is defined as the number of data point values n minus the number of fitted coefficients m estimated from the data points. $[degreesoffreedom = v = n - m]$. v indicated the number of independent pieces of information involving the n data points that are required to calculate the sum of squares. The Adjusted R-square is the best indicator of the fit quality, when comparing the two models of different characteristics that refer to the same data points.

$$Adjusted\ R - square = 1 - \frac{SSE\ (n-1)}{SST\ (v)} \tag{5.5}$$

Root Mean Squared Error: It is also commonly known as the fit standard error and the standard error of the regression. It is an estimated of the standard deviation of random component in the data.

$$RMSE = s = \sqrt{\frac{SSE}{v}} \tag{5.6}$$

5.3. INTERPOLANT FITTING

Figure 5.1shows the interpolant fitting. As it can be seen, the surface passes through all the data points, which are represented by blue points in the plot. It generates sharp corners in each point, what stresses the

evidence that this fitting type is not faithful when representing a deformed surface.

The sharp behaviour of interpolant fitting might be seen also in the Contour plot (centre). In this plot, it is possible to observe the typical shape of horse saddle. Finally, in the right plot shows the residuals of the fit, that in the case of the interpolant fitting, there are no residuals.

Despite this fitting not being able to be used to generate a surface function, it might be used as a "reference" when carry out other fitting in terms of surface trends.

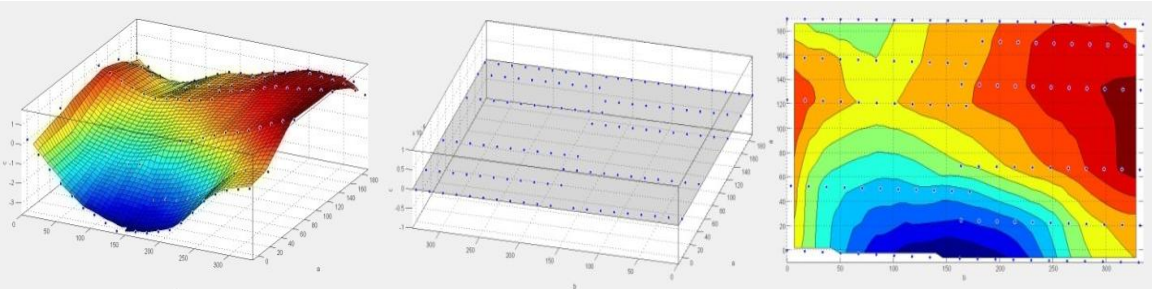

Figure 5.1Interpolantfitting:left: 3D Surface, center: Contour of the Surface. Right: Residuals

5.4. POLYNOMIAL FITTING

The initial problem can be defined as follows: given N data points (x_i, y_i) and N numbers $f_i, i = 1,2, \dots, N$, find a function $f(x, y)$ from some class and defined on a plane containing the data points for which $f(x_i, y_i) = f_i$ for $i = 1,2, \dots, N$. A class is defined as the polynomial function of the same order in both x and y and the first four ones are as follows.

Table 1 Polynomial Classes

Class	Basis Function
$\mathcal{P}_0$	1
$\mathcal{P}_1$	1 x y
$\mathcal{P}_2$	1 x y x^2 xy y^2
$\mathcal{P}_3$	1 x y x^2 xy y^2 x^3 x^2y xy^2 y^3

Thus, any function p, in the class $\mathcal{P}_2$, for example, must be of the form

$$p(x, y) = a_1 + a_2 x + a_3 y + a_4 x^2 + a_5 xy + a_6 y^2 \tag{5.7}$$

for some real numbers $a_0, a_1, a_2, \dots, a_6$. More generally, $\mathcal{P}_n$ is the class of polynomials containing all functions of the form x_i, y_i, where $0 \leq i + j \leq n$ and $i \geq 0, j \geq 0$. The classes $\mathcal{P}_0$ $\mathcal{P}_1$ $\mathcal{P}_2$ and $\mathcal{P}_3$are known as the spaces of constant, linear, quadratic and cubic polynomials respectively.

5.4.1. Least squares fitting of polynomial surfaces

As a result of any fitting, there is a difference between the original coordinates of a point and the coordinates obtained from the calculated function [66]. This difference is defined as $p(x_i, y_i) - f_i$. The objective is then to adjust p by choosing the coefficients $a_0, a_1, a_2, \dots, a_n$ so as to minimize,

$$E(p) = \sum_{i=0}^{N} (p(x_i, y_i) - f_i)^2 \tag{5.8}$$

E is a function of $a_0, a_1, a_2, \dots, a_n$ and will have a minimum only when $\frac{\partial E}{\partial a_i} = 0$ for $i = 1,2, \dots, 6$. These conditions yield to six linear equations of the unknowns $a_0, a_1, a_2, \dots, a_6$.

$$\begin{gathered}
(N+1)a_1 + \left(\sum x_i\right) a_2 + \left(\sum y_i\right) a_3 + \left(\sum x_i^2\right) a_4 + \left(\sum x_i y_i\right) a_5 + \left(\sum y_i^2\right) a_6 = \sum f_i \\
\left(\sum x_i\right) a_1 + \left(\sum x_i^2\right) a_2 + \left(\sum x_i y_i\right) a_3 + \left(\sum x_i^3\right) a_4 + \left(\sum x_i^2 y_i\right) a_5 + \left(\sum y_i^2 x_i\right) a_6 = \sum x_i f_i \\
\left(\sum y_i\right) a_1 + \left(\sum x_i y_i\right) a_2 + \left(\sum y_i^2\right) a_3 + \left(\sum x_i^2 y_i\right) a_4 + \left(\sum y_i^2 x_i\right) a_5 + \left(\sum y_i^3\right) a_6 = \sum y_i f_i \\
\left(\sum {x_i}^2\right) a_1 + \left(\sum x_i^3\right) a_2 + \left(\sum {x_i}^2 y_i\right) a_3 + \left(\sum x_i^4\right) a_4 + \left(\sum x_i^3 y_i\right) a_5 + \left(\sum y_i^2 {x_i}^2\right) a_6 = \sum {x_i}^2 f_i \\
\left(\sum x_i y_i\right) a_1 + \left(\sum {x_i}^2 y_i\right) a_2 + \left(\sum y_i^2 x_i\right) a_3 + \left(\sum {x_i}^3 y_i\right) a_4 + \left(\sum y_i^2 {x_i}^2\right) a_5 + \left(\sum {y_i}^3 x_i\right) a_6 = \sum x_i y_i f_i \\
\left(\sum {y_i}^2\right) a_1 + \left(\sum y_i^2 x_i\right) a_2 + \left(\sum y_i^3\right) a_3 + \left(\sum y_i^2 {x_i}^2\right) a_4 + \left(\sum y_i^3 x_i\right) a_5 + \left(\sum y_i^4\right) a_6 = \sum {y_i}^2 f_i
\end{gathered} \tag{5.9}$$

where all the summations are for *i* are from zero to *N*.

The equations are the same as in the case of normal equations for fitting a polynomial of the first degree, a plane surface, but in that case, only the first three equations are considered, discarding the last three ones ($a_4 = a_5 = a_6 = 0$). Similarly, for a fitted bilinear surface, only the first, second, third and fifth equations are considered ($a_4 = a_6 = 0$).

The equations may be conveniently expressed in matrix-vector form. In the case of the full set of equation seen before, it is introduced the $(N+1) \times 6$ matrix.

$$V = \begin{bmatrix} 1 & x_0 & y_0 & x_0^2 & x_0 y_0 & y_0^2 \\ 1 & x_1 & y_1 & x_1^2 & x_1 y_1 & y_1^2 \\ \cdot & & & & & \cdot \\ \cdot & & & & & \cdot \\ \cdot & & & & & \cdot \\ 1 & x_N & y_N & x_N^2 & x_N y_N & y_N^2 \end{bmatrix}, \tag{5.10}$$

and the column vectors,

$$a = \begin{bmatrix} a_1 \\ a_2 \\ a_3 \\ a_4 \\ a_5 \\ a_6 \end{bmatrix}, \quad f = \begin{bmatrix} f_0 \\ f_1 \\ \cdot \\ \cdot \\ \cdot \\ f_N \end{bmatrix} \tag{5.11}$$

The vector-matrix formulation takes the following form,$V^T V a = V^T f$

A solution of this equation for *a* determines the polynomial of the equation $p(x,y) = a_1 + a_2 x + a_3 y + a_4 x^2 + a_5 xy + a_6 y^2$ that best fit the data in the sense of the least squared deviations. Following, in the case of quadratic problem, if there are only six points of interpretation then $N + 1 = 6$ and so V is square. If the sic points are on the mid-sides and vertices of a triangle then V and $V^T V$ will be *non-singular.* That is $(V^T V)^{-1}$ exists and it means that there is a unique solution $a = (V^T V)^{-1} V^T f$, where the function $p(x,y)$ is now the *Interpolant function* to the data and the deviations are zero.

As for the case of a higher function's class, more coefficients are involved, as it is the case of the cubic functions:

$$p(x,y) = a_1 + a_2 x + a_3 y + a_4 x^2 + a_5 xy + a_6 y^2 + a_7 x^3 + a_8 x^2 y + a_9 xy^2 + a_{10} y^3 \quad (5.12)$$

On the other hand, the procedure is the same as the quadratic function. In general, the function used is either quadratic or cubic, it is necessary to use computer programs to solve the problem. Furthermore, since the number of points composing a project of surface modelling might be of well over 100, it is even more necessary to call on computer tools. The computed tool used to find the coefficients is Matlab, which can be used to find the coefficients that minimize the difference $p(x_i, y_i) - f_i$.

The Matlab tool Sftool allows generating a surface fitting of various polynomial degrees in both axis x and y up to the fifth degree. It means that multiple polynomial approximations may be carried out to adjust to the project requirements.

The first six polynomial classes of one plate surface specimen of the sample are presented in Figure 5.2. Looking at the residual plots (central plot), it can be observed that the residual trend decreases while the polynomial degrees are increasing. In the contour plots (right) it is also noticeable that shape gradually trends to be equal the one obtained in the interpolant fitting. The GOF parameters corresponding to the polynomial fittings are also presented in the Table 2.

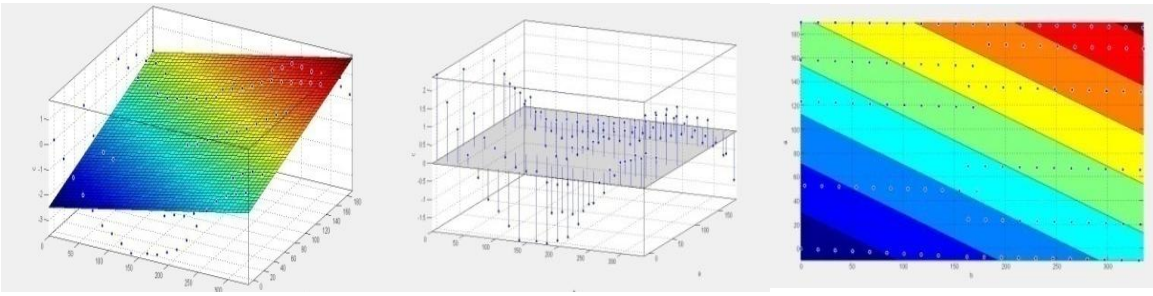

Figure 5.2 Second Polynomial Class fit, left: 3D Surface, centre: Contour of the Surface, right: Residuals

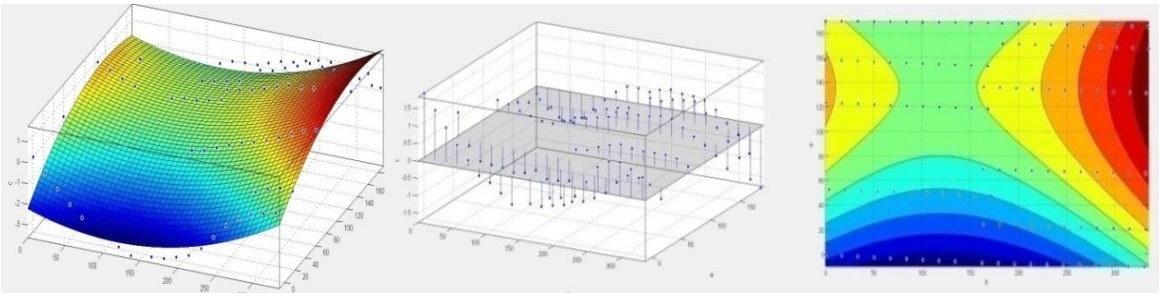

Figure 5.3Third Polynomial Class fit. left: 3D Surface. centre: Contour of the Surface, right: Residuals

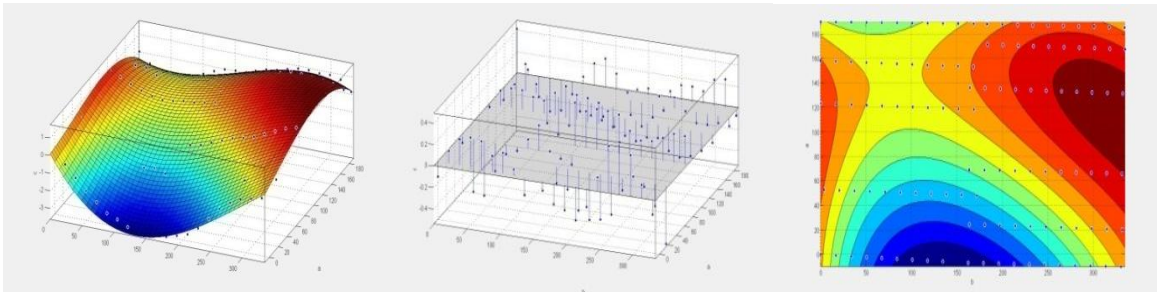

Figure 5.4 Fourth Polynomial Class fit. left: 3D Surface. centre: Contour of the Surface. right: Residuals

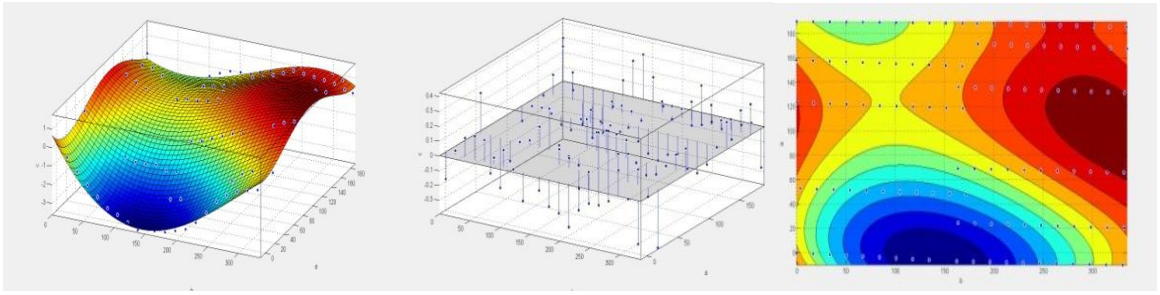

Figure 5.5 Fifth Polynomial Class fit. left: 3D Surface. centre: Contour of the Surface. right: Residuals

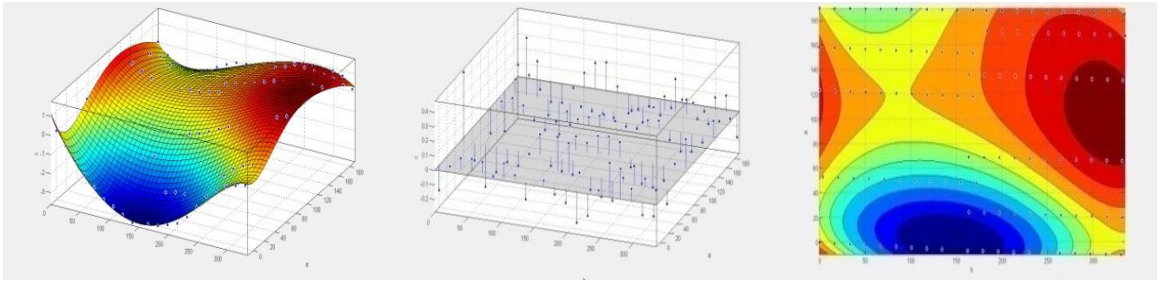

Figure 5.6 Sixth Polynomial Class fit. left: 3D Surface. centre: Contour of the Surface. right: Residuals

The second polynomial class generates a surface that by definition is completely flat and its orientation is such that the residuals are minimized. It is evident that this class is not applicable in the case that is studied here since what it is desired is to catch the deformed surface. The third class is capable to describe parabolic forms that are the first mode of deformations. As it is shown in the plots, this class is able to catch the main deformation. In the example plotted, it is possible to observe that the typical horse saddle shape, which was previously observed in the "reference" interpolant fitting.

As for the fourth class, with respect to the contour plots it does not seem to introduce much improvements compared to the third class, however, this class makes possible to catch more realistic imperfections owed to its ability to describe other deformations than parabolic forms, that is, the second mode of deformation. As can be seen from Table 2, the improvements attained in the higher polynomial class, in terms of GOF, are not noticeable. While the Adjusted R-square obtained with the fourth class is of 0.9683, the fifth and the sixth class are of 0.9821 and 0.9887 respectively that is only a 2% of improvement.

Table 2 GOF of first three Polynomial Class.

Fit Name	Fit Type	SSE	R-square	Deg of Free.	Adj R-squa	RMSE	Nº Coeff
Interpolant	linearinterp	1.03655E-26	1	0	NaN	NaN	117
Poly_First	poly11	87.1712	0.5611	114	0.5534	0.8744	3
Poly_Second	poly22	37.0033	0.8137	111	0.8053	0.5774	6
Poly_Third	poly33	5.8039	0.9708	107	0.9683	0.2329	10
Poly_fourth	poly44	3.1315	0.9842	102	0.9821	0.1752	15
Poly__Fifth	poly55	1.8500	0.9907	96	0.9887	0.1388	21

A part from the quality values of GOF, it is important to point out the fact that the corners and the borders behave differently. The use of higher polynomial classes might induces erroneous shape, for instance, in the corners and borders.

6.SENSITIVE ANALYSIS

In this thesis, several procedures and techniques are combined so as to successfully modelling real deformed plates and to be analysed using finite element methods. It is important to assess the accuracy of the techniques used in the present study and how sensitive they are to the governing parameters.

The principal factor to be considered corresponds to the photogrammetric measurements. Despite the fact its accuracy might be calculated mathematically, some tests are carried out to prove its correlation. In this sense, three tests are performed and presented in this chapter; the first one consists in making a plaster cast of a plate that might be used to take measurements. In the second test, measurements of a very deformed plate are taken from a quasi-perfect plate. With all the measurements taken, correlation with the measurements taken from Photogrammetry can be studied, however, since the x and y coordinates are not coincident, it makes necessary to apply the polynomial fitting. As it will be demonstrated later, it induces a polynomial intrinsic error that must be taken into consideration when analysing the results. The third test consists in dispose of 161 points over a surface that is as much flat as possible. The goal is to check out if Photogrammetry is able to catch such flatness. In order to take the most trustable real measurements during the trials a professional calliper gauge is used.

6.1. PLASTER CAST

The initial imperfections are defined as the deflections of a surface from its ideal perfect plane. The plane over which the plate is laying over might be defined as the reference plane, and the deflection at any point may be determined as the distance from that point to the reference plane. To measure those distances it would be necessary to drill the plate to introduce a calliper down to the reference plane. Since that is not possible, a plaster cast is made to catch and simulate the shape of the plate.

After several trials, plaster cast has been made successfully. To do so, some considerations have been taken into account regarding the orientation of the plate and the minimum thickness of the model to be properly managed later. By definition, there is no unique reference plane so it is necessary to determine a coordinate system in order to be able to carry out comparisons later. It is necessary to select three points to define such coordinate system. The three points have been decided to be coincident to the three corners. Since the plate is deformed, the fourth corner is not necessary to be in the same plane of the coordinate system.

The holes of the plaster cast are done following a pattern of the coordinates x and y. In addition, a procedure to automatically orientate the coordinates is done to adjust better the measurements to the data from Photo-modeller.

This manufacture of plaster cast presents some difficulties and the accuracy is not easy to ensure. Among the troubles to be faced, it is difficult to take measurements from a surface that presents some irregularities, the fragile material that needs to be of the minimum thickness for not to brake and the deviations produced when drilling the holes. Despite of this, high correlation between the measurements and the polynomial surface of the third order is found as can be seen in Table 3.

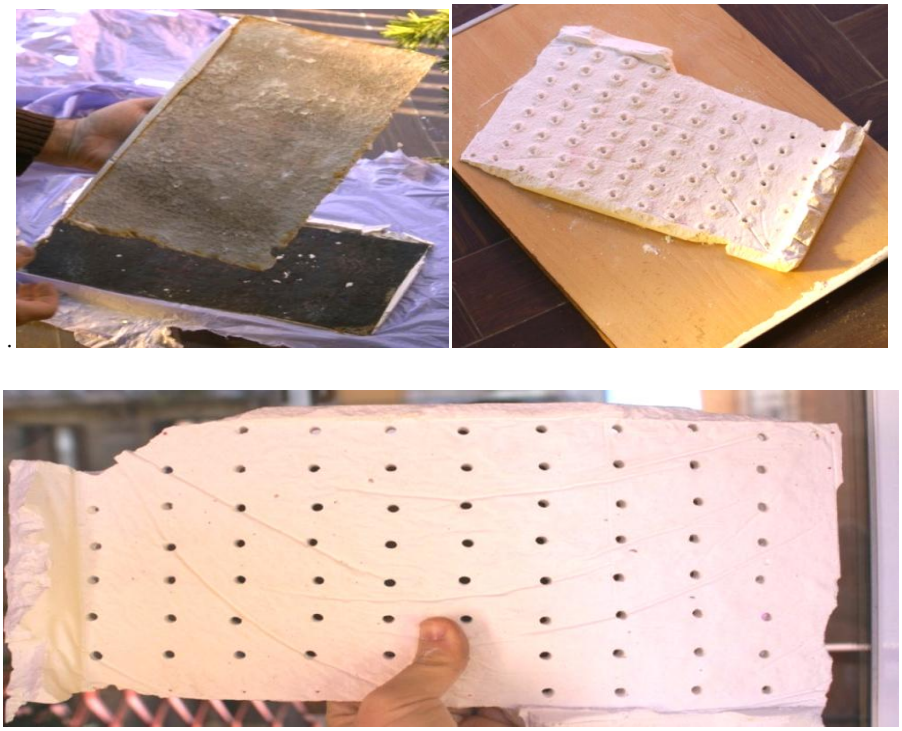

Figure 6.1Plaster cast manufacturing

6.2. QUASI-IDEAL PLATE

The procedure here is based on the use of a brand new steel plate, which has not been subjected to load before and because of that it is not expected to be deform and it has been called quasi-ideal plate Furthermore, this plate is re-forced by steel bar stiffener. Two tests are set up in two different ways, firstly, disposing the plate to be measured upside down and installing the quasi-ideal plate using magnets in such way torsion is avoided. Measurements have been carried out to increase the redundancy. On the other side, the second configuration consists in disposing the quasi-ideal plate over the plate to be measured. As mentioned before, the setting of the structural elements involved in the measurement must be done in a way that the coordinate systems coincide.

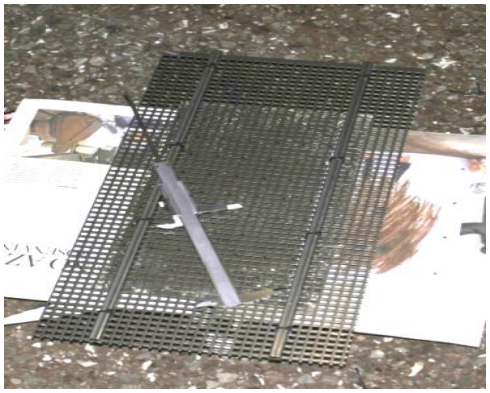

Figure 6.2 Measurements using "quasi-ideal" plate.

The results of both systems are presented in Table 3. Correlation with the polynomial surface of third order and the correlation between the different trials are calculated.

Table 3 Correlations between measurements.

	SSE	Media	SSR	SST	ST.DV	R^2
POLY33 - DOWN PLATE 1	121.0	6.723	1844.6	1965.6	1.173	0.938
POLY33 - GUIX	97.1	6.723	1693.8	1790.9	1.049	0.946
POLY33 - DOWN PLATE 2	76.7	5.268	2232.5	2309.3	0.939	0.964
POLY33 - OVER PLATE	89.6	5.237	2241.9	2331.5	1.015	0.958
DOWN PLATE 1 - GUIX	0.3098	0.0188	53.0783	53.3881	0.0541	0.9946
DOWN PLATE 2 - OVER PLAT	0.1518	0.0031	61.0144	61.1662	0.0416	0.9975
FLATNESS	9.9	84.442	184061.0	184070.8	0.249	0.9999

It is appreciable a little deviation in the correlations with the polynomials, such is owed to the intrinsic deviations produced in the polynomial fitting. This fact can be easily seen checking out the correlation graphs where a pattern is observed coinciding in both cases.

This pattern shows one of the drawbacks of the polynomial fitting of third order, consisting in small deviations on the maximum and minimum values. Nevertheless, this effect is proportional and it is appreciable only for extremely deformed plates.

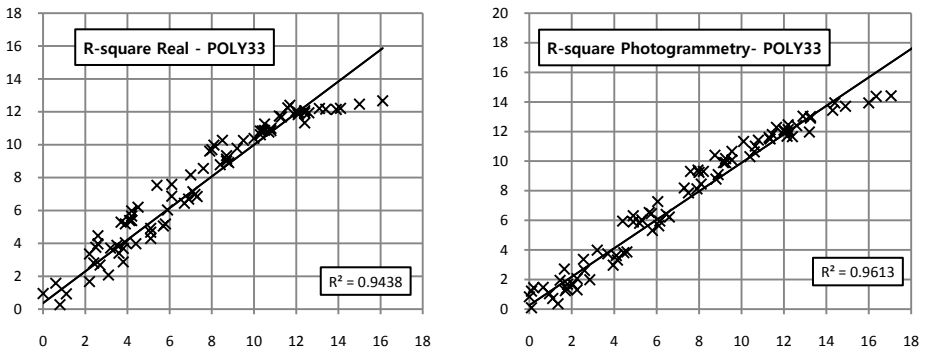

Figure 6.3 Correlation comparison.

6.3. FLATNESS TRIAL

The third study consists in taking photogrammetric measurements of a grid of points disposed on a completely flat surface, where the vertical component of the resultant points should be zero. To ensure the flattest surface a combination of very thick glasses are set. The *x* and *y* coordinates of the points might be easily calculated since they are distributed in a grid form.

The results are processed using Excel and compared to the values obtained from the Project information available from Photomodeller. The vertical components of the points are found to be inside of the range 0.04 mm to -0.04 mm, with an average of 0.0023 mm and with a standard deviation of 0.021. It is shown that the accuracy achieved that is about more than twice what is observed as Z maximum and minimum-. This is likely due to the inevitable deviations produced by the irregularities of the paper.

Table 4 Project Status. Flatness.

Overall RMS Vector Length: 0.0204 mm
Maximum Vector Length: 0.023 mm
Minimum Vector Length: 0.0194 mm
Maximum X: 0.0133 mm
Maximum Y: 0.0132 mm
Maximum Z: 0.0139 mm
Minimum X: 0.0105 mm
Minimum Y: 0.0103 mm
Minimum Z: 0.0125 mm

The points of the grid are distributed homogeneously, so that, the coordinates of each of the points are known. Having this information, it is possible to carry out a correlation between these known coordinates and those computed by Photogrammetry. The result is shown in the Table 3.

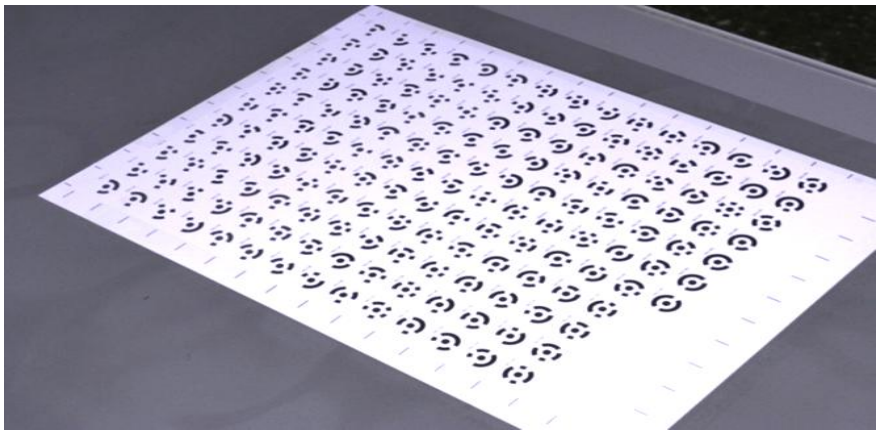

Figure 6.4 Flatness trial

7.STUDY CASE

The aim of the present work is to carry out an ultimate strength assessment of steel plates by using Photogrammetry techniques to measure the initial imperfections. The question is how to do it?

The first step is to identify what are the main stages of the process. Namely, there are three principal stages, Photogrammetry, Plate Modelling and Finite Element Analysis. The Photogrammetry stage produces a set of points that represent the surface shape of the plate. In the second stage, it creates a mathematical function that best represents the trend of the points of the initial imperfections of the plate. Finally, with the mathematical function a 3D model of the initial imperfection is built for assessing the ultimate strength of the specimen. Each of these stages is based on commercial software. For the Photogrammetry procedures is used a code called Photo-modeller Scanner, as for the plate modelling, Matlab and Excel is used to perform polynomial surface fitting and finally, the finite element analysis is done with ANSYS.

For each program, it is crucial to study the relevant factors that govern the quality of the results. For instance, when obtaining the points from Photogrammetry, it is significant to decide the number of photographs to be added to the project, the angles from which they are taken, the type of camera to use and so forth; or when modelling the 3D model in ANSYS, to decide the mesh size or the Boundary conditions to be applied. These factors are studied and presented in detail in the present chapter.

On the other side, each program processes and generates data that is necessary for the others, that means that a flow of data is generated between them. Furthermore, each program uses different types of data files or simply, they organize the data in a different way. This difficulty stress requires having a methodology to ensure the compatibility of the programs minimizes the flows of data speeding up the procedure and maximizes the quality of the results.

Figure 7.1represents the methodology proposed in this thesis. In such, the main stages are shown and the most relevant tasks carried out for each one are outlined. The central column indicates the principal steps of the process. Inside of the 'ROMBOS', is presented the tools, whether they are programmed, subprograms or the camera, and in the 'rectangles' is represented the results obtained from the upper tool. In the left column is shown the most important aspects related to the tools and on the right side, the characteristics of the results are shown.

The chapter is divided into three parts concerning the three stages described above. In the first part, the topics related to the application of the Photogrammetry techniques are approached and the decisions taken to obtain the results presented. In the second part, it is explained the scripts developed in Matlab and Excel in order to catch the data from Photo-modeller and automatically generate a script for ANSYS. Finally, the third part is related to the results obtained from FEM analysis.

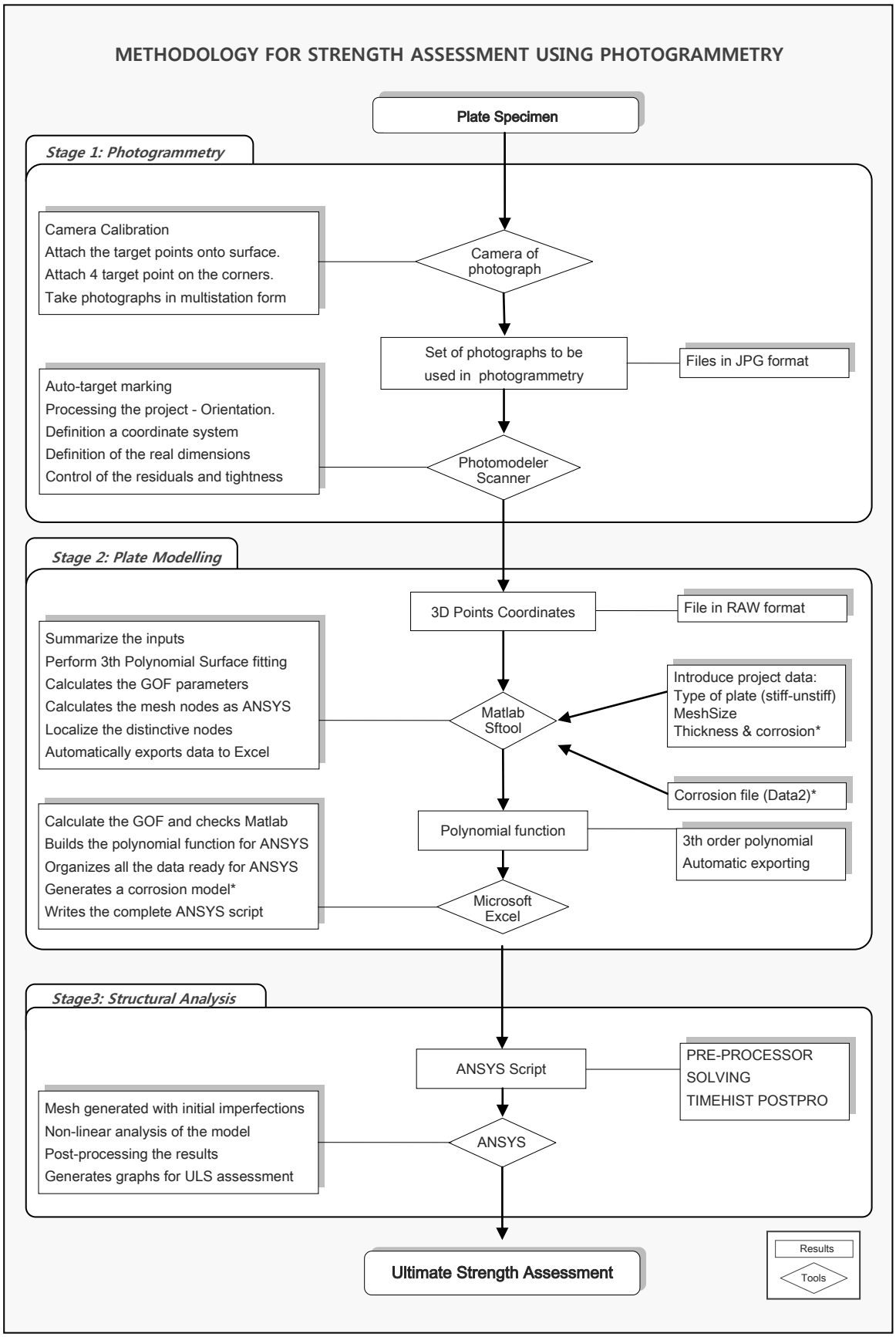

Figure 7.1 Scheme of the Methodology

Despite of the fact that the methodology proposed here is intended to take initial imperfections measurements with analytical Photogrammetry, an additional procedure has been studied related with local corrosion degradation, which has been based on the digital Photogrammetry. While the corrosion considered in the projects focused in the initial imperfections is modelled using statistical degradation parameters, the purpose of using digital Photogrammetry is to catch the roughness of the surface from the photographs. These two modelling alternatives are referred as *types of corrosion modelling* and they are explained in more detail in section 7.3.4.

7.1. TEST SPECIMENS

The plates, selected to be used in this thesis, belong to a girder box girder, specially treated to simulate the real characteristics of the plates found in marine structures. The set of specimens is composed by 3 un-stiffened plates plus 4 stiffened plates and the position they occupy in the whole structure is shown in Figure 7.2. The aspect ratio of the most of them is approximately equal to 2 and thicknesses are measured by a ultrasonic gauge. All information is shown in Table 5. The elasticity modulus and the Poisson coefficient are considered to be of E = 206 GPa and $v = 0.3$ respectively.

Table 5 Plate specimens

Name	X distance *(a)*	Y distance *(b)*	Aspect Ratio	Thickness	Slenderness	W0 (0.12)	W0 (0.3)	a/t
Plate4	175.9	341.6	1.9	2.70	2.5	2.10	5.3	65.1
Plate4_B	180.0	324.7	1.8	2.01	3.5	2.96	7.4	89.5
Plate7	176.1	327.0	1.9	2.02	3.4	2.82	7.0	87.2
Stiff3	189.5	334.2	1.8	2.90	2.6	2.27	5.7	65.3
Stiff4_B	180.0	323.9	1.8	2.90	2.4	2.05	5.1	62.1
Stiff7	175.1	322.3	1.8	2.50	2.7	2.25	5.6	70.0
Stiff 8	189.0	330.2	1.7	2.22	3.3	2.95	7.4	85.2

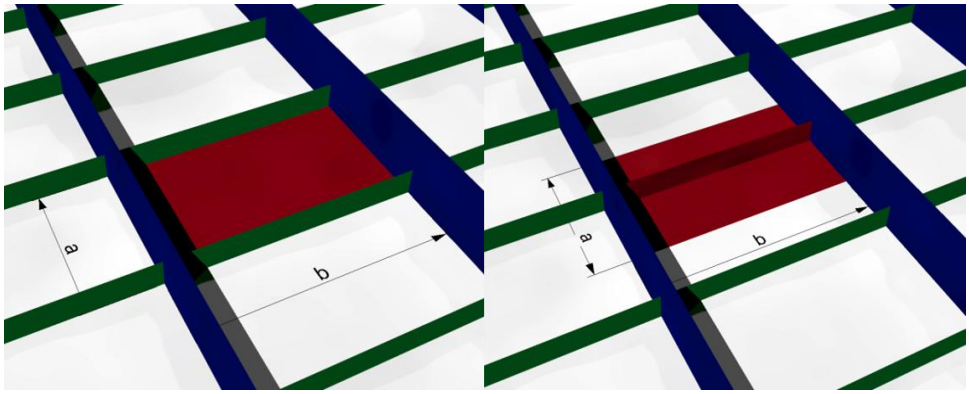

Figure 7.2 Images of the un-stiffened (left) and stiffened (right) plates

7.2. STAGE 1: PHOTOGRAMMETRY

A procedure of modelling plate shapes with initial imperfections by means of photogrammetric techniques is presented here. In order to solve the analytical photogrammetric equations, a commercial code called Photo-modeller has been used. This program helps in extracting measurements and 3D models from photographs, by using a camera as an input device. This software is divided into two sub-programs. The first sub-program is intended to create models of objects by using multi-station images. The model can be created either manually or automatically by using auto referencing marking codes and is called *Automatic Target Marking* (from now on ATM). The ATM is a procedure used to model the plates since it is more reliable and faster than manual one. On the other hand, the second sub-program, also called Photo-modeller Scanner, is aimed to create models by using stereographic photos. This second program has been used to estimate the level of corrosion of the plates, which is presented after.

7.2.1. Auto-marking coded target method

The objective is to model the deflections of the plates, and the way to do is by attaching reference points onto the surface of the plates, following the shape. These reference points are known as *coded target points* and they are physical codified points whose the program is able to find inside of a photograph.

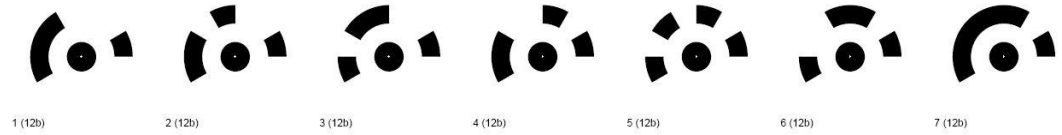

Figure 7.3 Coded Targets

The program incorporates a code, which has the capability of searching dots' forms along of an image. It detects the dots' edges and by deducing the shape of the dot, whether it is round or elliptic due to the inclination, it is able to determine the centre of the dot. Further, it reads the surround of the dot where a bit codification representing a real number is placed and assigns the number to the dot.

Figure 7.3shows an example of the coded target points, with the inner dot, the surrounding code, and down to the left of each target point, the number that the code represents and between the parenthesis the number of bits of the code, in this case, 12 bits. It is important to ensure that the target points are as much contrasted as possible, using black over white or vice versa strongly helps to better edge detection as can be seen in Figure 7.4- left. The whole process permits to the program to determine the coordinates of all the points in each photograph. Finally, by introducing all the coordinates from all the images in the collinearity equations, the third coordinate of the points might be calculated regarding the *multi-station* photogrammetric theory.

The coded target points can be generated from the program itself and its features may be modified in size to adjust to the project requirements. Furthermore, in order to ensure that the target points follows the shape of the plates with more fidelity, the targets might be disposed in magnetic strips as shown in Figure 7.4- right.

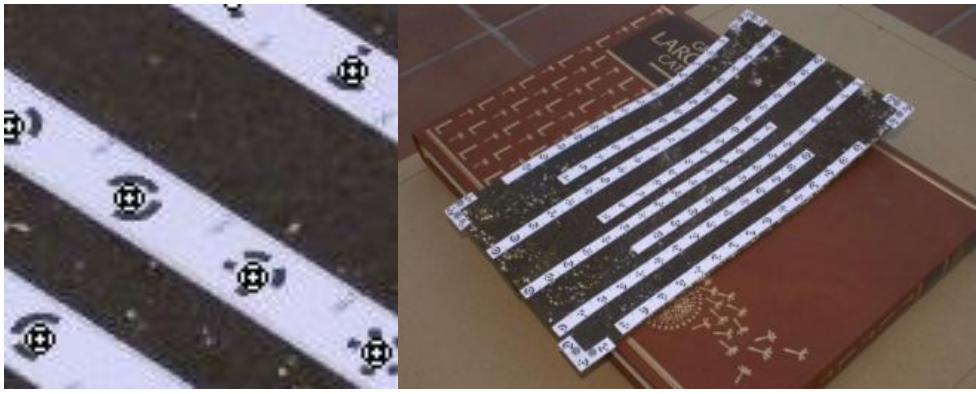

Figure 7.4 Left: Auto-marking target points. Right: Magnetic Strips onto the plate

The amount of point's forms a cloud of points positioned in an arbitrary 3D coordinate system as can be seen in Figure 7.5– right. However, to take measurements of the deflections it is desired that the points are referenced to a coordinate system based on a plate itself. This coordinate system should represent the hypothetical perfect plate without imperfections, so the points' deviation in the vertical axis from the imaginary plane is considered as plate deflections. To set this coordinate system three corners are used, that means that three of the coded target points must be coincident to three plate corners, as shown in Figure 7.5- right. The fourth corner does not necessarily belongs to the coordinate system plane. Finally, it is necessary to indicate a real distance between two certain points to give real dimensions of the 3D models.

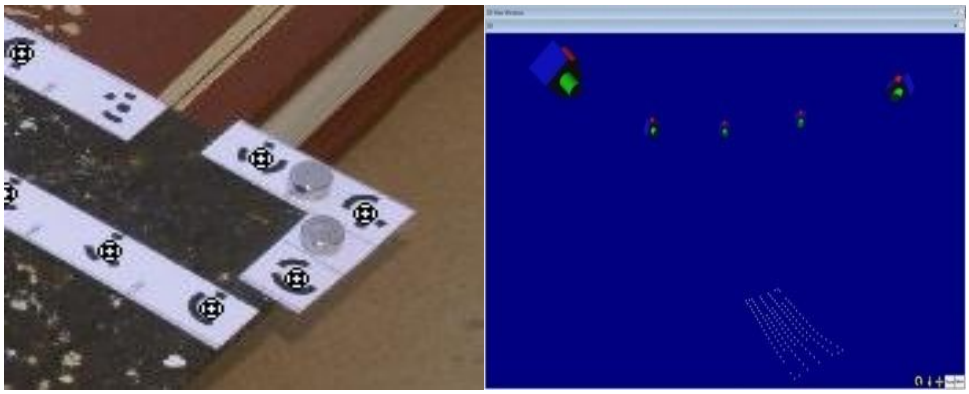

Figure 7.5. Left: Target point in the corner. Right: Cloud of points' 3D model.

7.2.2. Residuals

From the solution of the collinearity equations, the program is able to measure the accuracy of the project by measuring the distances between the expected point coordinates and the ones observed in the photographs, that is, the residuals. It also means that there is one residual for each point in each photograph. The program resumes all this information and lists the maximum residual attained for each point and in what photograph that happens.

For a project to be considered of high accuracy, the maximum residual reached should not be larger than 1 pixel. The dimensions of a pixel depend on the real distance that the image is covered, for example, in the case of a 10 Megapixel (3872 x 2892) photograph covering a rectangle of 0.5 x 0.30 meters, the length of 1 pixel equals to 0.12mm.

However, the accuracy of the project does not only depend on the maximum residual, which corresponds to a single point in a single photograph, being necessary to evaluate the rest of the points' residuals. It could happen that the maximum residual of a project was induced by a mistake in one single photo of the sample while the rest of the project is well executed, in that case, skipping the problematic photo could improve the project's accuracy without having to restart the project again. Because of that, any project must be studied in detail to figure out what are the sources of the residuals and what can be done to fix the issue.

Apart from the residuals, it is possible to analyse if any pattern in the residuals is produced. This can be done by observing the vectors of the residuals as shown in the Figure 7.6. For a better understanding, the scale of the arrows has been increased 2000 times.

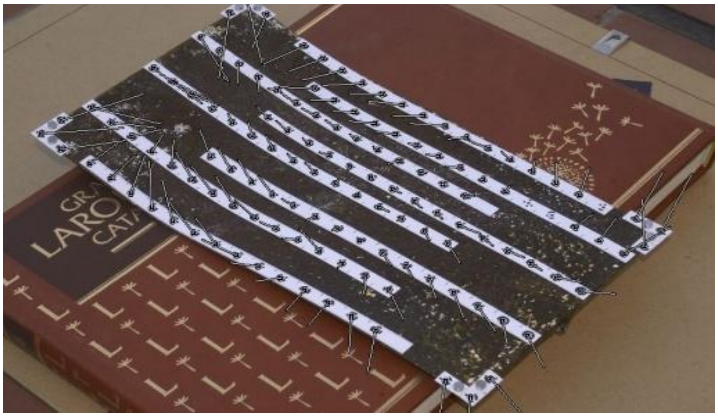

Figure 7.6 Residuals (increased 2000 times)

To perform measurements of higher accuracy more than what pixel permits, Photo-modeller incorporates what is called Sub-pixel marking. This computational process permits to the program to increase the measurements into a pixel by dividing it into 20 times. That means that an edge of a point can be detected with an accuracy up to 0.05 of a pixel for a very high-contrast low-noise circular targets down to 1 pixel accuracy for lower-contrast targets. The location of the geometrical centre of a point might be found by either the Centroid method or Least Squares method. Generally the Least Squares method is more accurate, especially on small targets[65].

Despite of the fact that is not easy to determine how the accuracy is improved by sub-pixel marking, it can be expected from five to twenty times improvement for a project that is mostly circular targets and done with a calibrated camera. So for a camera of 10 megapixels, it can be expected about 1 in 18,000 (0.2 of a pixel) to 1 in 78,000 (0.05 of a pixel) accuracy. In addition, in terms of millimetres, it would correspond to 0.025 to 0.006 mm.

7.2.3. Tightness

Tightness is a parameter used to indicate the accuracy of an Object Point's photo markings in conjunction with the accuracy of the camera station orientations. For each point, the tightness is displayed so point-by-point evaluation can be done. Furthermore, it possible to determine the overall RMS, what helps to study the quality of a project further than the maximum residual obtained.

The 3D position of an Object Point is computed by intersecting light rays from photographs. Due to measurement error, those light rays never intersect at the same precise point in the 3D space. To calculate the tightness it is necessary to know the closest distance between any two light rays (k and j) used in the computation of point $i$and find the largest of these closest distances. Then, if the size of the project is defined by entering the real distance between two known points, the tightness value can be computed as:

$$Tightnessofapointi = \frac{Largestdistancefromaraytoapoint}{SizeofthePoject} \times 100 \quad (7.1)$$

7.2.4. Project setting

When preparing a project, some considerations are to be taken into account in order to achieve high accuracy results. It is expected that the better the results are desired, the longer the time is necessary to complete a project, so that the understanding of how much each aspect influences to the quality of the results as well as to the time increasing is necessary to perform accurate project with the least efforts. In addition, some aspects affect the results without increasing the project time, so that it is also important to understand their relation with the results to take advantage of them.

7.2.4.1. Number of photographs

The number of photographs will compound a project is maybe the first important decision to be taken. Mathematically, with one photograph, a resection evaluation can be carried out and a minimum of two photographs is necessary to solve the collinearity equations on intersection condition, as it was seen before. Multi-station condition is composed of three or more than three photographs. From the Photo-modeller program, it is recommended to precede with a minimum of three photographs in spite of four on more photographs offer more reliable and confident results. Paradoxically, the larger the number of photos the higher the probability of increasing the residuals of the project and hence the more deviated the results, yet more confident the results are. That is due to the fact that the probability of one observed point in a photo to be deviated from the rest of the points in other photographs increases, while if the points are found to be coincident in a large number of photos, its coordinates are more trustable. The good news is that if the photographs are carefully well taken, the residuals do not increase when adding the photos to the project.

The number of photographs is affected in a high manner to the total time of the project, so that, it is important to know what the best number of images for a project is. Since this work is experimental, the highest reliable results are desired, so a number of eight photographs have proposed to be added in each project that is the number of photos recommended for calibration projects.

The procedure followed has been as follows: a) take 8 photographs from a plate with coded target points onto the surface, b) introduce them to the program and process the project, c) if the maximum residual is larger than 1 pixel, search the image where it is attained and discard it before process the project again, d) if the residual is not reduced, the photograph discarded is added again and the photograph with currently higher residuals is now discarded. This step is done till the maximum residual is reduced to at least one, e) if neither the photographs extracted helps to reduce the residuals, the number of photographs is reduced in one photograph and steps b) and c) are repeated, f) if 4 photographs are still too much to reduce the

residuals to 1 pixel, then the photographs need to be repeated. Despite the process presented appears to be arduous, good residuals are usually attained in the very beginning of the process when the photographs are taken carefully.

7.2.4.2. Number of coded targets

The number of coded target points to be used is also a determinant of the time invested per project. The larger the number of targets the more computer efforts is necessary. It has desirable reduced it to the minimum acceptable to decrease the time of computing. On the other hand, some plate shapes are very complex, so an excessive reduction means a loss of information and hence, erroneous results. For the models analysed here, it has been considered not less than 130 points for a plate size of 180 x 320 mm.

7.2.4.3. Internals of the camera

The collinearity equations depend on the parameters such as a focal length, lens distortion characteristics and lens position relative to the CCD, what is called the internals of the camera. In order not to introduce confusing values to the equations, these parameters should not be changed from photographs to photograph, and that means that the user:

- should not use a zoom lens on the camera unless the focal length can be locked securely,
- should not use interchangeable lenses unless one lens is left securely on the camera during the shoot for one Measurement Project,
- should not refocus the camera because in many consumer cameras, the lens focal length and lens distortion characteristics change as the lens is focused, and
- should not depend on autofocus cameras since the lens is focused out of user control.
- The user must follow dictates 1 and 2 from above and should take care with 3 and 4, but not be unnecessarily worried about focus effects, unless the focusing is changing considerably (i.e. some shots are focused at 1 foot and some at infinity).

7.2.4.4. Photograph features

As it was seen in the auto-marking procedure paragraph, it is desired that the target points appear in the images as much clear and contrasted as possible. The goal is to avoid blurry points because that causes large residuals. So that, images with large depth of field are expected since it decreases the probability of any point be out of focus. Using a flash and closing the lens' diaphragm as much as possible means highly contrasted images and sharp edges due to the large depth of field. This configuration requires the use of tripod because a closed diaphragm increases notoriously the exposure time. At the end, high accuracy results have been obtained, with residuals less than 0.3 pixels for a project of 6 photographs.

7.2.5. Calibration of the project camera

The camera used is a Sony Alpha 100, which is able to shoot photos up to 10 Megapixels, what permits to work far over the minimum recommended of 2 Megapixel. Before starting with any project, it is necessary to calibrate the camera and the lens under the conditions that are going to be used such as the focal length.

The quality of the results obtained in the project depends very much on the quality of the calibration.

The calibration procedure consists in taking photographs to a pattern of dots homogeneously distributed forming a grid from at least 6 different angles. This pattern, composed by 100 points, is provided by Photo-modeller and can be printed in a sheet of paper of several sizes. The larger the pattern is the higher the accuracy is achieved.

Since the program knows where any point is supposed to be, it can be computed what are the deviations induced by the lens, whether they are induced by a radial distortion or tangential distortion. Professional lens usually generate lower distortions, hopefully, whatever large the distortions are, the calibration process corrects them, and that permits the use of no-expensive cameras. From the calibration process, it is returned to a list of parameters corresponding to the lens, which are used to evaluate, and compare the quality of the calibrations. These parameters are divided into:

- Parameter deviation values - the calibration with smaller values is better
- Parameter correlations - the calibration with no correlations between parameters is better.
- Marking residuals (largest and RMS) - lower RMS marking residual is better.

Several calibrations have been carried out and finally the best two are selected. The first calibration has been done with a focal length of 35 mm and the other has been done with a focal length of 50 mm. In the first case, the overall RMS is equal to 0.116 pixels, and in the second case is equal to 0.138.

Table 6 Camera Calibration values

	35 mm		50 mm	
	Value (mm)	**Dev. (mm)**	**Value (mm)**	**Dev. (mm)**
FocalLength	34.4293	0.004	50.3055	0.007
Xp-principalpointx	12.1029	0.005	11.4465	0.009
Yp-principalpointy	7.8900	0.001	7.8319	0.003
Fw-formatwidth	24.2932	0.002	23.8921	0.002
Fh-formatheight	16.2206		16.0661	

	Value	**Deviation**	**Value**	**Deviation**
K1-radialdistortion1	6.59E-05	5.70E-07	-4.02E-06	4.50E-07
K2-radialdistortion2	-8.80E-08	2.60E-09	-2.61E-08	1.70E-09
K3-radialdistortion3	0.00E+00		0.00E+00	
P1-decenteringdistortion1	5.86E-06	1.20E-06	4.46E-05	1.40E-06
P2-decenteringdistortion2	0.00E+00		0.00E+00	

7.2.6. Models obtained

An amount of 7 specimens are modelled by using Photogrammetry techniques composed by 3 plates and 4 stiffened plates. The number of photos used to generate the models is 8 in order to be as much confident as possible to the results as indicated earlier. However, the number is reduced in two projects since more than 4 photographs are not strictly necessary.

The photogrammetric orientation values are presented in the following table. The first three values of each photo (Omega, Phi and Kappa) correspond to the axis rotational values and the three: Xc, Yc, Zc are the centring parameters. They are calculated by using the software Photo-modeller Scanner.

Table 7 Photogrammetric orientation parameters

	Orient.	Stiff 8	Stiff 3	Plate 7	Plate 4	Stiff 7	Plate4_B	Stiff4_B
Photo 1	Omega	0.0348	-0.1915	-54.5929	-28.9009	-0.2028	-68.1811	-41.4300
	Phi	0.0019	0.1715	-31.0470	-37.2692	0.0036	-27.9039	-41.4244
	Kappa	-0.0159	-0.1812	-140.9611	-88.6775	-0.0841	-137.4445	-91.9677
	Xc	0.0000	0.0081	-1.0164	-1.6615	0.0002	-0.9832	-1.4888
	Yc	-0.0017	0.0092	1.4600	1.0647	0.0101	1.8248	1.1929
	Zc	-0.0020	0.0000	-1.0751	-0.8759	0.0004	-1.4369	-1.1179
Photo 2	Omega	-7.2789	-10.7200	-53.4758	-3.3228	-9.1529	-37.3020	-10.3936
	Phi	21.4541	23.8445	-31.6297	-22.7252	23.6339	-38.9321	-31.5164
	Kappa	32.7981	32.4358	-141.4893	-36.8403	34.9259	-83.0367	-41.6998
	Xc	0.9940	1.1325	-1.0473	-1.0767	1.0521	-1.3841	-1.1901
	Yc	0.3433	0.4715	1.4311	0.1527	0.3844	1.0585	0.3806
	Zc	-0.1447	-0.2343	-1.0175	-0.1974	-0.3960	-0.8080	-0.3704
Photo 3	Omega	-36.6104	-41.0568	-23.1633	-0.1485	-37.3758	-8.7123	-0.1008
	Phi	28.9807	32.7305	-38.6463	-0.0431	30.8631	-23.5871	-0.1163
	Kappa	90.1340	90.2523	-86.7164	-0.0611	90.3084	-34.5831	0.0607
	Xc	1.2318	1.4824	-1.2949	-0.0022	1.3142	-0.8598	-0.0050
	Yc	1.3632	1.5165	0.6779	0.0072	1.4183	0.3100	0.0041
	Zc	-0.7986	-0.9768	-0.6043	0.0036	-1.0674	-0.2084	0.0028
Photo 4	Omega	-60.9093	-64.6924	-0.2909	-12.7954	-61.8054	-0.2663	-42.5104
	Phi	13.7936	17.8521	0.1216	20.2963	17.5779	-0.0360	40.0303
	Kappa	142.0895	135.1396	-0.1013	37.7120	138.8551	0.0608	89.3521
	Xc	0.6572	0.8784	0.0041	0.9984	0.7745	-0.0014	1.5193
	Yc	2.3358	2.3888	0.0104	0.5771	2.3538	0.0099	1.1649
	Zc	-1.4123	-1.6051	0.0014	-0.2456	-1.7017	0.0043	-1.0442
Photo 5	Omega	-64.7281	-71.4637	-12.8698	-35.8385	-65.9938		
	Phi	-6.8541	-5.7554	18.6574	27.9491	-5.9115		
	Kappa	176.5356	175.2043	44.1332	89.8852	178.0432		
	Xc	-0.2719	-0.2186	0.6798	1.4454	-0.3007		
	Yc	2.3969	2.6734	0.4523	1.5347	2.4097		
	Zc	-1.4952	-1.8339	-0.1408	-0.6411	-1.8296		
Photo 6	Omega	-57.0082	-60.6575	-34.7811	-58.3892	-57.3445		
	Phi	-26.8623	-29.1506	26.4255	19.1919	-28.6211		
	Kappa	-143.9280	-145.7560	88.6660	133.3608	-137.8163		
	Xc	-1.1959	-1.2821	0.9515	1.0116	-1.3725		
	Yc	2.0464	2.1776	1.0934	2.4477	2.0983		
	Zc	-1.3301	-1.5804	-0.5057	-1.2733	-1.6220		
Photo 7	Omega	-31.6290	-32.0639	-55.1958	-64.7945	-32.0369		
	Phi	-30.7305	-33.0504	11.1899	-3.5563	-31.5625		
	Kappa	-91.0688	-90.9034	136.4266	174.7467	-90.6248		
	Xc	-1.2865	-1.3077	0.3920	-0.1513	-1.3404		
	Yc	1.1956	1.1792	1.6007	2.7174	1.1337		
	Zc	-0.7043	-0.9347	-0.9357	-1.5266	-1.0347		
Photo 8	Omega	-7.1691	-5.6621	-64.5231	-51.5900	-6.0254		
	Phi	-19.8244	-18.8410	-14.2575	-31.7018	-17.6438		
	Kappa	-34.9641	-32.7738	178.8424	-138.5026	-37.5209		
	Xc	-0.9153	-0.8501	-0.5056	-1.6560	-0.8332		
	Yc	0.3199	0.2801	1.8291	2.0820	0.2627		
	Zc	-0.0539	-0.2317	-1.1901	-1.1553	-0.3462		

Table 8 shows the qualitative values of the projects carried out with Photo-modeller. As it can be, in the column of Max RMS (pixels) all the projects have maximum residuals smaller than one pixel.

Table 8 Quality parameters.

Name	Nº Photos	Coverage	Overall RMS	Max RMS	Min RMS	Overall RMS	Max RMS	Min RMS
			Pixels			Millimeters		
Stiff 8	8	89%	0.203	0.423	0.045	0.0224	0.0326	0.0218
Stiff3	8	89%	0.287	0.615	0.077	0.0587	0.0810	0.0568
Plate7	8	88%	0.277	0.603	0.081	0.0267	0.0289	0.0261
Plate4	8	89%	0.183	0.424	0.044	0.0194	0.0212	0.0187
Stiff7	8	89%	0.181	0.424	0.051	0.0176	0.0205	0.0171
Plate4_B	4	89%	0.193	0.544	0.019	0.0335	0.0917	0.0289
Stiff4_B	4	89%	0.127	0.329	0.017	0.0152	0.0247	0.0142

In the following figures, the images used for generating the 3D model on the left side and the 3D model itself on the right side are shown. The coordinates of the points of each specimen may be exported in RAW files, which will be used to generate mathematical functions as developed in the next chapter.

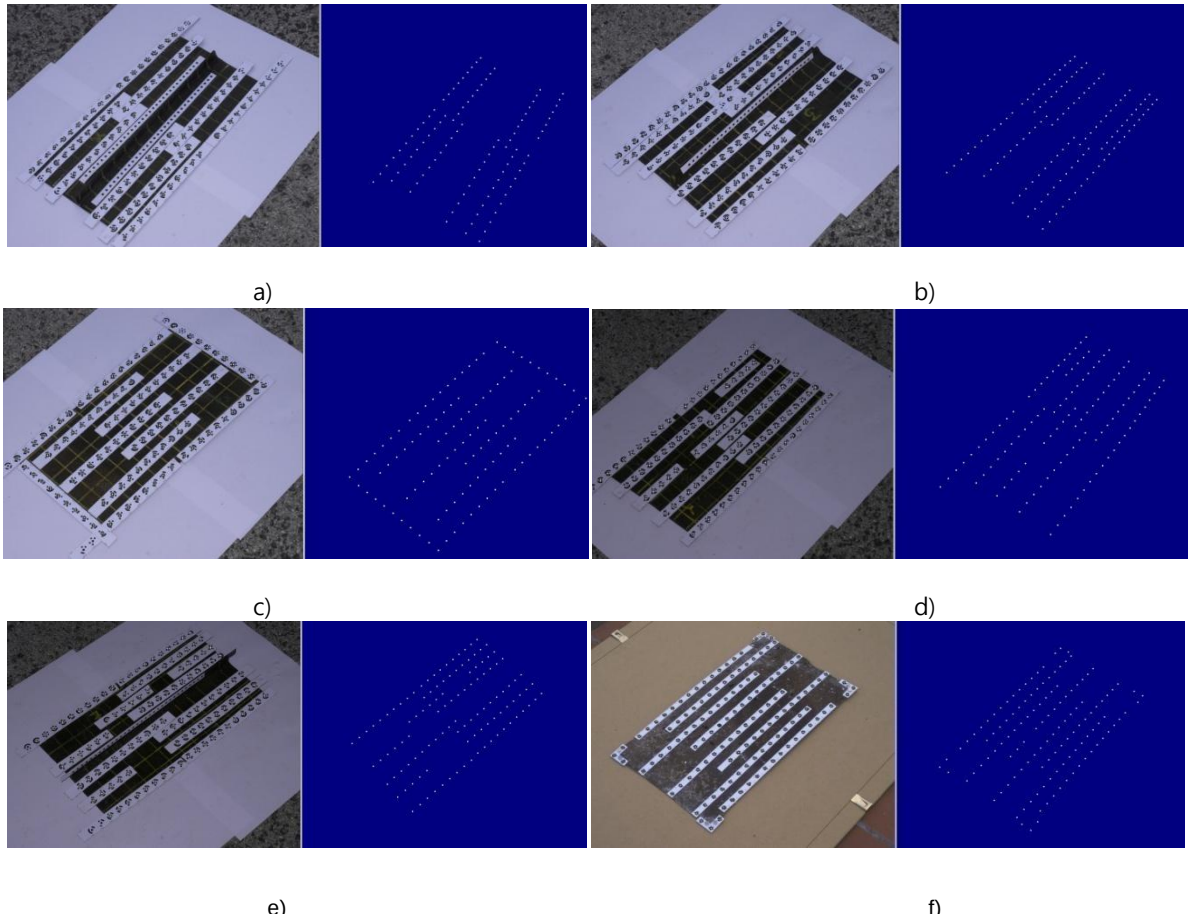

Figure 7.7 Photograph and model. (a) Stiffened 8 (b) Stiffened 3 (c) plate7 (d) plate 4 (e) Stiffened7 (f) plates 4_B

7.3. STAGE 2: PLATE MODELLING

The models of the deformed surface of the plates are generated using polynomial functions. However, it is required to decide what is the best degree of the polynomial function to be used. It depends on the complexity of the plate shape to be modelled. If the shape is totally flat, a fitting of first order in both x and y axis would be enough. However, if the plates were fully wavy, it would be necessary to use a higher order. The higher degree allows a more complex shape to be reproduced in a good quality, on the other side, the use of higher polynomial degree will involve an increase of the number of coefficients, and hence, the computational efforts. Furthermore, more wavy surfaces are created, and that can generate erroneous shapes, especially on the borders of corners.

The plates that are considered in this thesis are small pieces of a girder box. According to Hughes[67], if a rectangular plate has a single half wave longitudinally and transversely, its longitudinal curvature will be smaller than the transversal one and that means that it will resist better to buckling, and because of that, the plate itself will try to achieve a buckling shape such that the longitudinal and transversal curvatures are as equal as possible. It means that there is a relation between the longitudinal and transversal ratio (a/b) and the initial mode of deformation.

The dimensions of the plates studied have a aspect ratio a/b = 2 approximately. Thus, it is expected not to observe more than two half waves in the longitudinal axis, so at least third polynomial degree is necessary. To study the fitting behaviour of several polynomial degrees functions, it has been performed series of fittings, starting from the first degree until the fourth one. The order has been increased for both x and y axis separately. From each fitting has been calculated the correlation between the surface generated and the photogrammetric points. The goal is to study when the increase of the coefficients is not compensated with a gain of correlation.

Table 9 Adjusted R^2 of the fittings

X Deg.	Y Deg.	Plate 4 B	Plate 4 L	Plate 7	Stiff 3	Stiff 4 B	Stiff 7	Stiff 8
1	**1**	0.219	0.0791	0.0935	0.5534	0.1945	0.0627	0.6057
2	**1**	0.3773	0.2639	0.2655	0.6744	0.2024	0.4041	0.6696
3	**1**	0.4502	0.255	0.2678	0.6842	0.1918	0.4344	0.7031
4	**1**	0.443	0.2476	0.2581	0.6863	0.1846	0.4255	0.7275
1	**2**	0.7562	0.7576	0.746	0.6687	0.7576	0.4335	0.659
2	**2**	0.8137	0.965	0.9234	0.8053	0.7557	0.5559	0.7063
3	**2**	0.9326	0.9759	0.9393	0.9274	0.7516	0.6399	0.745
4	**2**	0.9489	0.9786	0.9411	0.9375	0.7459	0.6359	0.7673
1	**3**	0.815	0.7705	0.7779	0.8078	0.9505	0.515	0.7065
2	**3**	0.8786	0.9818	0.9823	0.9539	0.9564	0.6792	0.8042
3	**3**	**0.9451**	**0.9833**	**0.9826**	**0.9683**	**0.9563**	**0.6763**	**0.8068**
4	**3**	0.9647	0.9879	0.985	0.982	0.9741	0.8557	0.8424
1	**4**	0.8153	0.7683	0.778	0.8046	0.967	0.667	0.7107
2	**4**	0.8972	0.9868	0.9848	0.9544	0.9735	0.8482	0.8283
3	**4**	0.9654	0.9881	0.9851	0.9705	0.9736	0.8468	0.8315
4	**4**	0.965	0.9881	0.9849	0.9821	0.9743	0.8284	0.8514

Figure 7.8 represents the trend of the coefficient of determination (R^2) performed for all the plates studied. The trend is drawn by a surface of the second order and right after the values are available in Table 9. It can be observed that the R^2 increases while the degree in each axis increases. Despite the surface is appearing to decrease, when the degree reaches the third order, the R^2 obtained is of the same magnitude, meaning that for plates of a/b=2 fourth class of polynomial is enough to faithfully model their shapes.

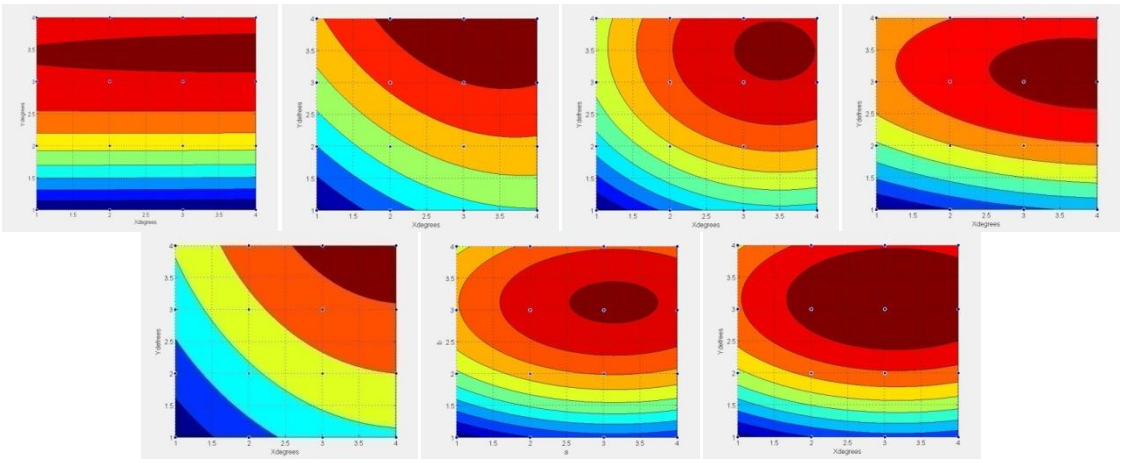

Figure 7.8 Correlation of the fittings depending on the degree of the polynomial function.

7.3.1. Polynomial Fitting

As has been seen, during many years the procedure to model the initial imperfections has been based on the Fourier sine series of one or three terms depending of the modelled surface: square or rectangular (a/b=3) plates respectively. The same plates are modelled by using the Fourier assumption and the coefficients of determination (R^2) with the data points is calculated by Sftool. These results are compared to those obtained with the polynomial methodology.

Table 10 GOF of Fourier fittings

Fit Name	SSE	R-square	Deg of Free.	Adj R-squa	RMSE	Nº Coeff
Plate4_b	217.87	0.552	126	0.541	1.315	4
Plate4	64.41	0.678	115	0.670	0.748	4
Plate4	75.07	0.625	117	0.621	0.801	2
Plate7	34.59	0.740	108	0.733	0.566	4
Plate7	47.43	0.644	110	0.641	0.657	2
Stiff3	163.71	0.173	113	0.151	1.204	4
Stiff4_b	1324.69	0.506	126	0.494	3.242	4
Stiff7	90.24	0.060	113	0.035	0.894	4
Stiff8	83.03	0.055	98	0.035	0.920	4

The amplitude of the Fourier terms is calculated using the Custom Function tool from Matlab that finds the variables that minimizes the residuals. Table 2 shows the GOF obtained from the fittings carried out using the Fourier series of 3 terms for the longitudinal direction. Additionally, it is added an independent term "c" allowing the program to centre the function so the fitting to be improved.

Very high correlations are obtained for the un-stiffened plates. That might be explained due to the fact that they present only the first mode of deformation and mainly, because the borders remain quite on the same plane as it can be seen in the contour plots.

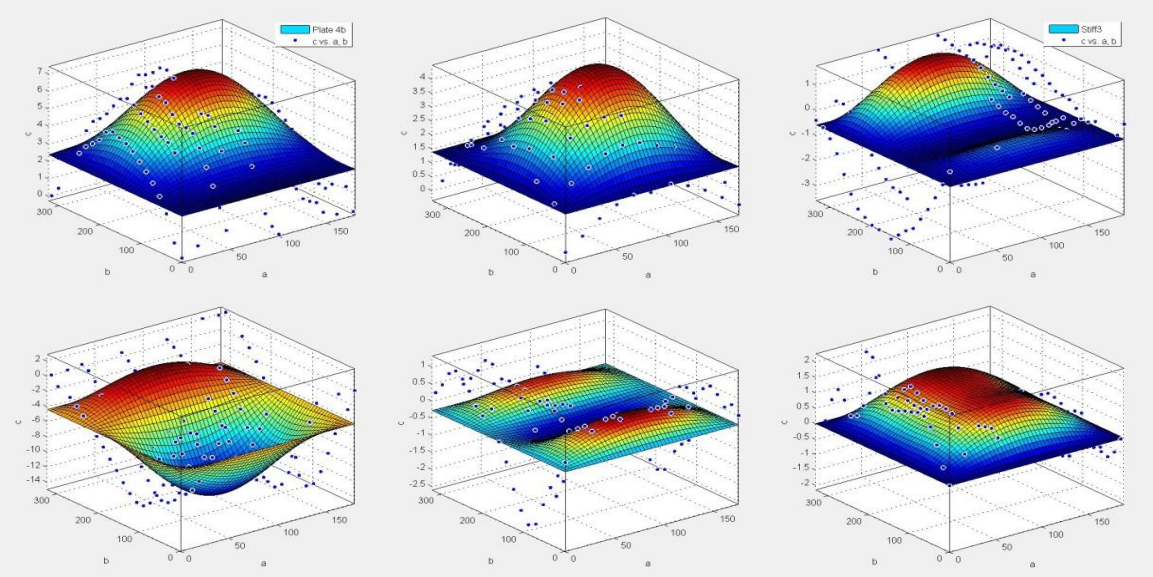

Figure 7.9 Fittings based on Fourier series

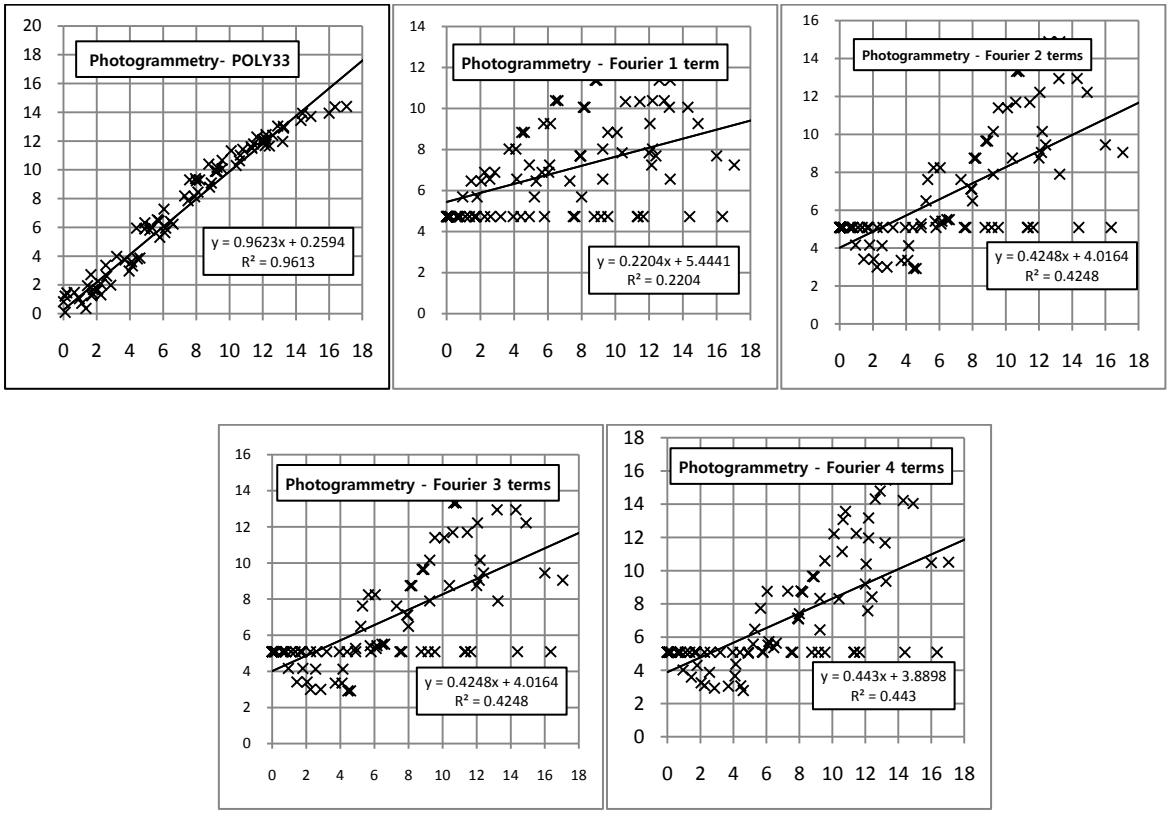

Figure 7.10 Fourier series correlations

If the number of terms of the Fourier function is reduced, only a very small correlation decrease is observed as shown for the plates 4 and 7, in both cases three terms are used. One of the main differences observed between the modelling of a plate surface by using polynomials or Fourier Series, is the fact that the trigonometric functions remain zero deformation in all the borders of the specimen, while the polynomials permit to model deformations in the borders and to improve the correlation with the real plate surface.

Finally, the correlation obtained with several Fourier functions of one, two and three longitudinal terms and only one transverse term are studied. Additionally, a Fourier function of 3 terms in longitudinal and 2 in transversal direction is also studied, observing a very little improvement as can be seen from Figure 7.10.

7.3.2. Models of plate surfaces

It has been observed that the third order polynomials, or so-called the fourth class of polynomials, are the most convenient polynomial functions of the set of plates of the present work. The lower degrees do not represent the plate faithfully and in the higher degrees do not signify a higher correlation and even in some cases it has been observed a decrease of the adjusted R-square due to the fact that the degrees of freedom increases. Only in one case, it has been observed a considerable improvement of the adjusted R-square, corresponding to the stiffened plate number 7. Matlab is used to compute the ten coefficients corresponding to the fourth class of polynomials and it has been found that while un-stiffened plates are better adjusted with only one-half wave, the stiffened plates demonstrate higher irregular shapes.

Some plates are better represented than others, and that is caused by the distortions from the dominant shape that are found in some case, for example, the stiffened plate number 7. The lower correlations correspond to those cases where the amplitude of the initial deformations are small. Contrarily, if the initial deflections are more evident, the correlation improves. In the same sense, if the plate is extremely deformed, the third order polynomial face some difficulties to represent the upper values, as it may be seen in case of the Stiffened 4B plot, where a trend is visible in the upper values.

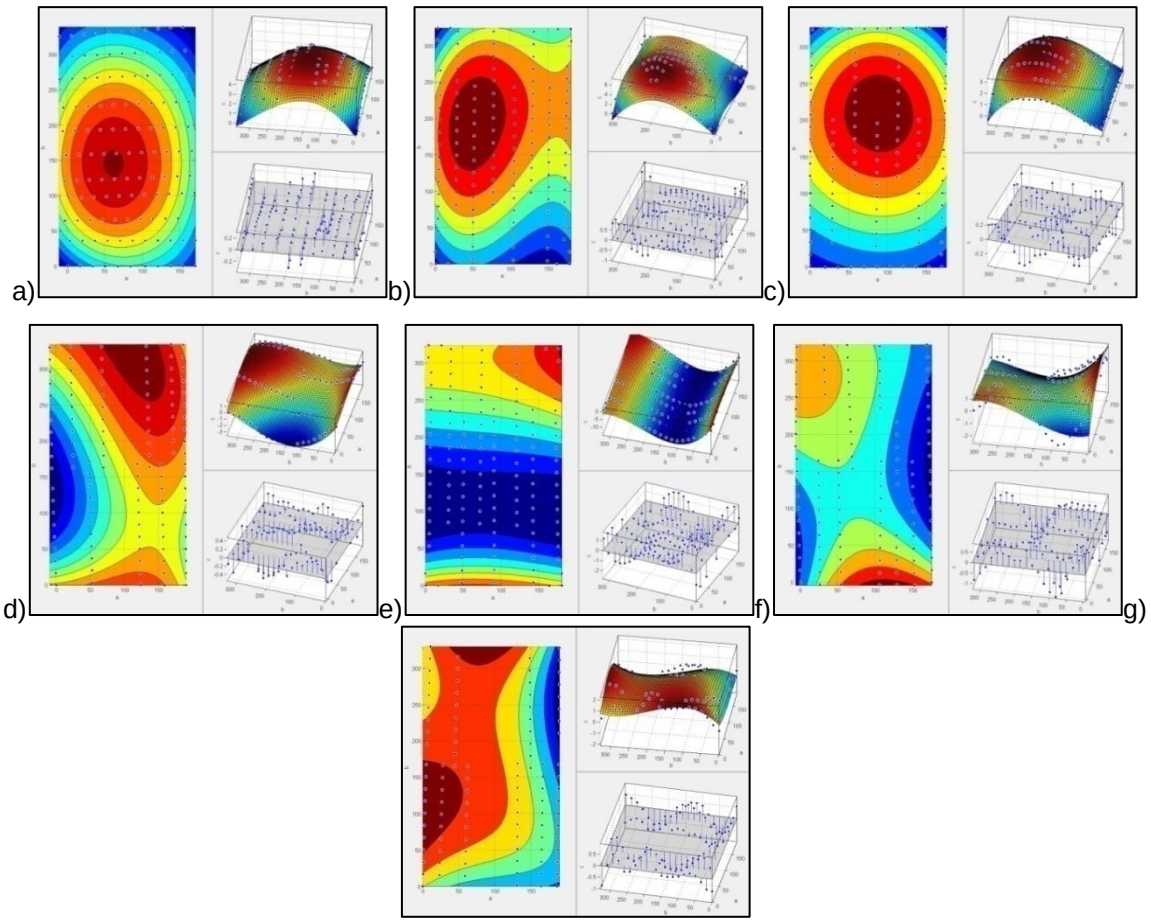

Figure 7.11 Plate modelling with polynomial fitting: (a) Plate 4 (b) Plate 4_b (c) Plate 7 (d) Stiffened 3 (e) Stiffened 4_b (f) Stiffened 7 (g) Stiffened 8

Finally, it is detected that in one case, corresponding to the Stiffened 4_b, a pattern in the correlation is visible. That is caused by the difficulties that third order polynomial presents in catching extreme deformations. While the maximum value measured by Photogrammetry is about 17 mm, the polynomial function is reaching a value of 15 mm. That could be solved by increasing the polynomial order.

The lowest value is obtained in the stiffened plate number 7. As it was outlined before, in this plate was observed that the fourth polynomial degree in the longitudinal direction would strongly improve the correlation because of the mode of deformation.

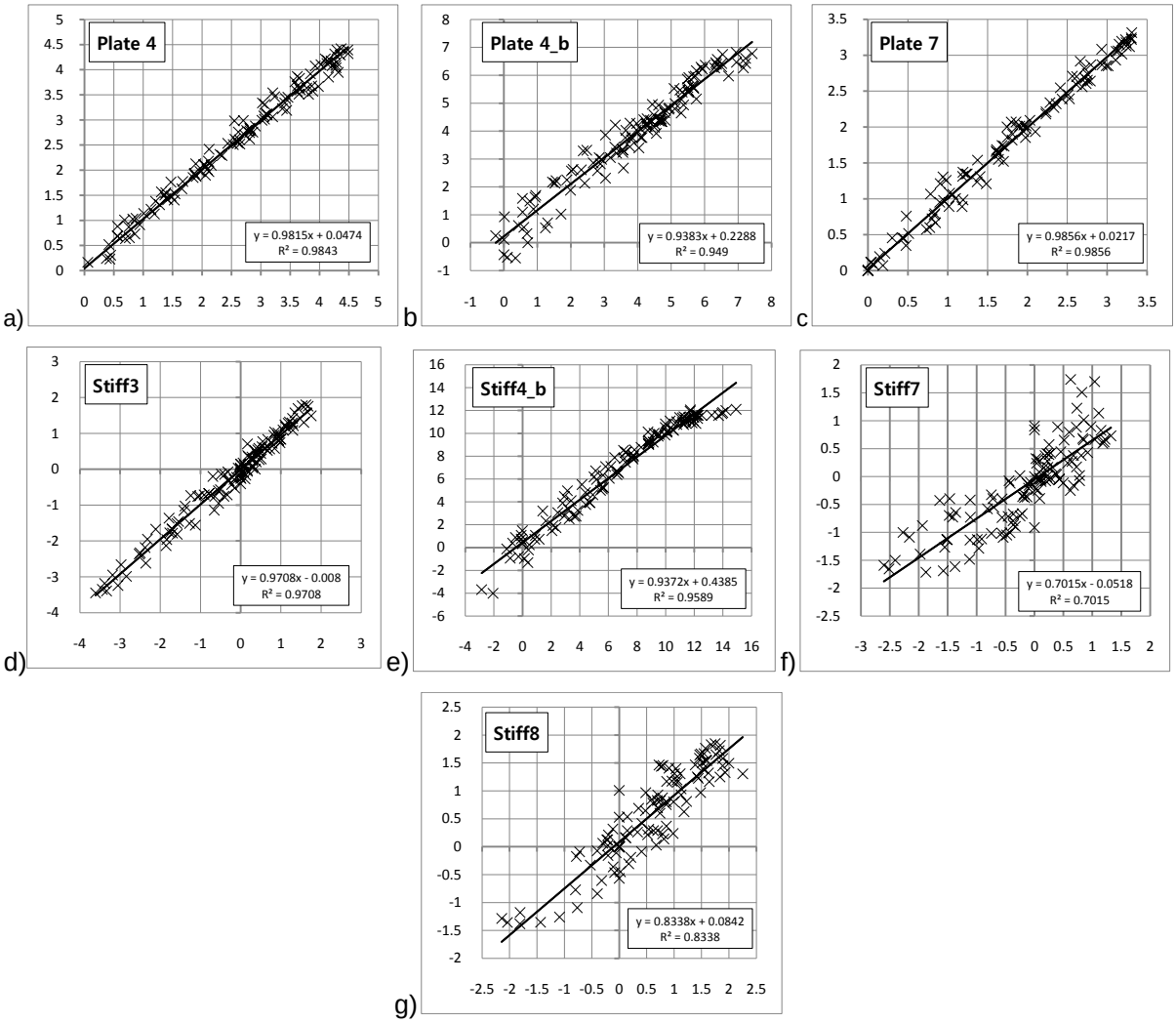

Figure 7.12 Correlation: (a) Plate 4 (b) Plate 4_b (c) Plate 7 (d) Stiffened 3 (e) Stiffened 4_b (f) Stiffened 7 (g) Stiffened 8

7.3.3. Data Systematization

In this section, a proposal to systematize the procedure for generating a script to run in ANSYS finite element analysis software is presented taking into account the data of the plate and some other parameters are necessarily to be defined. ANSYS scripts may be created automatically by using two programs, Matlab and Excel. On one side, the first program is intended to do both, to perform a surface fitting as previously seen, and to calculate the nodes of the mesh that will be generated in ANSYS. On the other side, Excel is mainly intended to write the script that will be ran in ANSYS.

The starting point of designing this procedure is to define what data is needed to carry out by a FEM analysis and how the program MATLAB needs this data to be arranged. This program allows working using commands in a script but to be functional it has to be written in a very restrained way. The objective is to find a way, whether with Matlab or Excel, to organize the project data that might be read by ANSYS. Figure 7.13shows all data necessary to proceed and how the two programs will be used to generate it.

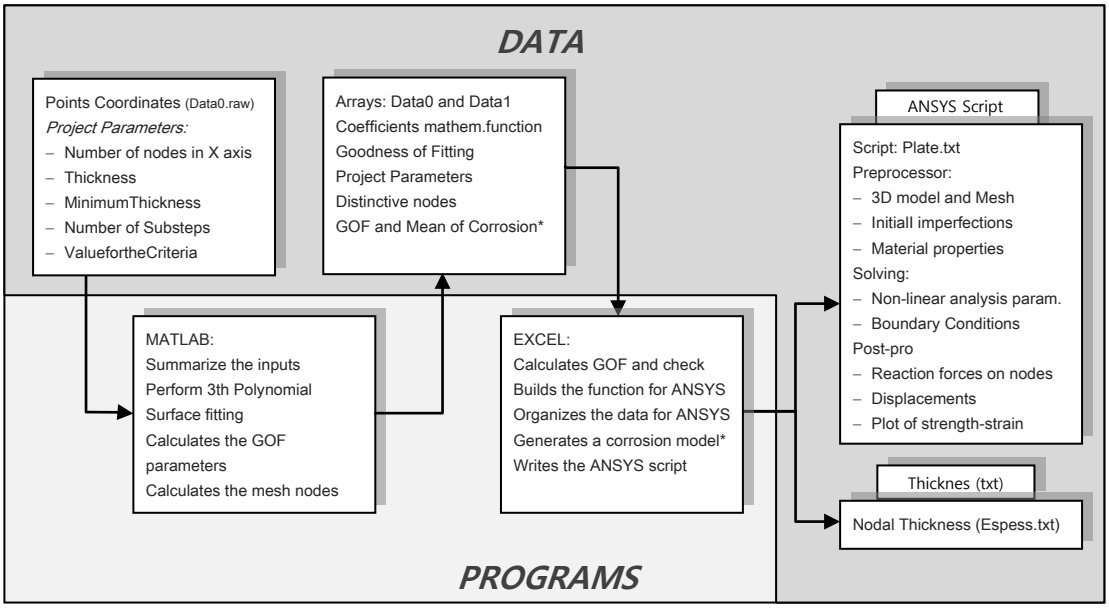

Figure 7.13Figure Systematization of the data

As it can be observed, the proposed procedure is sequential, that means that there is no need to use each program more than once. This organization simplifies the number of steps to avoid possible mistakes when managing large amounts of data. Both programs are somehow interacting with the 'User', who is asked to define some relevant parameters.

The first program to be used is Matlab, in which a macro has been written to carry out the following steps. It starts reading two sets of data. On one hand, it reads the file containing the coordinates of the points that was created with Photo-modeller (Data0.raw). At the same time, the macro asks the User for so-called *Project Parameters:*

- *Number of nodes in X-axis:* Defining the number of nodes in X-axis, leading to the element size created in the finite element model by ANSYS. The larger number of nodes the more refined the mesh is. It permits to the User to carry out several simulations only varying this parameter. This parameter accepts values from 3 nodes up to 30.
- *Height of the stiffener.* When modelling a stiffener plate, it is necessary to determine what the height of the stiffener is. By definition, it will be always set in the middle of the plate.
- *Thickness:* This parameter defines what the thickness of the plate is.
- *Minimum Thickness:* As has been seen in Section 3.3, the corrosion can be modelled as taking into account the degradation parameters. Some of these parameters are defined based on the experience, and the designer has to enter the minimum thickness of the plate.

- *Number of Substeps:* Number of steps inside one loading step to be used in non-linear analysis, the smaller the number, the faster the calculations, yet the smaller the accuracy of the results.
- *Value for the Criteria:* Control termination of the solution based on the arc - length method. Defines the maximum displacement that a control node can reach. When it happens, the simulation stops.

The way these parameters are defined depending on the type of analysis the User is carrying out. So that, they have to be organized in a specific way, as can be seen in Figure. The first step regards the two types of corrosion modelling, one based on statistical degradation parameters, and the other one, based on measurements done by the digital Photogrammetry of the plate roughness, which will be explained later.

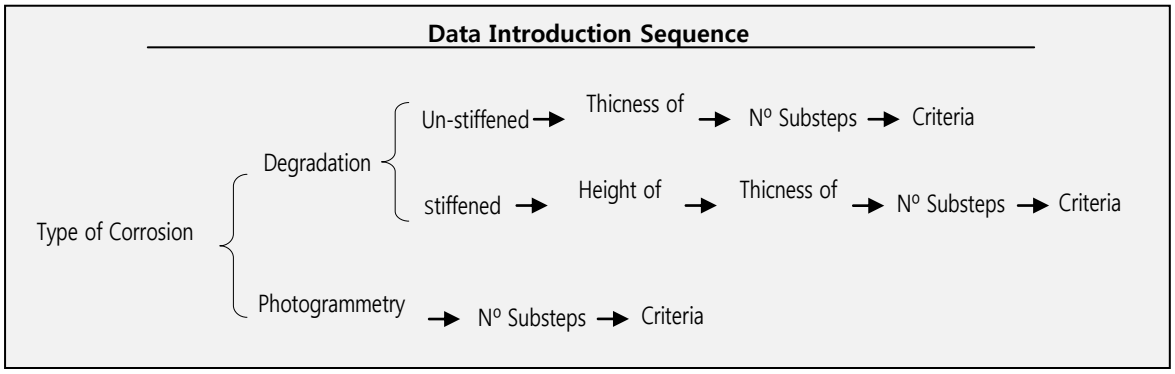

Figure 7.14Data introduction sequence

Being all these data entered in Matlab, the macro is able automatically to carry out the third polynomial surface fitting and to calculate the coefficients that minimize the residuals, and it computes the GOF to be checked out. The macro also calculates the mesh size about the number of nodes in X-axis and generates an array with nodes that will be further created by ANSYS pre-processor and their coordinates, named Data1. The reason to create this array at this point is to make possible to find those nodes that will be need later when carrying out post-processing, such as the nodes belonging to the edges.

Finally, Matlab automatically saves all the data generated in specific cells of an Excel file previously prepared. Such file is designed in a way that once the data from Matlab are entered; it is able automatically to write script files in txt to be ran in ANSYS. An excel's file carries out GOF analysis of the fitting and compares the results imported from Matlab. The results are displayed so as to the User to check if some data are mistaken. All the data corresponding to the PRE-PROCESSOR is organized with Excel, being the most utile for the polynomial function. Taking into account the polynomial coefficients, a *DO routine is entered into the script to be run with ANSYS. This way, the model of the deformed plate is as the real one. The main dimensions, the material properties, and other parameters are automatically prepared for the ANSYS script writing.

Excel's file also writes the SOLVING and POST-PROCESSOR commands for ANSYS. In the former case, Excel uses the information introduced by the User in Matlab and that automatically are stored in Excel's file. The boundary conditions are adjusted at this point, and they can be manually modified. As for the latter, Excel uses the array of nodes calculated in Matlab, as well as the distinctive nodes corresponding to the edges to set the reaction forces and displacements to be caught in the HIST-POST PROPCESSOR. Doing this, it is possible to plot the strain-strength graphs and to analyse the ultimate strength.

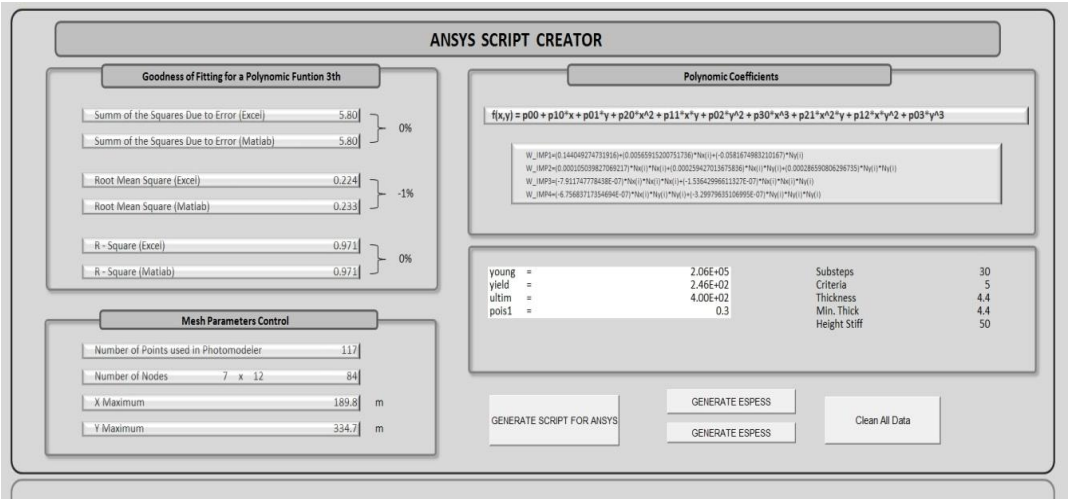

Figure 7.15 Capture of the Excel interface

7.3.4. Corrosion Modelling

Despite the fact that this thesis has a principal objective to model the initial imperfection of steel plates by using analytical Photogrammetry, a study has been carried out to model corroded surface based on digital photogrammetric measurements. As indicated in Section 3.3, the corroded plate surface can be modelled based on degradation parameters of corrosion that induces a reduction of the strength capacity of the plate. These parameters are based on real mechanical measurements. This approach has been used for modelling the corroded plates in the analysis carried out in this thesis. This type of modelling it has been called *Degradation Parameters type.*

In this type of modelling, the User has to set the thickness of the plate and the 'minimum' degraded thickness of the plate. The larger the difference between the thickness and the minimum thickness, the larger the degradation of the plate is. The thickness of each node is randomly assigned in a way that the mean thickness and the standard deviation are attained. These two parameters depend of the mean and standard deviation of the so-called *corrosion depth* parameters. The mean, standard deviation and COV used for the present analysis are 1.5, 2.5 and 0.8 respectively. Figure 7.14 shows an example in which a corroded plate has been modelled as a residual plate of 5mm and with a minimum thickness of 2mm.

The objective of corrosion depth modelling based on the digital Photogrammetry is to catch the surface degradation. The digital Photogrammetry is able to detect not only the trend of the shape but also the roughness of the surface in very small details. Knowing the roughness, as well as the location of each node of the finite element model it is possible to determine the corrosion characteristics corresponding to any particular node.

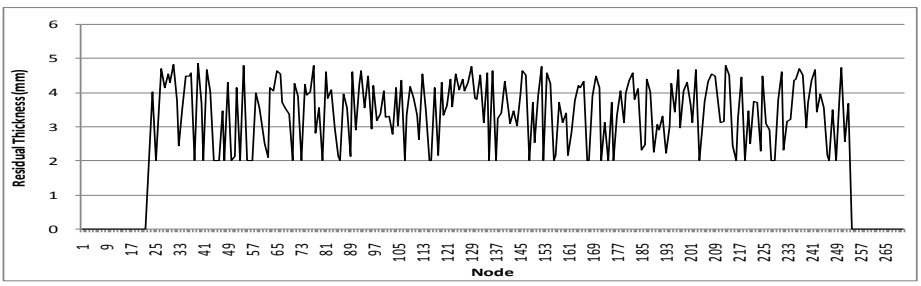

Figure 7.16 Corrosion node distribution

The procedure is composed of the following steps: a) select an arbitrary node of the mesh whom coordinates are known, b) select all the points from the cloud surrounding that node, c) fit a first order polynomial surface to that set of points and d) compute the RMSE and R-square of the fitting as well as the mean of the heights of the points. This is done for each node of the mesh. Having this information there are several ways to proceed, such as considering the mean or generates qualitative indexes. The way chosen in this work is to choose the RSME.

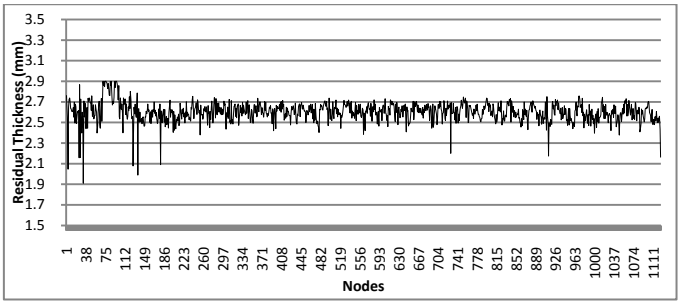

Figure 7.17 Corrosion node distribution from Digital Photogrammetry

From Photo-modeller, it is possible to obtain a very dense cloud of points, where each point belongs to the real surface. As an example, for a plate sizing 180x320 mm, the number of points might be of over 1.500.000. To proceed, a routine is defined in Matlab. It is aimed to select each node of the mesh created by Matlab itself with regard the mesh size and to be equal to the one of the finite element model, and searches all the points surrounding it. With these points are created a set of points from which the mean value and standard deviation are computed. The results obtained are stored in an array called Data2, which is automatically exported to the Excel file.

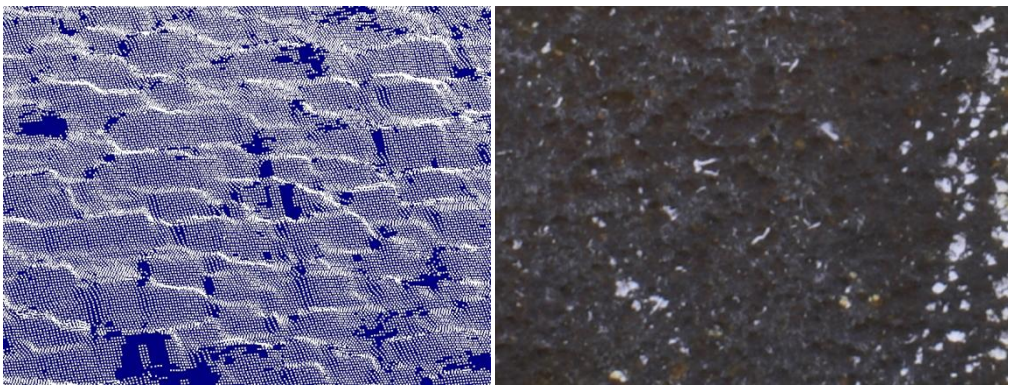

Figure 7.18 Cloud of points for corrosion modelling

In both types of corrosion modelling, Excel file creates an export file called 'Espess'. This file is read by a command included in the ANSYS script and assigns the thickness corresponding to each node. The procedure using the digital Photogrammetry requires large computational efforts since it needs the mesh to be very refined to respect the roughness of real corroded plate surface. On the other hand, a further investigation should be needed to analyse the accuracy of the cloud of points because some wavy patterns seem to be appearing. Strength Assessment Simulations

7.4. FINITE ELEMENT ANALYSIS

One of the objectives of this thesis is to assess the ultimate strength of plates, which geometry has been modelled using photogrammetric measurements. The buckling and post-buckling behaviour are analysed for all specimens. The analysis is carried out based on Finite Element Method using commercial software ANSYS.

Following the methodology introduced in the previous chapter, it is possible to prepare a finite element model to be run using ANSYS. Relying on script macros, the model of the plates may be created. The parameters necessary to solve the problem can be defined and finally, the response data might be obtained to study the ultimate strength results.

The plates are modelled by nonlinear shell elements SHELL181 of four nodes and each node having 6 degrees of freedom. This type of element permits to set up non-linear and multi-linear material properties. The nonlinear material properties are defined as MISO, that is, multi-linear isotropic hardening and three points are defined as zero stress-zero strain; yield point/young modulus-yield point and 0.2 -ultimate strength.

7.4.1. Mesh Size

There are four requirements that should be satisfied in order to achieve a monotonically convergent solution:

- Continuous behaviour of the approximation displacement function within the element, that is, no oscillations of the line trend.
- Compatibility along the common nodes, boundary or surfaces between adjacent elements, that is, no spaces and gaps between elements.
- Ensure the constant variation of the field variable ϕ and its derivatives, that is, permit the rigid body motion of the element if need to be.
- Geometric isotropy for the same behaviour in each direction, that is, the possibility of increasing the degree of order matching the number of coefficients with the number of nodes, removing, if necessary, some of the higher order elements.

The convergence for the problems considered in this thesis is studied to decide what the most appropriate mesh size to be used is. In the y-axis, it is plotted the Ultimate Strength of the plate and in the x-axis, the number of nodes of the mesh.

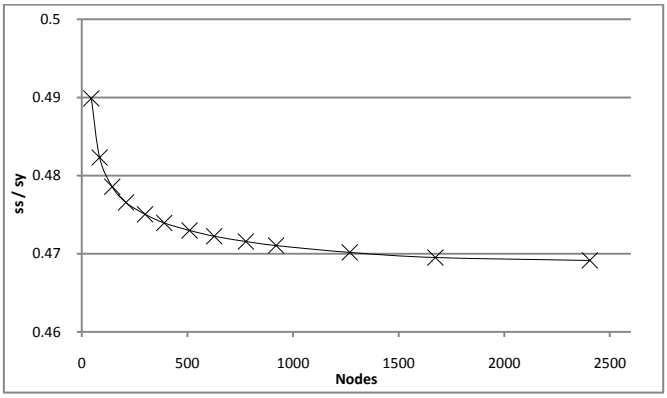

Figure 7.19 Monotonic convergence

From the graphs it might be concluded that, firstly, the solution converges monotonically, and secondly that no significant improvement of the results are obtained from meshes more refined than 1000 nodes. So that, the mesh is defined by the use of 25x36 nodes approximately.

7.4.2. Boundary Conditions

The specimens that originally are part of a global integral structure depend not only on the geometry and material properties but also on the position they occupy in the structure. Two boundary conditions are considered, differently for un-stiffened plates and stiffened plates.

Table 11 shows the boundary conditions that are considered here. In the case of plates, the longitudinal edges are constrained in both $x - axis$ and $z - axis$, representing the longitudinal stiffeners surrounding it. As for the transversal axis, the displacements of the edge $Y = 0$ are fully constrained and in the edge of $Y = L$ the longitudinal uniaxial pressure is applied. The rotations are allowed on the corresponding plane such as a simply supported structure is modelled. Regarding the stiffened plates, the boundary conditions are very similar. The main difference consists in leaving one of the longitudinal axis free. In both cases the nodes where the pressure is applied are coupled, that means that all the modes displace in the same way.

Table 11 Boundary Conditions

Boundary Conditions of UN-STIFFENED PLATES							Boundary Conditions of STIFFENED PLATES					
	Rotation			Displacement			Rotation			Displacement		
	X	Y	Z	X	Y	Z	X	Y	Z	X	Y	Z
Y=0	F	F	F	C	C	C	F	F	F	C	C	C
X=a	F	F	F	C	F	C	F	C	F	C	F	F
Y=b	F	F	F	C	F	C	F	F	F	C	F	C
X=0	F	F	F	C	F	C	F	C	F	F	F	F

For each of the specimens, two scenarios are presented: deformed shape considering the measurements taken from Photogrammetry and deformed shape taking into account the trigonometric deformations with a maximum amplitude of $w_0 = 0.12\,\beta^2$ as proposed by Antoniou [33]. The following plots present the stress-strain curves in which the stresses are presented as a ratio of the yield stress point of the material, so-called Average Stress Ratio (ASR), and the strain is presented relative to the yield strain of the material.

7.4.3. Un-stiffened Plates

The first specimens to be analysed are the un-stiffened plates: Plate 4, Plate 4B and Plate 7. Initially the plates are considered not to be affected by the corrosion. As it was expected, the deformations induce a decrease of the load carrying capacity of the plates and the ultimate strength is reduced to the half of the yield stress approximately. As it can be seen, in the three cases the UTS reached in the models deformed using Fourier functions are slightly higher than the ultimate strength capacity attained in the models based on the photogrammetric measurements.

When studying the stresses and the deformation of the plates in more detail it may be observed some

differences between the two types of modelling. As an example, the behaviour of the Plate 4B is studied in more detail.

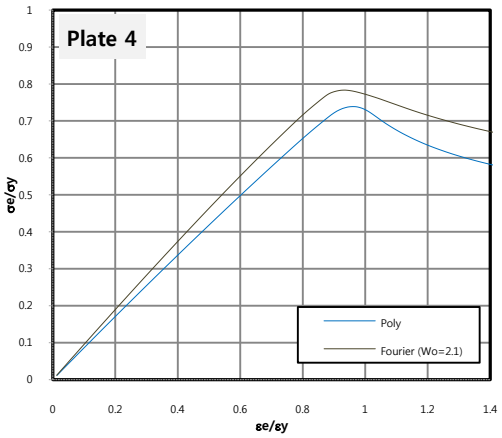

Figure 7.20 Un-Stiffened 4. Strength-Strain curves of different deformation modelling types

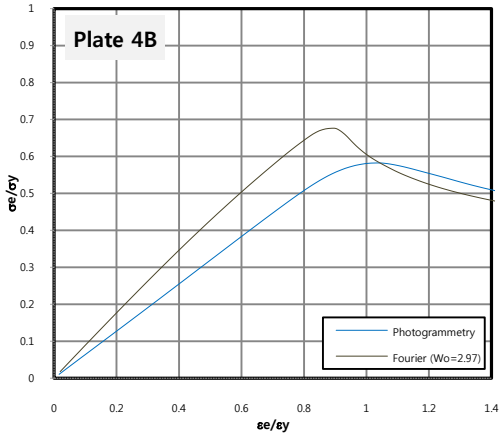

Figure 7.21 Un-Stiffened 4B. Strength-Strain curves of different deformation modelling types

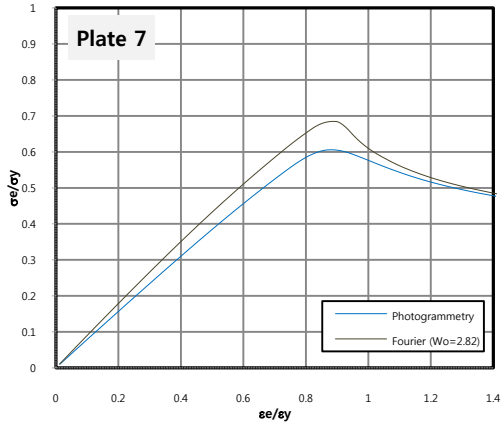

Figure 7.22 Un-Stiffened 7. Strength-Strain curves of different deformation modelling types

Figure 7.23a plots the $z-axis$ deformation and Figure 7.23b, the Von Misses stresses on the plate modelled using the Fourier functions, both corresponding to the moment at which the ultimate strength is reached. It is appreciable that there is symmetry in both axes. This symmetry is found from the beginning of the load application up to the UTS, and after this point, the plate behaves asymmetrically. On the other side, Figure 7.23c and Figure 7.23d show the deformations of the $z-axis$ and Von Mises stresses respectively of the plate modelled using the photogrammetric measurement. In this case, it is not observed the symmetry seen before and consequently, a decrease of the strength is observed. Furthermore, the strain at which the UTS may vary depending of the level of asymmetries.

As can be seen from Figure 7.11, the model of the plate 4b was found to be less symmetric than plates 4 and 7, because of that, the response of the plate, represented by the strength-strain plate, is noticeable different compared with the Fourier model. In all the cases, the buckling shape is the same, and that could

be explained because the initial mode of deformation defined by Photogrammetry is the same as the one generated with trigonometric functions, the first mode. However, that does not necessarily mean that all the un-stiffened plates will be of the same mode and consequently, different behaviours could be found.

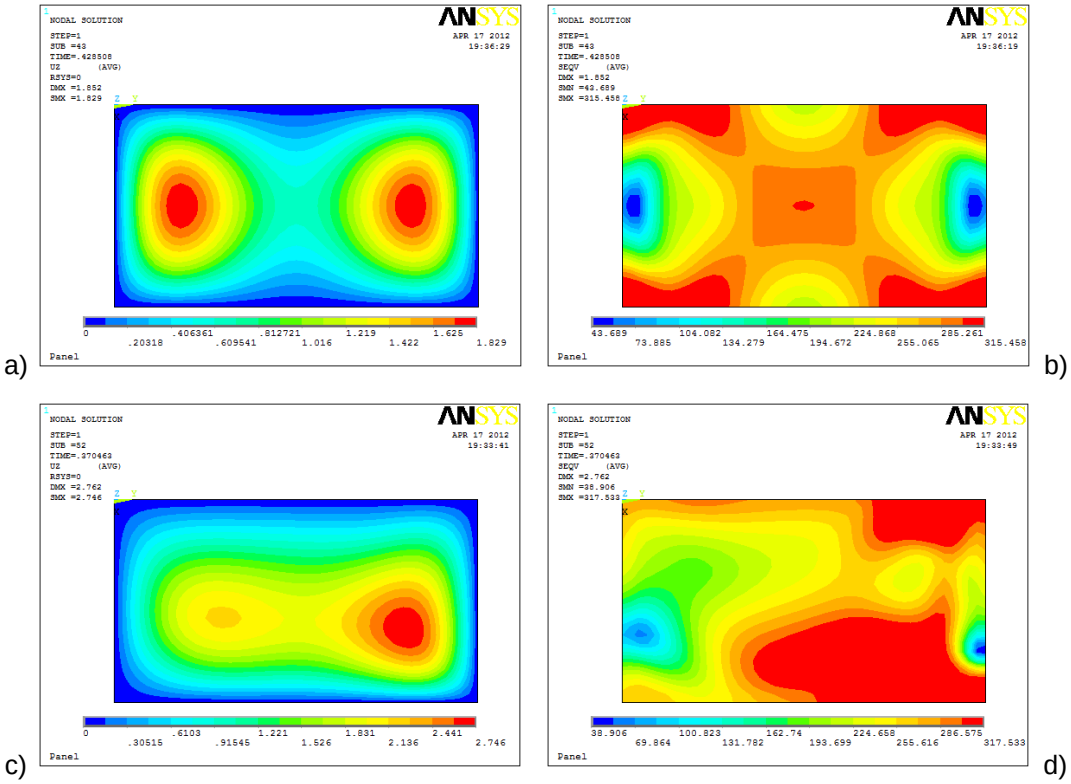

Figure 7.23 Plate 4B deformation plots

7.4.4. Stiffened Plates

Similar procedure has been used with the stiffened plates. Because of the presence of the stiffener attached to the plate and due to the fact that the boundary conditions are different, the results obtained are different. Attending to the graphs, it is appreciable that stiffened specimens 4, 7 and 8 perform similarly while the stiffened plate number 4B behaves in a different manner. This is because of the fact that the initial deformations of the specimen 4B conduce to a very early plate overall buckling.

It has been seen that asymmetries cause a strength reduction in un-stiffened plates, however, in stiffened plates the asymmetries may cause a rise of the ultimate strength compared to the values obtained with the Fourier models.

Attending to the plots of displacement it may be seen that the plates are influenced not only by the slenderness but also by the shape of the initial deformations. Within the pre-buckling part, the initial imperfections are amplified once the load is applied and as the buckling capacity is approached, the plate gradually changes the shape in order to adopt its lowest energy shape. In the case of the Fourier models, the initial dominant shape is one-half sine wave while the lowest energy corresponds to two half-sine waves. The transition from the first shape to the other is done in a short piece of time and consequently the

strength-strain curve presents a sharp slope change. Such event can also be checked out from the figures of displacements and stresses.

On the other hand, the models analysed using photogrammetric measurements present asymmetries in both axis similar to the un-stiffened plates. These asymmetries are found to be very influential in the behaviour of the plate for mainly two reasons. The first reason is related to the lowest energy shape, that, while in the models done with Fourier functions is found to be of two-half sine waves, in the photogrammetric models are of different shapes in each case. As an example, Figure 7.28and Figure 7.29 show the shapes of the plates 3 and 8 at the ultimate strength capacity. The plots on the left correspond to the plate modelled using trigonometric Fourier functions while the plots on the right show the model based on photogrammetric measurements.

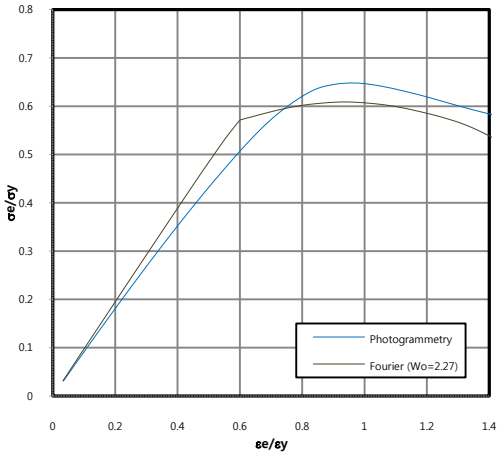

Figure 7.24 Stiffened 3. Strength-Strain curves of different deformation modelling types

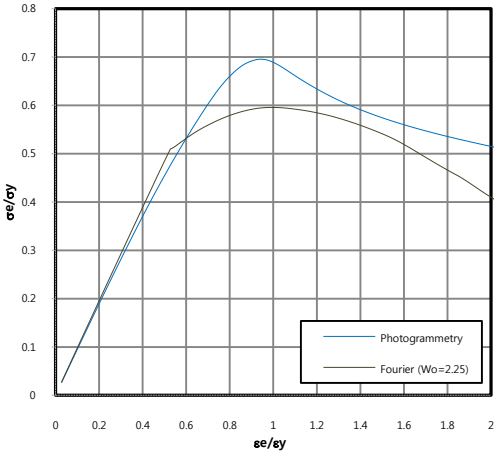

Figure 7.25 Stiffened 7. Strength-Strain curves of different deformation modelling types

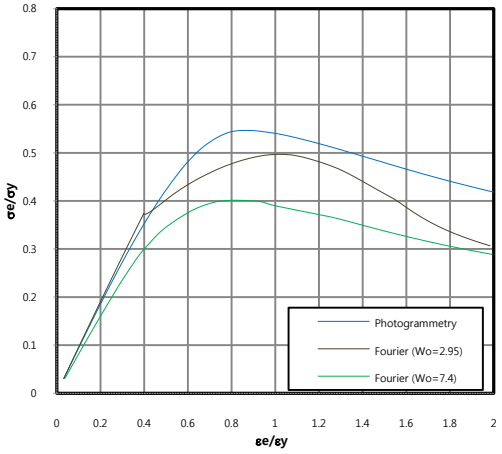

Figure 7.26 Stiffened 8. Strength-Strain curves of different deformation modelling types

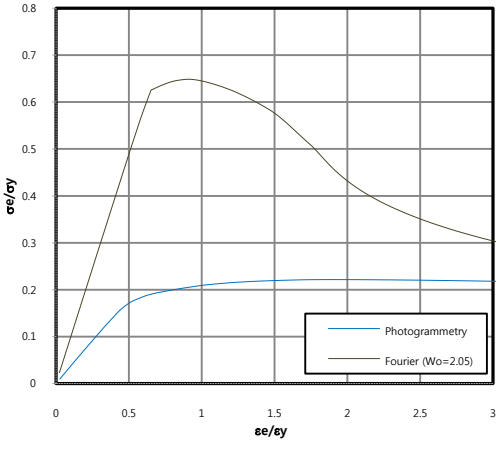

Figure 7.27 Stiffened 4B. Strength-Strain curves of different deformation modelling types

As it can be seen, the displacements of the Fourier models are symmetric and the lowest energy shape has been found always to correspond to the second mode of deformation that is of two-half sine waves. On the

other hand, the shape of the photogrammetric models at the ultimate strength point may adopt various forms, being dominated by the initial out-of-plane deviations, and because of that, the strength varies in each case.

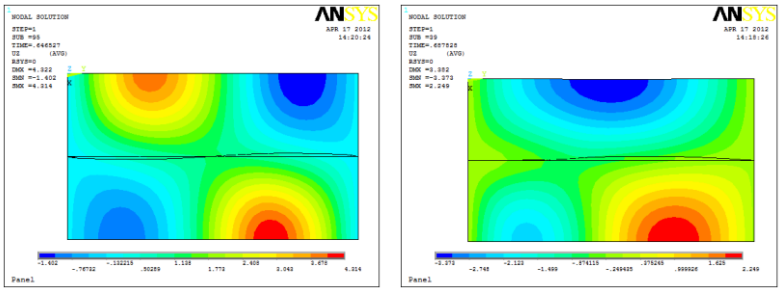

Figure 7.28 Displacements at the Ultimate Strength of the specimen Stiff 3.Fourier and Photogrammetric model.

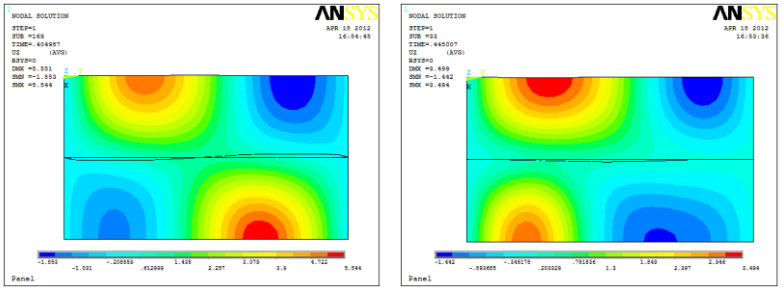

Figure 7.29 Displacements at the Ultimate Strength of the specimen Stiff 8.Fourier and Photogrammetric model.

The second reason is related to the transition of the shapes that plates adopt. Since the initial distortions of the photogrammetric models are more dominant than the one of Fourier cases, the plates do not perform any transition, and thus, there is no any sudden change of the strength-strain curve slope. Evidently, the asymmetries observed in the displacements may be seen in the von Misses stresses. Figure 7.30represents a stress distribution of the stiffened plate 7when the ultimate strength is reached.

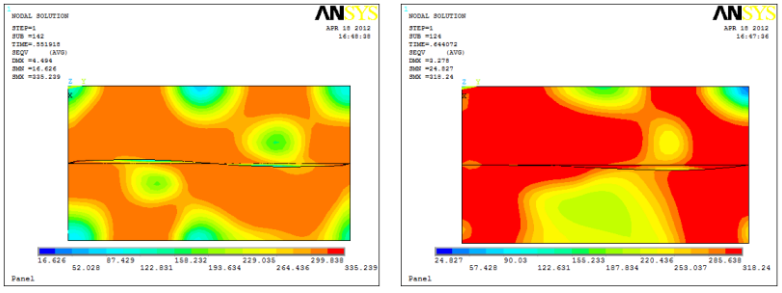

Figure 7.30 Stresses of the plate Stiff 7, Fourier model and Photogrammetric model, respectively.

7.4.5. Corroded Plates

In the latter section of this chapter, it has been carried out an analysis where the corrosion is modelled using the digital Photogrammetry. This procedure has been done using the specimen stiffened 4B, which has been treated as a un-stiffened plate. Using Photo-modeller, it has been created a cloud of points following the surface roughness from photographs, having this cloud the corrosion may be computed as explained in the Section7.3.4.

To make a comparison of the results, three simulations based on three different models of corrosion degradation are carried out. The first model considers the plate without any corrosion and the thickness has been set up of 2.9 mm; the second, takes into account the corrosion, modelled using digital photogrammetry (Type 2) where the mean value thickness is of 2.61mm, the standard deviation is 0.0964 mm and the COV is 0.037; the third model is randomly corroded by using the same parameters obtained from photogrammetry, that is, mean value thickness of 2.63 mm, standard deviation 0.097 mm and COV 0.037 (Type 1).All the models have been deformed using Fourier functions with an amplitude of $Wo = 2.05$ and the results are shown in the Figure 7.31.

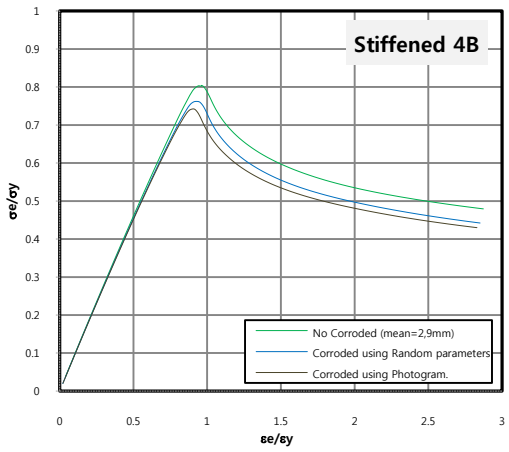

Figure 7.31 Types of corrosion modelling

It can be observed that despite the statistical values of the two corrosion types modelling to be the same, the plate behaves slightly different. The Figure 7.32shows the displacements of the plate and the stresses at UTS of the non-corroded model (left), corroded model using a random distribution (central) and corroded model using the photogrammetric data (right). It is observed that the displacements and stresses in the photogrammetric model are more irregular compared to the random distributed model. The displacement figures also show that in the case of the random distributed model the plate reaches the maximum load carrying capacity being more symmetric than the photogrammetric model.

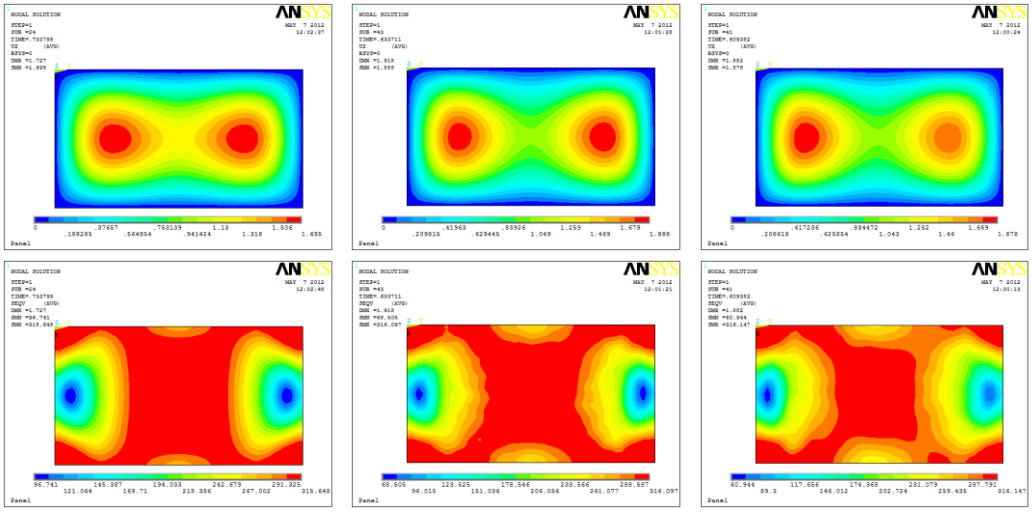

Figure 7.32 Displacements and Stresses of non-corroded model, Random corroded model and Photogrammetric corroded model, respectively

7.5. DISCUSION

The Table 12 shows the ultimate strength of plates based on different initial imperfection models: modelled using Fourier functions and modelled using polynomial functions from photogrammetric measurements. Apart from the case of the stiffened plate 4B, the un-stiffened plates showed more optimistic UTS in the models based on Fourier functions while in the stiffened plates more optimistic results are obtained from the photogrammetric ones.

The results obtained from the photogrammetric models are more variant and even in one case -stiffened 4B- the results are completely different from the Fourier models. This is owed to the fact that models based on Photogrammetry consider the geometrical particularities of each plate that might be deformed in a different manner than the others.

Table 12 Ultimate Strength of the plates with regard to the type of modelling

Name	Thickness	Slenderness	ϕ uF/ϕ y	ϕ uPH/ϕ y
Plate4	2.70	2.5	0.78	0.74
Plate4_B	2.01	3.5	0.68	0.58
Plate7	2.02	3.4	0.68	0.61
Stiff3	2.90	2.6	0.61	0.65
Stiff4_B	2.90	2.4	0.65	0.22
Stiff7	2.50	2.7	0.60	0.70
Stiff 8	2.22	3.3	0.50	0.55

When comparing the behaviour of un-stiffened plates modelled with Fourier and Photogrammetric basis, the following conclusions may be drawn:

- The initial deformation of the un-stiffened plates, modelled by the Photogrammetry, are similar to those generated by the trigonometric Fourier functions. The initial mode of deformation is found to be the same, the first mode. However, despite both models being more alike than the case of stiffened plates, two singularities are still remarkable: the small asymmetries that are not considered in Fourier models and the out-of-plane borders. These singularities and the fact that the initial

amplitude is not the same bring the results to be different.

- The difference of strength between the two modelling types is approximately of 10% in the studied cases. The lower values obtained for the photogrammetric models might be induced by the asymmetries found in those models.

- The more differentiate strength-strain curve corresponds to plate 4B, that it is found to be the more asymmetrical shape in the plate modelling stage. The differences are found not only in the ultimate strength but also in the strain that it is reached.

From the comparison between the behaviour of stiffened plates modelled with the Fourier and Photogrammetric basis, the following conclusions may be drawn:

- The strength-strain curves obtained from models done with Fourier functions and Photogrammetric models are slightly different in terms of the shape as well as the ultimate strength is reached.

- In the case of the un-stiffened plates, the asymmetries cause an ultimate strength reduction when compared to the Fourier models. On the other hand, it seems to provoke a strength improvement in the case of stiffened plates. Such effect might be caused by the opposition of the initial imperfections to the lowest energy configuration shape, strengthen to specimen.

- In one case, stiffened plate 4B, the plate is initially very deformed and plate-induced overall buckling is easily identifiable. Such imperfections bring the specimen to lose its load carrying capacity very early. This eventuality is a proof that the photogrammetric strength assessment ensures a more accurate knowledge of the real strength capacity of plates.

Finally, from the procedure of corrosion modelling, the following conclusions may be outlined:

- Digital photogrammetric procedure is able to catch the distribution of the corrosion depth along the surface of the plate. If it is the case that in some parts of the plate the degradation of the plate is more severe, then, the plate may lose its strength capacity due to these particularities and may induce an asymmetrical deformation. In the example carried out in this work, such asymmetries have been detected in the photogrammetric model, which leads to the loss of its load carrying capacity earlier than the one modelled by the use of random parameters.

8. CONCLUSIONS AND FUTURE WORK

8.1. CONCLUSIONS

Along the years, the initial imperfections of plates have been modelled using the Fourier functions to assess their load carrying capacity. In this thesis, it has been proposed a new procedure, based on photogrammetric techniques, that allows the generation of models taking into account the real shape of plates.

This procedure involves several steps that are identified and organized in such a way so that the strength assessment may be carried out in an easy and reliable manner. The procedure is mainly composed by three stages that are coincident with three dusting techniques: Photogrammetric modelling, Surface Fitting, and Finite Element Analysis. The background of these techniques was discussed herein as well as their potentialities and drawbacks. In order to achieve the final objective, it is proposed a methodology that integrates the three techniques. This methodology is designed in a way that the accuracy is maximized while the number of the steps and the time is minimized.

Based on this methodology, the faithful geometry models of seven plates, three un-stiffened and four stiffened ones, originally belonging to a box girder were analysed. These models have been used to carry out finite element analysis. The results obtained are used to perform some comparisons between the photogrammetric models of initial imperfection and other types of modelling. It has been proved that photogrammetric models are able to catch the asymmetries present in the real plates. Such asymmetries are very influential to the plate configuration.

Finally, it has been presented a procedure to study the corrosion of plates by using the digital Photogrammetry. This procedure that relies on stereographic photographs permits to generate very fine cloud of points of the surface of the plate. In order to compute the corrosion of the plate, the dispersions of the cloud around a certain point have been related to the roughness of the surface. This procedure has allowed detecting the real distribution of the corrosion degradation along the plate and as a result, different behaviour has been observed.

8.2. FUTURE WORK

The study presented in this thesis is based on seven real specimens that are modelled and analysed by finite element method. It would be recommending testing these specimens against ultimate strength in order to develop comparisons between the experimental and numerical results. In addition, and since the methodology allows to carry out plates' analysis in a fast and easy way, it would be possible to enhance the number of specimens to be studied and compared.

Noteworthy is that the procedure developed is based on third order polynomial surface fitting to represent the plates under study. Such technique has been proved useful for a specific range of dimensions and aspect ratios, however, for larger plates or structures it would be necessary to develop other techniques based on

parametric fitting such as Beizer and B-splines. It would permit to carry out a strength assessment of ship hull blocks in the post-manufacturing phases or directly of whole ship hulls before launching or in operation surveys.

Finally, this work initiates a way to assess the level of corrosion based on digital Photogrammetry. Despite the investigations are not going far, the solutions here proposed would be used to find new reliable methods to measure the degradation of marine structures from stereographic images.

9. REFERENCES

1. Paik, J.K. and B.J. Kim, *Ultimate strength formulations for stiffened panels under combined axial load, in-plane bending and lateral pressure: a benchmark study.* Thin-Walled Structures, 2001.

2. Paik, J.K. and S.J. Kwan, *Nonlinear finite element methods models for Ultimate Strength analysis of steel stiffened-plate Structures under combined biaxial compression and lateral pressure actions. Part 1: Plate elements.* Thin-Walled Structures, 2008: p. 10.

3. Chi, L.E.W., G.Y. Grondin, and A.E. Elwi, *Interaction Buckling Failure of Stiffened Steel Plates.* University of Alberta - Department of Civil & Enviromental Engineergins, 2006(Structural Engineering Report No. 264).

4. Carlsen, C.A.a.C., J., *The specification of post-welding Distortion Tolerances for Stiffened plates in compression.* The Structural Engineer, 1978. **56A**(5): p. 133-141.

5. Guedes Soares, C., *Uncertainty Modelling in Plate Buckling.* Structural Safety, 1988. **5**: p. 17-34.

6. Frankland, J.M., *The strength of Ship Plating under edge compression.* U.S Experimental Model Basin Progess Report, 1940. **469**.

7. Smith, C., *Compressive strength of welded steel ship grillages.* Trans RINA, 1979. **117**: p. 325–359.

8. Guedes Soares, C. and J.M. Gordo, *Compressive Strength of Rectangular Plates Under Biaxial Load and Lateral Pressure.* Thin-Walled Structures, 1996. **24**: p. 231-259.

9. Koelman, H.J., *Application of a photogrammetry-based system to measure and re-engineer ship hulls and ship parts: An industrial practices-based report.* Computer-Aided Design, 2010. **42**(8): p. 731-743.

10. Zaplatic, T., *Dimensions and Shape Control of Sub-assembled Sections using Digital Photogrammetry.* 2008.

11. Julia Armestoa, et al., *FEM modeling of structures based on close range digital photogrammetry.* Automation in Construction, 2009. **18**(5): p. 559-569.

12. Ljubenkov, B., T. Zaplatic, and K. Ziha, *Measurements for reliability of ship design.* Production and operation interacion, 2008.

13. Remondino, F. and F. Menna, *Image-based Surface Measurement for Close-Range Heritage Documentation*, in *The International Archives of the Photogrammetry, Remote Sensing and Spatial Information Sciences*2008: Beijing, China.

14. Menna, F., et al. *Digital Photogrammetry: A Useful Tool For Shipbuilding Applications*. in *Proceedings of the 13th Congress of International Maritime Association of Mediterranean, IMAM*. 2009. Istanbul, Turkey.

15. Chen, B.Q., Y. Garbatov, and C. Guedes Soares, *Measurement of weld induced deformations in three-dimensional structures based on photogrammetry technique.* Journal of Ship Production and Design, 2011. **27**(2): p. 51-62.

16. Chen, B., Y. Garbatov, and C. Guedes Soares. *Displacement Measurement of Box Girder Based on Photogrammetry*. in *Proceedings of the 11th International Symposium on Practical Design of Ships and other Floating Structures (PRADS 2010), paper PRADS2010-20083*. 2010. Rio de Janeiro, Brasil: Aped - Apoio e Produção Ltda.

17. Chen, B.Q., Y. Garbatov, and C. Guedes Soares. *Automatic Approach for Measuring Deformations in Complex Structures Using Photogrammetry Technique*. in *Proceedings of the XXII Pan American Conference of Naval Engineering, Maritime Transportation & Ports Engineering*. 2011. Buenos Aires, Argentina.

18. Grytten, F., et al., *Out-of-plane deformation measurements of an aluminium plate during quasi-static perforation using structured light and close-range photogrammetry.* International Journal of Solids and Structures, 2007. **44**(17): p. 5752-5773.

19. Jiang, R., D.V. Jáuregui, and K.R. White, *Close-range photogrammetry applications in bridge measurement: Literature review.* Measurement, 2008. **41**(8): p. 823-834.

20. Whiteman, T., D.D. Lichti, and I. Chandler, *Measurements of Deflections in concrete beams by close-range digital photogrammetry.* 2002.

21. Dias-da-Costa, D., J.J.Valença, Eduardo N. B. S., *Laboratorial test monitoring applying photogrammetric post-processing procedures to surface displacements.* Measurement, 2011. **44**(3): p. 527-538.

22. Bambach, M.R., *Photogrammetry measurements of buckling modes and interactions in channels with edge-stiffened flanges.* Thin-Walled Structures, 2009. **47**(5): p. 485-504.

23. Sechidis, L., V. Tsioukas, and P. Patia, *An automatic process for the extraction of the 3d model of the human back surface for scoliosis treatmen.* Department of Cadastre Photogrammetry and Cartograph.

24. Petros, P., *Medical imaging challenges photogrammetry.* ISPRS Journal of Photogrammetry and Remote Sensing, 2002. **56**(5–6): p. 295-310.

25. Luhmann, T., *Close range photogrammetry for industrial applications.* ISPRS Journal of Photogrammetry and Remote Sensing, 2010. **65**(6): p. 558-569.

26. Karman, T.V. and E.E. Sechler, *The strenth of thin plates in compression.* Transactions of AS;E, 1932. **54**: p. 53-57.

27. Faulkner, D., *A Review of Effective Plating for use in the Analysis of Stiffened Plating in Bending and Compression.* Journal of Ship Research, 1975. **19**: p. 1-17.

28. Kamiski, M.L. and J. Amadhl, *ULTIMATE STRENGTH.* 14th International Ship and Offshore structures congress 2000, Japan, 2000. **Volume 1**: p. 68.

29. Carlsen, C.A., *Simplified collapse analysis of stiffened plates.* . Norwegian Maritime Research, 1977. **5**(1-4): p. 135-177.

30. Guedes Soares, C., *Design Equation for the Compressive Strength of Unstiffened Plate Elements with Initial Imperfections.* Journal of Constr. Steel Research, 1988. **9**: p. 287-310.

31. Cui, W.a.M., A., *Effects of Welding distortions and residual stresses on the ultimate strength of long rectangular plates under uniaxial compression.* Marine Structures, 1988. **11**(6): p. 251-269.

32. Dowling, P.J. and P.A. Frieze, *Ultimate Load Behavior of Plates in Compression.* Steel plated Structures: International symposium [London 1978]. Ed by P.J. Dowling, J.E. Harding and P.A. Frize., 1977. **Chap. 2**: p. 24-50.

33. Antoniou, A.C., *On the maximum deflection of plating in newly built ships.* Journal of Ship research, 1980. **24**(1): p. 31-39.

34. !!! INVALID CITATION !!!

35. Kmiencik, M., Jastrzerbksi, T. and Kuzniar, J. , *Statistics of ship plating distortions.* Marine Structures, 1995. **8**(2): p. 119-132.

36. Yao, T.F., M. Yanagihara, D., Varghese, B. and Niho, O. , *Influences of welding imperfections on buckling/ultimate strength of ship bottom plating subjected to combined bi-axial thrust and lateral pressure.* Thin-Walled Structures. Research and Developement., 1998: p. 425-432.

37. Fujikubo, M., Yao, T., Varghese, B. , *Buckling/Ultimate Strength of Rectangular plates subjected to combined in-plate loads.* Transactions of West-Japan Society of Naval Architects, 1997. **93**: p. 81-89.

38. Garbatov, Y., M. Tekgoz, and C. Guedes Soares, *Uncertainty Assessment of the Ultimate Strength of a Stiffened Panel*, in *Advances in Marine Structures*, C. Guedes Soares and W. Fricke, Editors. 2011, Taylor & Francis Group: London, UK. p. 659-668.

39. Sheikh, I.A., G.Y. Grondin, and A.E.Elwi, *Stiffener Tripping in stiffened steel plates.* Structural Engineering Report No. 236, 2001. **University of Alberta**.

40. Smith, C.S., Davidson, P.C. and Chaptman, J.C., *Strength and stiffenes of ships plating under in-plane compression and tension. .* Transactions of the Royal Institution of Naval Architects, 1988. **130**: p. 227-296.

41. Poisson, S., *Mémoire sur l'équilibre et le mouvement des corps élastiques.* Academia Royale Sci. Inst. France, 1829. **8**: p. 357-570.

42. Navier, L., *Extrait des recherches sur la flexion des plans élastiques.* Nouvean Bulletin des Sciences par la Sociéte Philomatique de Paris, 1823: p. 98-102.

43. Kirchoff, G., *Über das Gleichgewicht und die Bewegung einer elastischen Scheibe.* Journal für die reine und angewandte Mathematik, 1850: p. 51-88.

44. Timoshenko, S., S. Woinowsky-Krieger, and S. Woinowsky, *Theory of plates and shells.* Mc Graw-Hill, 1959.

45. Bryan, G.N., *On the stability of a plane plate under thrusts in its own plane.* Proc London Math Soc, 1981. **22**: p. 54-67.

46. Cox, H.L., *Buckling of Thin Plates in Compression.* Rep. and Memor., 1933. **1553, 1554**.

47. Ventsel, E. and T. Krauthammer, *Thin Plates and Shells - Theory, Analysis and Applications.* University Park, Pennsylvania, 2001.

48. Guedes Soares, C. and J.M. Gordo, *Compressive Strength of Rectangular Plates Under Transverse Load and Lateral Pressure.* Journal of Constructional Steel Research, 1996. **36**: p. 215-234.

49. Panayotova, M., Y. Garbatov, and C. Guedes Soares. *Factor Influencing Corrosion of Steel Structural Elements Immersed in Steawater*. in *Proceedings of the International Conference on Marine Science and Technology (Black Sea´04)*. 2004. Varna, Bulgaria: Union of Scientists of Varna.

50. Hart, D., S. Rutherford, and A. Wichham, *Structural Reliability Analysis of Stiffened Panels.* Transactions Royal Institution of Naval Architects (RINA), 1986. **128**: p. 293-310.

51. Shi, P. and S. Mahadevan, *Corrosion fatigue and multiple site damage reliability analysis.* International Journal of Fatigue, 2003. **25**: p. 457-469.

52. Garbatov, Y., C. Guedes Soares, and G. Wang, *Nonlinear time dependent corrosion wastage of deck plates of ballast and cargo tanks of tankers.* Journal of Offshore Mechanics and Arctic Engineering, 2007. **129**(1): p. 48-55.

53. Guedes Soares, C. and Y. Garbatov, *Reliability of Maintained, Corrosion Protected Plates Subjected to Non-Linear Corrosion and Compressive Loads.* Marine Structures, 1999: p. 425-445.

54. Guedes Soares, C., et al., *Corrosion Wastage Model for Ship Crude Oil Tanks.* Corrosion Science, 2008. **50**(11): p. 3095-3106.

55. Guedes Soares, C., et al., *Influence of Environmental Factors on Corrosion of Ship Structures in Marine Atmosphere.* Corrosion Science, 2009. **51**(9): p. 2014-2026.

56. Guedes Soares, C., Y. Garbatov, and A. Zayed, *Effect of Environmental Factors on Steel Plate Corrosion under Marine Immersion Conditions.* Corrosion Engineering, Science and Technology 2011. **46**(4): p. 524-541.

57. Silva, J.E., Y. Garbatov, and C. Guedes Soares, *Ultimate strength assessment of ageing steel plates subjected to random non-uniform corrosion wastage*, in *Advances in Marine Structures*, C. Guedes Soares and W. Fricke, Editors. 2011, Taylor & Francis Group: London, UK. p. 213-220.

58. Silva, J.E., Y. Garbatov, and C. Guedes Soares, *Reliability Assessment of a Randomly Nonuniform Corroded Plate Subjected to Compressive Load*, in *Maritime Technology and Engineering*, C. Guedes Soares, et al., Editors. 2012, Taylor & Francis Group: London, UK.

59. Fryer, J.G., *Photogrammtry* Close Range Photogrammetry and Machine Vision, 1996.

60. Thompson, E.H., *Photogrammetry and surveying,* 1977.

61. Konecny, G., *100 Years of the Society ISPRS.* ISPRS Journal of Photogrammetry and Remote Sensing, 2010.

62. Center_for_Photogrammetric_Training, *History of Photogrammetry.* Ferris State University. Michigan, USA, 2008.

63. Cooper, M.A.R. and S. Robson, *Theory of close range Photogrammetry.* Close Range Photogrammetry and Machine Vision, 1996.

64. P., E., *A comparison between photogrammetry and laser scanning.*

65. Inc, E.s., *Photomodeler Scanner Tutorials.* 1992-2008.

66. Lancaster, P. and K. Salkauskas, *Curve and Surface Fitting.* Harcourt Brace Jovanovich, Publicers, 1987.

67. Hughes, O.F., *Buckling and ultimate strength of plates. Ship Structural Design: A Rationally-based, Computer-Aided, Obtimisation Approach.* The society of Naval Architecs and Marine Engineers, 1988(12): p. 404-439.